NTNU

Norwegian University of
Science and Technology

A Comparison of Observers for Estimation of the Bottomhole Pressure.

Eirik Nyland Opsanger

Master of Science in Engineering Cybernetics

Submission date: June 2009

Supervisor: Ole Morten Aamo, ITK

Co-supervisor: Glenn-Ole Kaasa, StatoilHydro

Norwegian University of Science and Technology
Department of Engineering Cybernetics

Problem Description

The first objective of this thesis is to evaluate and compare given adaptive observers for the bottom hole pressure. The analysis is to be made using a high-fidelity model.
The second part is to derive a new friction model from field data.

Topics that should be addressed are:
-Literature review on estimation schemes and drilling model.
-Compare properties and performance of the following estimation schemes:
  -Nonlinear adaptive observer, Stamnes2007
  -Passive identifier with and without filter in adaptation law, Kaasa2008
  -Optimal Estimator for Polynomial systems
  -Nonlinear observer, Grip2009

If time permits
-Prove stability of the optimal estimator
-Prove stability for Grip observer.

-Based on data from a North Sea well, derive a more accurate friction model.
  -Approximate the friction model with B-spline (or other) basis functions.
  -Simulate some of the observers with the new friction model.

Assignment given: 09. January 2009
Supervisor: Ole Morten Aamo, ITK

Preface

This thesis is the result of the work done in the final semester of the Master of Technology program at the Department of Engineering Cybernetics at the Norwegian University of Science and Technology. The thesis has been performed during the spring 2009 and is the last part of the Master of Technology program.

I would like to thank my supervisor Professor Ole Morten Aamo and PhD student Øyvind Stamnes here at NTNU for their help and guidance during the work. I also appreciate the suggestions and answers to my questions from Dr. Glenn-Ole Kaasa at StatoilHydro, Porsgrunn. It has been interesting and instructive to work with a problem from StatoilHydro. The problem considered is a challenge for the petroleum industry, so to contribute with a small piece is motivating.

Trondheim, June 3, 2009

Eirik Nyland Opsanger

Abstract

New offshore oil recourses that are developed are more difficult to drill and increase the requirements to the technology in the offshore industry. A relatively new technology is Managed Pressure Drilling where a choke topside is used to control the bottom hole pressure. The bottom hole pressure measurement is unreliable, which motivates the need for an observer.

Different methods for estimation will be presented and compared in this thesis. Proofs of convergence are outlined for the Stamnes observer, derived for the Grip observer and some stepping stones for further work are presented for the Optimal Polynomial Filter. Each observer is simulated with a simple step in the mud pump to verify the estimation laws. The results show that all observes estimated the bottom hole pressure correctly for this simple case. A more realistic case, a pipe connection, is also simulated for each observer. The case includes zero flow from the mud pump, which reveals that all observers miss the estimation convergence in this case, but that the estimate converges when there is flow from the mud pump.

One of the states that affects the bottom hole pressure is the pressure loss due to friction in drill string and annulus. Earlier work modeled these losses as quadratic with respect to the flow through the bit, which are simplifications. To improve the estimate of the bottom hole pressure, new and better friction models are needed.

Measurement data from Gullfaks C are analyzed to get new knowledge of friction loss in the drilling string and annulus. For the drill string the quadratic friction model is found to be good enough, catching the main behavior. On the other hand, the friction loss in the annulus is a more complicated function of flow. The annulus friction is approximated with sets of basis functions and the weighted sum of these functions gives an approximation to the friction curve. Each weight is estimated to get the friction loss estimate.

The use of the weighted sum of four 1st-order b-spline functions give a good approximation to the real friction curve, and the weight for each basis function is estimated. This is tested in simulations both with a simple case and the pipe connection case.

The simulations show that the annulus friction loss and the bit pressure are estimated correctly.

Contents

List of Figures

List of Tables

Nomenclature

β_a	Bulk modulus of fluid in annulus.
β_d	Bulk modulus of fluid in drill string.
ρ_a	Density in annulus.
ρ_d	Density in drill string.
F_a	Friction factor in annulus.
F_d	Friction factor in drill string.
g	Gravity.
h_{bit}	The vertical height of the drill bit.
K_c	Choke constant.
M_a	Mass equivalence in annulus.
M_d	Mass equivalence in drill string.
P	Covariance matrix.
p_0	Pressure outside system.
p_c	Pressure over choke.
p_p	Mud pump pressure.
p^a_{fric}	Pressure loss due to friction in annulus.
p^d_{fric}	Pressure loss due to friction in drill string.
q_{back}	Flow from the back pressure pump.
q_{bit}	Flow through drill bit.
q_{choke}	Flow through the choke.
q_p	Flow through mud pump.

q_{res} Flow to/from reservoir.

V_a Volume in annulus.

V_d Volume in drill string.

z_c Choke opening. $z_c \in [0, 1]$

Design variables

$\mathbf{\Gamma}$ Adaption gain. $\mathbf{\Gamma}^\top = \mathbf{\Gamma} > 0$.

$\mathbf{x}$ State vector for Optimal filter estimator.

μ_i Radius of support for continuous basis functions.

$B(t)$ Scaling matrix for measurement noise, Optimal filter estimator.

$b(t)$ Scaling matrix for process noise, Optimal filter estimator.

c_i Center of support for basis functions.

H Scaling matrix for Optimal filter estimator.

l_1 Observer gain. $l_1 > 0$.

τ_f Time constant of low pass filter.

Defined parameters

$\boldsymbol{\phi}$ Regressor.

$\boldsymbol{\theta}$ Unknown parameters.

a_1 $\frac{\beta_d}{V_d}$

a_2 $\frac{1}{M}$

F $F_a + F_d$

M $M_a + M_d$

$v_1(t)$ $V_a(t)$

$v_2(t)$ $-\dot{V}_a(t)$

$v_3(t)$ $h_{bit}(t)$

Part I

Background

Chapter 1

Introduction

This first chapter gives background information about offshore drilling, pressure control and the idea behind observers. It is assumed that the reader has knowledge about these topics, so just a very short overview is given.

At the end, the chapter covers the scope and outline of the thesis.

1.1 Drilling, Control problem and Managed Pressure Drilling

When difficult reserves are discovered, advanced technology is required to be able to drill well. The subject considered in this thesis is the problem of keeping the bottom hole pressure under control during drilling.

Figure 1.1 shows a simple sketch of a typical offshore drilling setup, which will be briefly explained. The *top drive* is a motor used to rotate the *drill string*, with the *drill bit* at the end. The area around the bit is called *the open (bottom) hole*. Drilling mud is used during drilling to clean the bottom hole and to maintain the pressure. The mud is pumped down with the main mud pump and flows through the drill string down to the drill bit and taking the cuttings up through the annulus. The cuttings are taken out, while the mud is sent back into the drill string.

After drilling some distance, the open hole wall is covered with cement, called *casing*. This makes the hole stable concerning pressures from the formation. Before the open hole is cased, the pressure from the formation must be balanced with pressure from the mud.

If the bottom hole pressure becomes too low (below the pore pressure) there can be influx from the reservoir, which in worst case can lead to an uncontrolled blow out [Skalle, 2005]. Another issue is that the drill bit can be stuck due to formation collapse. This may lead to a twist-off of the drill string and lead to large economic losses, since the well probably would have to be drilled again.

If the bottom hole pressure profile becomes too high (over the fracture

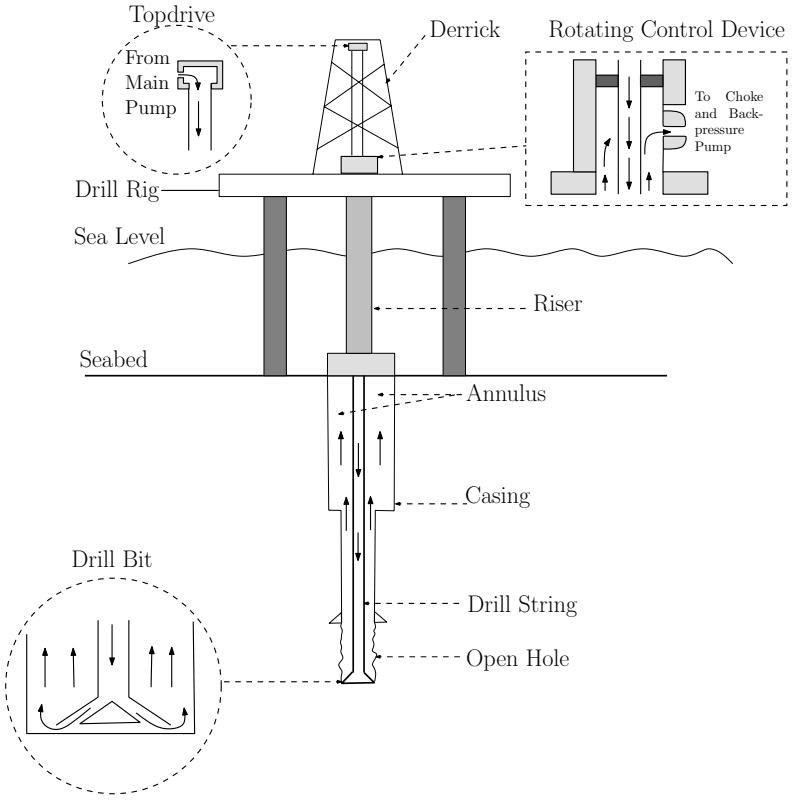

Figure 1.1: Example of drilling system. Modified version of figure from [Stamnes, 2007].

pressure), the wall of the well can be destroyed and the drilling has to be stopped. A worst case scenario is that the entire installation can be lost as a cause of an underground blowout.

Many of the easy wells (large pressure margins) have already been drilled, so new technology is required to drill the "undrillable reserves" and meet the increasing demand for oil. This, together with reduced drilling costs, motivates the need for precise pressure control. Drilling costs have lately (2008/2009) been an even more important part, after the problems in the world economics.

As will be derived in Chapter 2 there are different ways to change (control) the pressure in the open hole. One solution is to change the mud density since this will change the hydrostatic pressure. An evident disadvantage with this solution is that change of density includes a large time lag. It will also be a problem to achieve precise control.

Another method to control the pressure is the use of Managed Pressure Drilling (MPD), defined by *IADC Underbalanced Operations Committee* as *"an adaptive drilling process used to precisely control the annular pressure profile throughout the well bore. The objectives are to ascertain the down hole*

pressure environment limits and to manage the annular hydraulic pressure profile accordingly" [Hannegan et al., 2004]. MPD gives more accurate control over the down hole pressure, which reduces formation damage, reduces loss of circulation mud and gives improved rate of penetration [Kaasa, 2007].

To control the pressure with MPD, a choke is used to set the outflow from the annulus topside. If the choke is closed, the bottom hole pressure increases and vice versa. The technology is relatively new to the offshore drilling industry, but e.g. StatoilHydro has done some MPD-testing at Gullfaks C and Grane fields.

The complete bottom hole pressure profile is very complex and hard to obtain. It is a function of geometry, fluid velocity, friction, density etc. Because of this, the pressure at the bit is usually used for control. The margins are smallest at the bit, which justifies the use of this value for control. In the cased part of the well, there will be no pressure problems.

One of the parameters affecting the bottom hole pressure will be taken closer into consideration in this thesis, namely the friction loss. In the first part of the thesis the friction is assumed to be quadric w.r.t. the flow, but new models are derived in the last part. Better understanding of the friction loss will result in better estimation of the bottom hole pressure.

1.1.1 Important equipments

Some of the drilling equipments in Figure 1.1 are important for the modeling in Chapter 2. These parts are given a short introduction here. See also Figure 2.1 for the relation between the states and the drilling setup.

Main pressure pump The main pressure pump (mud pump) is, as the name implies, the major component in the circulating system. The pump gets the mud to circulate in the system.

The dynamics of the mud pump are not taken into account in this thesis, instead the flow rate is taken as the main actuator directly.

Back pressure pump The back pressure pump is a backup pump for the main pump. When the main pump must be turned off, e.g. for a pipe connection, the back pressure pump is used to maintain the pressure in the open hole.

The back pressure pump is used in simulations of a drilling scenario later in the thesis. As for the mud pump, the flow rate is given and no dynamics are considered.

Control choke The control choke is the manipulated variable in the system. The choke is closed to increase the bottom hole pressure, and the choke is opened to decrease the pressure.

A simple PI-controller is used in the drilling cases, otherwise the choke opening is kept constant (open loop).

Drill bit The drill bit is the last part of the drill string and is used to crush or cut the rocks. A wide range of different bits are available for different formations and selecting the right bit is an important task for a drilling engineer.

The pressure at the bit is used to represent the open hole pressure.

1.1.2 Observer

Observers are used in control systems when measurements are not good enough. This can be because the measurements include noise, have low sampling frequency, is unreliable or because the state is not measured at all. For the MPD-problem observers are needed to get a continuous value for the pressure at the bit, in addition to estimate unknown parameters.

One point that makes the estimation problem challenging for this system is that the flow through the bit is not measured. In real drilling this value is known with a unreliable measurement with low sampling frequency (mud pulse telemetry), but this is not used in any of the observers that will be presented.

Different observers are presented and compared in this thesis.

1.2 Scope

The first goal of this thesis is to compare given observers for the bottom hole pressure. Proofs of convergence will also be derived for some observers, while others are tested with simulations.

The second goal is to find new friction models for the friction in the drill string and annulus, based on measurement data. The annulus friction should also be estimated in this case.

1.3 Thesis outline

The thesis is divided into 5 parts:

1. Part 1 (Chapters 1 - 2) gives motivation, background information about drilling and presents a low order model used for observer design.
2. Part 2 (Chapters 3 - 8) is the main part of the thesis, with presentations of the observers, proofs and simulation results.
3. Part 3 (Chapters 9 - 11) present a new friction model which is derived from drilling data, together with different approximations and simulations.
4. Part 4 (Chapter 12) concludes the thesis and suggests further work.
5. Part 5 (Chapters A-C) contains appendices with more detailed derivations and additional simulation results.

Chapter 2

Modeling

To be able to design observers, a model of the system is needed. In this chapter a simple ODE model is derived. The model is originally developed in the internal document [Kaasa, 2007] and also given a good review in [Stamnes, 2007].

The modeling is based on mass and momentum balances and a short overview is given here for the completeness of the thesis. Some derivations are given in Appendix A. The modeling gives three ordinary differential equations and considers single phase flow only.

The system is divided into two control volumes as shown in Figure 2.1, the drill string and the annulus. The two volumes are connected with the drill bit. The figure also shows the states used to describe the system.

2.1 Pressure dynamics

There are two pressures that are modeled, the main pump pressure and the choke pressure. In Appendix A a mass balance is used to get an expression for the pressure dynamics, given in Equation (A.7). Using this equation and Figure 2.1 it is easy to see that the pressure dynamics for the pump pressure (p_p) are given by

$$\frac{V_d}{\beta_d}\dot{p}_p = q_p - q_{bit} - \dot{V}_d \tag{2.1}$$

where V_d is the drill sting volume, β_d is the bulk modulus of the mud, q_p is the flow from the mud pump and q_{bit} is the flow to the drill bit.

The same mass balance is also used to find the dynamics for the choke pressure, which are

$$\frac{V_a}{\beta_a}\dot{p}_c = q_{bit} + q_{back} + q_{res} - q_{choke} - \dot{V}_a \tag{2.2}$$

where V_a is the volume of the annulus, β_a is the bulk modulus of the fluid in the annulus, q_{back} is flow from back pressure pump, q_{res} is flow from the

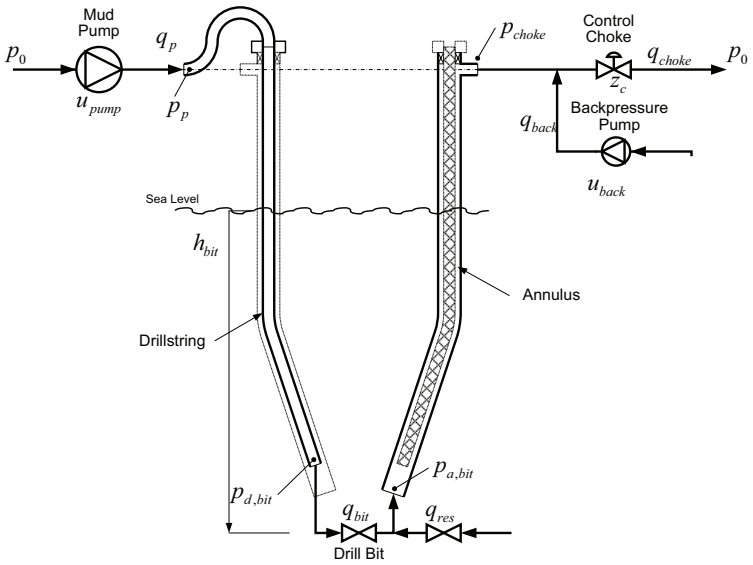

Figure 2.1: Division of the system into two control volumes. Slightly modified figure from [Kaasa, 2007]

reservoir and q_{choke} is flow through the choke, modeled by the classic orifice equation [Merritt, 1967]

$$q_{choke} = K_c z_c \sqrt{\frac{2}{\rho_a}(p_c - p_0)} \tag{2.3}$$

where $z_c \in [0, 1]$ is the valve opening, K_c is a valve constant and p_0 is the pressure outside the system (1 bar).

2.2 Flow dynamics

Both the pump pressure dynamics and the dynamics for the choke pressure depend on the flow through the bit, q_{bit} (which connects the two control volumes). The dynamics for q_{bit} is derived using a momentum balance for each of the two control volumes.

The flow in the two control volumes given by [Stamnes, 2007]

$$M_a \dot{q}_a = p_{bit} - p_c - F_a|q_a|q_a - \rho_a g h_{bit} \tag{2.4}$$

$$M_d \dot{q}_d = p_p - p_{bit} - F_d|q_d|q_d - \rho_d g h_{bit} \tag{2.5}$$

where $M_d = \rho_d \int_0^{L_{dN}} \frac{1}{A_d(x)} dx$ and $M_a = \rho_a \int_0^{l_w} \frac{1}{A_a(x)} dx$. ($L_{dN}$ and l_w are the drill string and annulus lengths, while $A_d(x)$ and $A_a(x)$ are cross-section areas of the drill string and annulus.) ρ_d and ρ_a are densities in drill string and annulus, g is gravity and h_{bit} is the vertical depth of the bit (not the same

as the length of the well). F_d and F_a are friction factors for the drill string and annulus, which means that the friction losses are assumed to be quadratic w.r.t. q_{bit}. [1]

When density is considered in the modeling it should be a function of height in the drill sting/annulus, however the average density is used to simplify the equations.

The dynamics for the flow through the bit are found by summing Equations (2.4) and (2.5) and inserting $q_a = q_{bit} + q_{res}$ and $q_d = q_{bit}$ (See Figure 2.1). Assuming constant flow to/from the reservoir implies $\dot{q}_a = \dot{q}_{bit}$ and the bit flow dynamics are

$$\begin{aligned} M\dot{q}_{bit} = \quad & \underbrace{p_p - p_c}_{\text{Pressure difference}} \quad \underbrace{-F_d|q_{bit}|q_{bit}}_{\text{Friction in drill string}} \\ & \underbrace{-F_a|q_{bit}+q_{res}|(q_{bit}+q_{res})}_{\text{Friction in annulus}} \underbrace{+(\rho_d - \rho_a)gh_{bit}}_{\text{Hydrostatic pressure}} \end{aligned} \tag{2.6}$$

where $M = M_a + M_d$. There is usually a check valve in the bit to prevent flow from annulus back into the drill string. It is then assumed that $q_{bit} \geq 0$.

Rearranging Equation (2.4) gives the expression for the bit pressure

$$p_{bit} = p_c + M_a\dot{q}_{bit} + F_a|q_{bit}+q_{res}|(q_{bit}+q_{res}) + \rho_a g h_{bit} \tag{2.7}$$

$$\begin{aligned} &= \frac{M_a}{M}p_p + \frac{M_d}{M}p_c + (\frac{M_d}{M}F_a - \frac{M_a}{M}F_d)|q_{bit}+q_{res}|(q_{bit}+q_{res}) \\ &\quad + (\frac{M_d}{M}\rho_a + \frac{M_a}{M}\rho_d)gh_{bit} \end{aligned} \tag{2.8}$$

From Equation (2.7) we see that the bit pressure consist of three parts in steady state. It is pressure from the control choke, pressure due to friction and hydrostatic pressure. From this equation the different methods of pressure control (change ρ_a or p_c) mentioned in Section 1.1 should be obvious.

2.3 Assumptions

The following assumptions are made for the model (2.1), (2.2) and (2.6).

Assumption 1. *Isothermal conditions in the fluid.*

Assumption 2. $\sum m_{in} = \sum q_{in}\rho$ *and* $\sum m_{out} = \sum q_{out}\rho$

Assumption 3. *The change w.r.t. time in average pressure is the same as the change in pressure anywhere in the control volume.*

[1] New friction models, based on drilling test measurements, are derived later in this thesis.

Assumption 4. *ρ is constant in the flow dynamics, compressible flow effects due to pressure variations will be neglected, this implies that the flow will be considered rigid. The density is assumed to be constant in the control volume.*

Assumption 5. *q_{res} is constant.*

2.4 Summary of model and notation

The design model is summarized in Table 2.1 and used in the rest of the thesis.

Table 2.1: Summary of the design model.

Plant	$\dot{p}_p = a_1(q_p - q_{bit})$ $\dot{p}_c = \frac{\beta_a}{v_1}(q_{bit} + q_{back} + q_{res} - q_{choke} + v_2)$ $\dot{q}_{bit} = a_2(p_p - p_c) - a_2 F_d \lvert q_{bit}\rvert q_{bit}$ $\quad -a_2 F_a \lvert q_{bit} + q_{res}\rvert (q_{bit} + q_{res}) - a_2(\rho_d - \rho_a) g v_3$
Constants	$a_1 \triangleq \frac{\beta_d}{V_d}$ $a_2 \triangleq \frac{1}{M_a + M_d}$
Time varying	$v_1(t) \triangleq V_a(t)$ $v_2(t) \triangleq -\dot{V}_a(t)$ $v_3(t) \triangleq h_{bit}(t)$

Assumption 6. *The flow to/from the reservoir is disregarded in the rest of the thesis.* $q_{res} \equiv 0$.

Part II

Comparison of different observers

Chapter 3

The Stamnes observer

A nonlinear adaptive observer was derived in [Stamnes, 2007; Stamnes et al., 2008] based on the modeling from Chapter 2 and Table 2.1. This observer is well documented with proofs of convergence and simulations.

The observer uses a change of coordinates to estimate the flow through the bit. From the Lyapunov analysis the dynamics for the adaptation error are chosen, driven by $\tilde{q}_{bit}$. But since q_{bit} is not measured, a new change of coordinates is used to derive the adaptation law. The fact that the observer does not use q_{bit} in the estimation is an advantage.

3.1 Observer

As mentioned earlier, the main goal is to estimate p_{bit} which is given in Equation (2.8) as

$$\begin{aligned} p_{bit} = &\frac{M_a}{M}p_p + \frac{M_d}{M}p_c + (\frac{M_d}{M}F_a - \frac{M_a}{M}F_d)|q_{bit}|q_{bit} \\ &+ (\frac{M_d}{M}\rho_a + \frac{M_a}{M}\rho_d)gh_{bit} \end{aligned} \tag{3.1}$$

where p_p, p_c, h_{bit} are measured and $M = M_d + M_a$, ρ_d and F_d are assumed to be known. Using the notation from Section 2.4 and define

$$\theta_1 = \frac{F_a + F_d}{M_a + M_d} \tag{3.2}$$

$$\theta_2 = \frac{(\rho_d - \rho_a)g}{M_a + M_d} \tag{3.3}$$

Equation (3.1) can be written as

$$\begin{aligned} p_{bit} = &p_c + M_a(a_2(p_p - p_c) - \theta_1|q_{bit}|q_{bit} + \theta_2 v_3 \\ &+ (M\theta_1 - F_d)|q_{bit}|q_{bit} + (\rho_d g - M\theta_2)v_3 \end{aligned} \tag{3.4}$$

and an estimate of p_{bit} is

$$\begin{aligned}\hat{p}_{bit} = p_c + M_a(a_2(p_p - p_c) - \hat{\theta}_1|\hat{q}_{bit}|\hat{q}_{bit} + \hat{\theta}_2 v_3 \\ + (M\hat{\theta}_1 - F_d)|\hat{q}_{bit}|\hat{q}_{bit} + (\rho_d g - M\hat{\theta}_2)v_3\end{aligned} \tag{3.5}$$

As Equation (3.5) shows, expressions for $\hat{q}_{bit}$ and $\hat{\boldsymbol{\theta}}$ are needed to find the estimate $\hat{p}_{bit}$. [Stamnes et al., 2008] introduces the following change of coordinates (idea from [Tan et al., 1998]) to solve this issue

$$\xi_1 \triangleq q_{bit} + l_p p_p \tag{3.6}$$

The time-derivative is (using Equations (2.1) and (2.6))

$$\dot{\xi}_1 = \dot{q}_{bit} + l_1 \dot{p}_p \tag{3.7}$$

$$= a_2(p_p - p_c) - a_2(F_d + F_a)|q_{bit}|q_{bit} - a_2(\rho_d - \rho_a)g v_3 + l_1 a_2(q_p - q_{bit}) \tag{3.8}$$

The observer for q_{bit} is then taken as

$$\dot{\hat{\xi}}_1 = a_2(p_p - p_c) - \hat{\theta}_1|\hat{q}_{bit}|\hat{q}_{bit} - \hat{\theta}_2 v_3 + l_1 a_2(q_p - \hat{q}_{bit}) \tag{3.9}$$

$$\hat{q}_{bit} = \hat{\xi}_1 - l_1 p_p \tag{3.10}$$

where $l_1 > 0$ is the observer gain. Note that $\tilde{\xi}_1 = \xi_1 - \hat{\xi}_1 = \tilde{q}_{bit}$.

The initial condition is given by

$$\hat{\xi}_1(0) = \hat{q}_{bit}(0) + l_1 p_p(0) \tag{3.11}$$

3.1.1 Proof outline

The most important stages from the Lyapunov proof in [Stamnes, 2007] is repeated here. The following Lyapunov candidate is used

$$V_1(\tilde{\xi}_1, \tilde{\boldsymbol{\theta}}) = \frac{1}{2}\tilde{\xi}_1^2 + \frac{1}{2}\tilde{\boldsymbol{\theta}}^\top \boldsymbol{\Gamma}^{-1}\tilde{\boldsymbol{\theta}}, \tag{3.12}$$

where $\boldsymbol{\Gamma} = \boldsymbol{\Gamma}^\top > 0$ is the adaptation gain. By choosing

$$\dot{\tilde{\boldsymbol{\theta}}} = -\boldsymbol{\Gamma}\boldsymbol{\phi}\tilde{\xi}_1 \tag{3.13}$$

the derivative of V_1 becomes

$$\dot{V}_1 \leq -l_1 a_1 \tilde{\xi}_1^2 \tag{3.14}$$

It is argued in [Stamnes, 2007] that this implies $\hat{q}_{bit} \to q_{bit}$ as $t \to \infty$ $\forall q_{bit} > 0$, but it does not guarantee that $\hat{\boldsymbol{\theta}} \to \boldsymbol{\theta}$ as $t \to \infty$. However, $\dot{\hat{\boldsymbol{\theta}}} \to 0$.

3.2 Adaptation law

To get convergence of $\hat{q}_{bit}$ the error dynamics were chosen as $\dot{\tilde{\boldsymbol{\theta}}} = -\boldsymbol{\Gamma}\boldsymbol{\phi}\tilde{\xi}_1$ in Equation (3.13). Since q_{bit} is assumed not to be measured, the adaption law $\dot{\hat{\boldsymbol{\theta}}} = -\dot{\tilde{\boldsymbol{\theta}}} = \boldsymbol{\Gamma}\boldsymbol{\phi}\tilde{\xi}_1$ can not be used. ($\tilde{\xi}_1 = \tilde{q}_{bit}$, which is unknown.) To get around this problem a change of coordinates are used

$$\sigma \triangleq \boldsymbol{\theta} + \boldsymbol{\eta}(\hat{q}_{bit}, v_3) \tag{3.15}$$

where $\boldsymbol{\eta}$ is a designed function of known/measured signals. The adaptation law is stated as

$$\hat{\boldsymbol{\theta}} = \hat{\boldsymbol{\sigma}} - \boldsymbol{\eta}(\hat{q}_{bit}, v_3) \tag{3.16}$$

The time derivative of $\hat{\boldsymbol{\sigma}}$ is[1]

$$\dot{\hat{\boldsymbol{\sigma}}} = -l_1 \frac{\partial \boldsymbol{\eta}}{\partial \hat{q}_{bit}}(-a_1 \hat{q}_{bit} + q_p) + \frac{\partial \boldsymbol{\eta}}{\partial \hat{q}_{bit}}\dot{\hat{\xi}} + \frac{\partial \boldsymbol{\eta}}{\partial v_3}\dot{v}_3 \tag{3.17}$$

with the initial conditions

$$\hat{\boldsymbol{\sigma}}(0) = \hat{\boldsymbol{\theta}}(0) + \boldsymbol{\eta}(\hat{q}_{bit}(0), v_3(0)) \tag{3.18}$$

By using the coordinate change in Equation (3.6) the error dynamics for $\boldsymbol{\theta}$ may be written

$$\dot{\tilde{\boldsymbol{\theta}}} = \dot{\tilde{\boldsymbol{\sigma}}} \tag{3.19}$$

$$= l_1 a_1 \frac{\partial \boldsymbol{\eta}}{\partial \hat{q}_{bit}}\tilde{\xi}_1 \tag{3.20}$$

The chosen dynamics for $\dot{\tilde{\boldsymbol{\theta}}}$ (Equation (3.13)) and Equation (3.20) give

$$-l_1 a_1 \frac{\partial \boldsymbol{\eta}}{\partial \hat{q}_{bit}} = \boldsymbol{\Gamma}\boldsymbol{\phi} \tag{3.21}$$

Several choices for $\boldsymbol{\eta}$ is now possible, but for simplicity [Stamnes, 2007] chose $\boldsymbol{\eta}$ from integrating the regressor $\boldsymbol{\phi} = [-|\hat{q}_{bit}|\hat{q}_{bit} \quad v_3]^\top$ w.r.t. $\hat{q}_{bit}$. This gives

$$\boldsymbol{\eta}(\hat{q}_{bit}, v_3) = \boldsymbol{\Gamma}\begin{bmatrix} \frac{|\hat{q}_{bit}|^3}{3l_1 a_1} \\ -\frac{v_3 \hat{q}_{bit}}{l_1 a_1} \end{bmatrix} \tag{3.22}$$

The partial derivative of $\boldsymbol{\eta}$ is needed in Equation (3.17) and is given by

$$\frac{\partial \boldsymbol{\eta}}{\partial \hat{q}_{bit}} = \boldsymbol{\Gamma}\begin{bmatrix} \frac{|\hat{q}_{bit}|\hat{q}_{bit}}{l_1 a_1} \\ -\frac{v_3}{l_1 a_1} \end{bmatrix} \tag{3.23}$$

$$\frac{\partial \boldsymbol{\eta}}{\partial v_3} = \boldsymbol{\Gamma}\begin{bmatrix} 0 \\ -\frac{\hat{q}_{bit}}{l_1 a_1} \end{bmatrix} \tag{3.24}$$

[1] Take the derivative of Equation (3.15) and insert (3.10).

3.3 Properties and limitations

The Stamnes observer is given by Equations (3.5), (3.9), (3.10), (3.16), (3.17), (3.22), (3.23) and (3.24) and has the following properties and limitations:

- $\tilde{p}_{bit} \to 0$ as $t \to \infty$
- $\tilde{q}_{bit} \to 0$ as $t \to \infty$
- $\dot{\hat{\boldsymbol{\theta}}} \to 0$ as $t \to \infty$
- The observer adapts to unknown β_a, but this is not considered in this thesis.
- The q_{bit} measurement, which is available with low sampling rate, should be used to some extent.
- There is an unsolved issue when $q_{bit} = 0$. A solution is proposed in [Stamnes, 2007], but further work could be done to prove stability.

3.4 Simulation result

To test the observer a simulation with the design model is made. The mud pump is stepped from $1000\frac{ltr}{min}$ to $500\frac{ltr}{min}$ after 1000 seconds. This simulation will be done for each observer through the thesis. A more realistic case is simulated in Chapter 7 where a pipe connection is considered. Since the system states (e.g. mud pump pressure) behaves exactly equal for the observers, these figures are placed in Appendix B.1 for the step-test. Also the same tuning parameters and the initial values were used for all observers. These can be seen in Table 3.1.

Table 3.1: Design parameters used for step test.

Parameter	Value
Γ	$\text{diag}([10^5, 5 \cdot 10^{-9}]$
l_1	10^{-5}
γ_0	10
τ_f	$\{1, 20, 50\}$
$\hat{q}_{bit}(0)$	700 [ltr/min]
$\hat{\theta}_1(0)$	28.1836 [-]
$\hat{\theta}_2(0)$	$-8.3640 \cdot 10^{-6}$ [-]

The simulation for the Stamnes-observer is shown in Figure 3.1. As can be seen in Figures 3.1(a) and 3.1(b) both $\tilde{q}_{bit}$ and $\tilde{p}_{bit}$ tends to zero as expected. It should also be noted that this happens, even when $\tilde{\theta} \neq 0$ as shown in 3.1(c) and 3.1(d). This coincides with the proof and expectations.

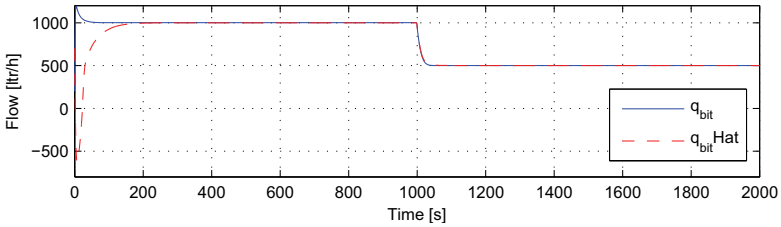

(a) q_{bit} and $\hat{q}_{bit}$.

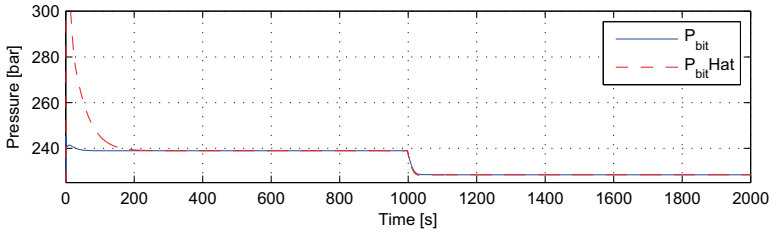

(b) p_{bit} and $\hat{p}_{bit}$.

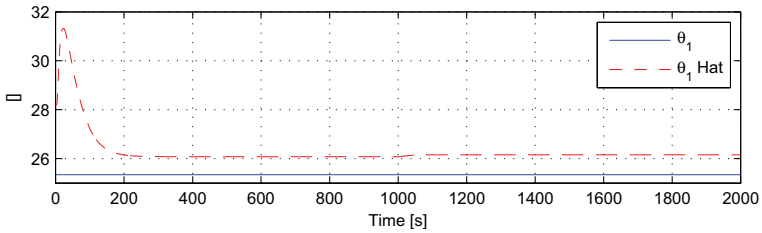

(c) θ_1 and $\hat{\theta}_1$

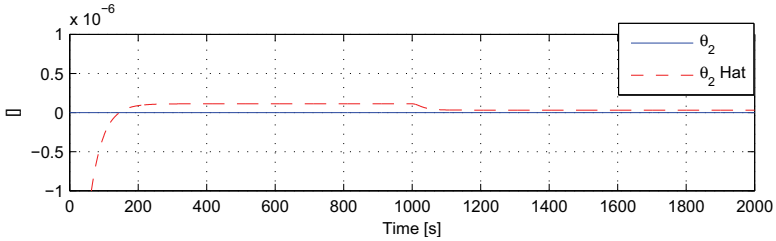

(d) θ_2 and $\hat{\theta}_2$

Figure 3.1: States and parameters for step test with Stamnes observer.

Chapter 4

Identifiers driven by $\tilde{q}_{bit}$

Two estimation methods driven by $\tilde{q}_{bit}$ are proposed in the internal document [Kaasa, 2009]. The estimation algorithms use the same design model as in Chapter 3 and the same observer for q_{bit}. The main difference from Chapter 3 is the implementation of the adaptation methods. Convergence proof is not derived for the adaptation law with a low pass filter.

4.1 Identifier driven by estimation error

In Chapter 3 the dynamics for $\tilde{\boldsymbol{\theta}}$ were chosen as $\dot{\hat{\boldsymbol{\theta}}} = -\dot{\tilde{\boldsymbol{\theta}}} = \boldsymbol{\Gamma}\boldsymbol{\phi}\tilde{\xi}_1$. It was argued that q_{bit} was not known and thus not used, which resulted in a derivation with change of coordinates. However, Equation (2.1) is

$$\frac{V_d}{\beta_d}\dot{p}_p = q_p - q_{bit} - \dot{V}_d \tag{4.1}$$

which can be rearranged to

$$q_{bit} = q_p + \dot{V}_d - \frac{V_d}{\beta_d}\dot{p}_p \tag{4.2}$$

$\dot{V}_d$, V_d and β_d are assumed to be known, so q_{bit} can be calculated if $\dot{p}_p$ is known. It is reasonable to assume p_p known (q_p is the actuator of the system), so the derivative can be found by e.g. an Euler-method.

The adaptation law is then taken as

$$\begin{aligned}\dot{\hat{\boldsymbol{\theta}}} &= \boldsymbol{\Gamma}\boldsymbol{\phi}(\hat{q}_{bit}, v_3)\tilde{q}_{bit} \\ &= \boldsymbol{\Gamma}\boldsymbol{\phi}(\hat{q}_{bit}, v_3)(q_p + \dot{V}_d - \frac{V_d}{\beta_d}\dot{p}_p - \hat{q}_{bit})\end{aligned} \tag{4.3}$$

where $\boldsymbol{\phi} = [\frac{F_a+F_d}{M} \quad \frac{(\rho_d-\rho_a)g}{M}]^\top$ as in the last chapter. This should ensure that $\tilde{q}_{bit}$ converges to zero since the error system is strictly passive. The observer

for q_{bit} is the same as in Chapter 3, written as

$$\dot{\hat{\xi}} = -l_1 a_1 \hat{q}_{bit} + a_2(p_p - p_c) + \hat{\boldsymbol{\theta}}^\top \boldsymbol{\phi}(t, \hat{q}_{bit}) + l_1 a_1 q_p \tag{4.4}$$

$$\hat{q}_{bit} = \hat{\xi} - l_1 p_p \tag{4.5}$$

$$\begin{aligned}\hat{p}_{bit} = p_c + M_a(a_2(p_p - p_c) - \hat{\theta}_1|\hat{q}_{bit}|\hat{q}_{bit} + \hat{\theta}_2 v_3 \\ + (M\hat{\theta}_1 - F_d)|\hat{q}_{bit}|\hat{q}_{bit} + (\rho_d g - M\hat{\theta}_2)v_3\end{aligned} \tag{4.6}$$

This method for adaptation is simple, but requires q_{bit} which is not available as a measurement. The use of Equation (4.2) solves this issue by using top side measurements, but introduces more model uncertainties. If e.g. the bulk-modus in the drill string is set wrong, this will influence q_{bit} directly.

4.1.1 Simulation result

The step-test for the passive identifier is shown in Figure 4.1. The tuning and initial conditions values are the same as in the last chapter. As seen from the figure, the results are very similar to the results with the Stamnes observer. This is as expected since the adaptation law in the Stamnes observer is just a smart implementation method to avoid the use of q_{bit}.

Both $\hat{q}_{bit}$ and $\hat{p}_{bit}$ (Figures 4.1(a) and 4.1(b)) converge to their true values.

Figure 4.1(c) shows that $\hat{\theta}$ is estimated wrong, but is at least constant. A look at Figure 4.1(d) may indicate that $\hat{\theta}_2 = \theta_2$ but a numerical analysis reveals that the value is just almost correct. More precisely is $\hat{\boldsymbol{\theta}}^\top \boldsymbol{\phi} = 0$, which is the same as the results for the observer in the last chapter.

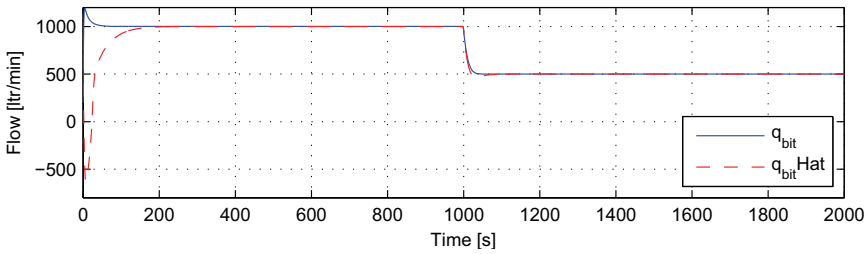

(a) q_{bit} and $\hat{q}_{bit}$.

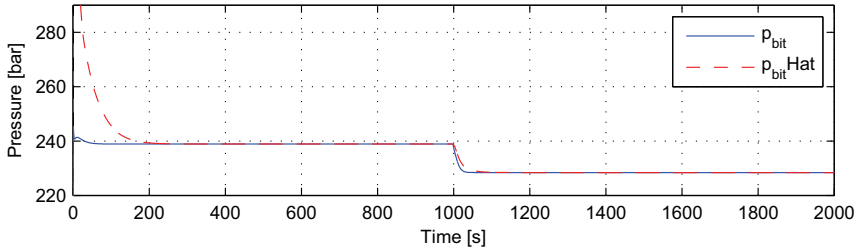

(b) p_{bit} and $\hat{p}_{bit}$.

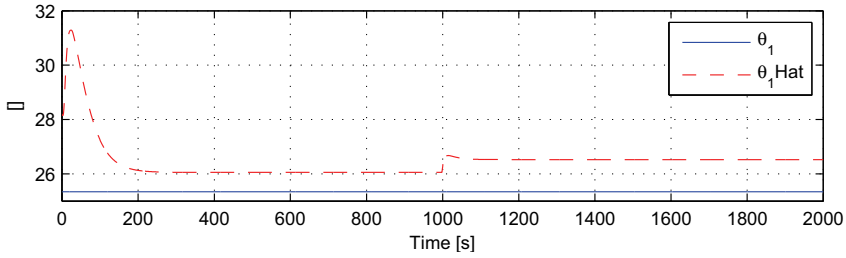

(c) θ_1 and $\hat{\theta}_1$

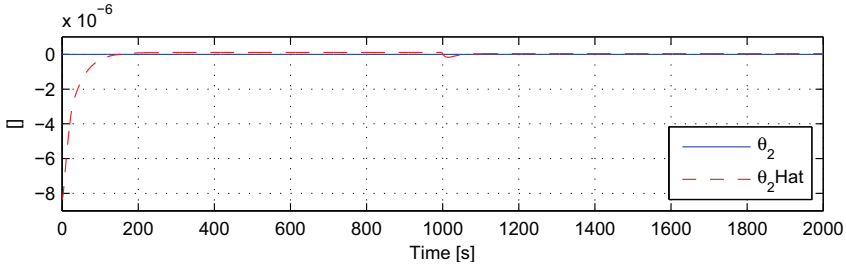

(d) θ_2 and $\hat{\theta}_2$

Figure 4.1: States and parameters for step test with passive identifier driven by $\tilde{q}_{bit}$.

4.2 Identifier driven by the filtered estimation error

As another approach to the adaptation problem, an adaptation law driven by the low-pass filtered estimation error is proposed in [Kaasa, 2009]. The low pass filtered error should be more robust to noise and smooth out changes in $\tilde{q}_{bit}$. Define

$$\tilde{q}_f \triangleq \frac{1}{\tau_f s + 1}\tilde{q}_{bit} \tag{4.7}$$

where τ_f is the time constant of the low pass filter. The estimator for $\boldsymbol{\theta}$ is then taken as

$$\begin{aligned}\dot{\hat{\boldsymbol{\theta}}} &= \boldsymbol{\Gamma}\boldsymbol{\phi}(\hat{q}, v_3)\tilde{q}_f \\ &= \boldsymbol{\Gamma}\boldsymbol{\phi}(\hat{q}_{bit}, v_3)\frac{1}{\tau_f s + 1}\tilde{q}_{bit} \\ &= \boldsymbol{\Gamma}\boldsymbol{\phi}(\hat{q}_{bit}, v_3)(q_p - q_{bit}) + \boldsymbol{\Gamma}\boldsymbol{\phi}(\hat{q}_{bit}, v_3)\frac{s}{\tau_f s + 1}p_p \end{aligned} \tag{4.8}$$

Note that (4.8) $\rightarrow$ (4.3) as $\tau_f \rightarrow 0$.

The law from Equation (4.8) can be written in state space form and implemented as

$$\dot{\hat{\boldsymbol{\theta}}} = \boldsymbol{\Gamma}\boldsymbol{\phi}(\hat{q}_{bit}, v_3)\tilde{q}_f \tag{4.9}$$

$$\dot{x}_f = -\tilde{q}_f + q_p - \hat{q}_{bit} \tag{4.10}$$

$$\tilde{q}_f = \frac{1}{\tau_f}(x_f - \frac{V_d}{\beta_d}p_p) \tag{4.11}$$

4.2.1 Simulation result

The step-test for the estimator driven by the low pass filtered $\tilde{q}_{bit}$ is shown with different time constants in Figure 4.2.

As seen for all variables, the introduction of the low pass filter gives some more oscillations than the step test in Figure 4.1. However, the steady state results is same; the pressure and flow estimate converge, but the parameters are wrong.

The oscillations are as expected, since a filter will introduce a phase lag. The oscillations increase with increased time constant in the filter, but increased time constant will give a better filter. The filter is not utilized in this simulations, so it may be worth to try in it other simulations later.

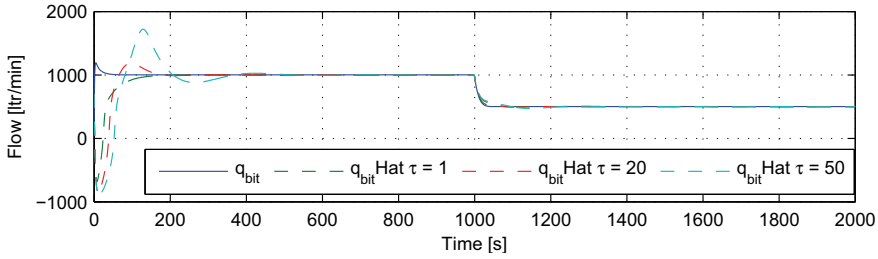

(a) q_{bit} and $\hat{q}_{bit}$.

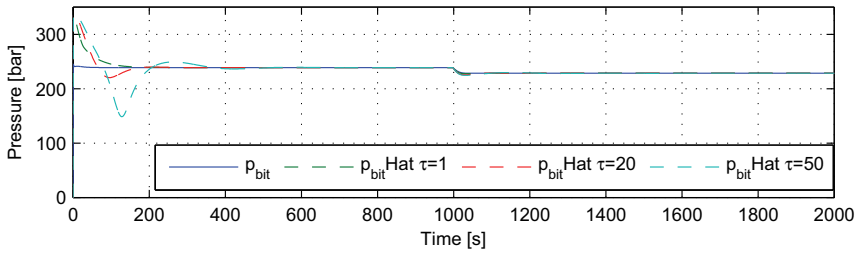

(b) p_{bit} and $\hat{p}_{bit}$.

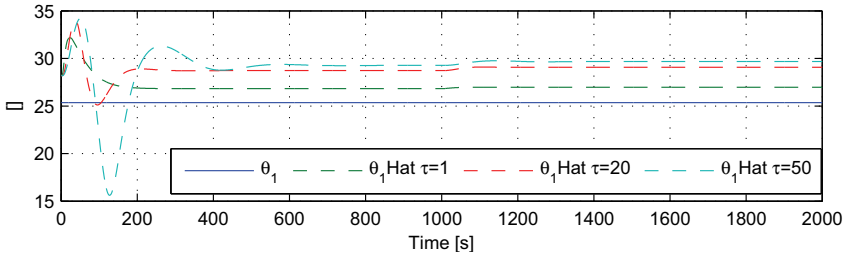

(c) θ_1 and $\hat{\theta}_1$

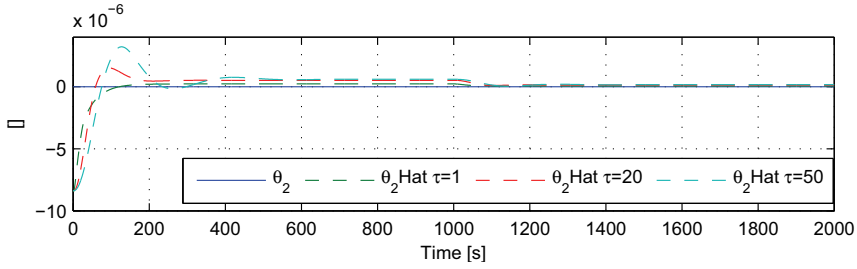

(d) θ_2 and $\hat{\theta}_2$

Figure 4.2: States and parameters for step test with passive identifier driven by filtered $\tilde{q}_{bit}$.

Chapter 5

Optimal filter estimator

Optimal filters have been applied to a wide rage of applications for many years, e.g. with the well known Kalman filter. The use of an optimal filter for estimation in this chapter is based on the work in [Basin et al., 2006, 2007] and applies to polynomial systems. As the derivation will show, these results are very similar to a Kalman filter. A comparison will therefore be made later in this chapter.

The system is written in a state space form and all the states are estimated. The filter is driven by noise, assumed to be white Gaussian. It is a goal for this chapter to derive theoretical results.

5.1 Simplified system

To make the calculations easier and to see the structure of the observer and compare it with other estimation techniques, a simplified version of the drilling system is applied.

The following assumptions are made

Assumption 7. *p_c is a given signal. $\rho_d = \rho_a$. The total friction factor, F, is the only unknown.*

These assumptions give the following simplified system from Equations (2.1), (2.2) and (2.6).

$$\frac{V_d}{\beta_d}\dot{p}_p = q_p - q_{bit} \tag{5.1}$$

$$M\dot{q}_{bit} = p_p - p_c - F|q_{bit}|q_{bit} \tag{5.2}$$

When using the system from Equations (5.1) and (5.2) the state vector is defined as

$$\mathbf{z} \triangleq \begin{bmatrix} p_p(t) \\ q_{bit}(t) \\ F \end{bmatrix} \tag{5.3}$$

where p_p is measured, while q_{bit} and F (the friction factor) are to be estimated. The dynamics are given by Equations (5.1) and (5.2) and with the assumption $q_{bit} > 0$ it can be written in state space form as

$$\dot{\mathbf{z}} = \begin{bmatrix} \frac{\beta_d}{V_d}(q_p(t) - z_2) \\ a_2(z_1 - p_c(t) - z_3 z_2^2) \\ 0 \end{bmatrix} + b_z(t)W_1(t) \tag{5.4}$$

$$= f_z(z,t) + b_z(t)W_1(t) \tag{5.5}$$

where $b_z(t) \in \mathbb{R}^{3\times 3}$ is a weight matrix for the process noise and $W_1(t) \in \mathbb{R}^3$ is a Wiener process. Other signals and parameters should be familiar from the last chapters, if not see Nomenclature in the beginning of the thesis. The measurement with noise is written as

$$\mathbf{y} = \begin{bmatrix} 1 & 0 & 0 \end{bmatrix} \mathbf{z} + B_z(t)W_2(t) \tag{5.6}$$

$$= C_z\mathbf{z} + B_z(t)W_2(t) \tag{5.7}$$

where $B_z(t) \in \mathbb{R}$ is a weight matrix for measurement noise and $W_2(t) \in \mathbb{R}$ is a Wiener process.

The estimator is optimal in the sense that it minimizes the Euclidian 2-norm

$$J = E[(\mathbf{z}(t) - \hat{\mathbf{z}}(t))^\top (\mathbf{z}(t) - \hat{\mathbf{z}}(t))], \tag{5.8}$$

at each time t. As suggested in [Stamnes, 2008], it can be desirable to scale the states in Equation (5.8). This is done by minimizing

$$J = E[(\mathbf{z}(t) - \hat{\mathbf{z}}(t))^\top K (\mathbf{z}(t) - \hat{\mathbf{z}}(t))], \tag{5.9}$$

where $K = H^{-\top}H^{-1}$ is a square, diagonal, positive definite matrix. The following change change of coordinates is used

$$\mathbf{z} = H\mathbf{x} \tag{5.10}$$

Equation (5.9) may then be written

$$J = E[(H\mathbf{x}(t) - H\hat{\mathbf{x}}(t))^\top H^{-\top}H^{-1}(H\mathbf{x}(t) - H\hat{\mathbf{x}}(t))] \tag{5.11}$$

$$= E[(\mathbf{x}(t) - \hat{\mathbf{x}}(t))^\top (\mathbf{x}(t) - \hat{\mathbf{x}}(t))] \tag{5.12}$$

The state space system from Equations (5.5) and (5.7) can now be written in x coordinates

$$\dot{\mathbf{x}} = H^{-1}f_z(H\mathbf{x},t) + H^{-1}b_z(t)W_1(t) \tag{5.13}$$

$$\triangleq f(\mathbf{x},t) + b(t)W_1(t) \tag{5.14}$$

$$y = C_z H\mathbf{x} + B(t)W_2(t) \tag{5.15}$$

$$\triangleq C\mathbf{x} + B(t)W_2(t) \tag{5.16}$$

where

$$\mathbf{f}(\mathbf{x},t) = \begin{bmatrix} \frac{\beta_d}{h_1 v_1}(q_p(t) - h_2 x_2) \\ \frac{1}{h_2} a_2 (h_1 x_1 - p_c(t) - h_2^2 h_3 x_2^2 x_3) \\ 0 \end{bmatrix} \tag{5.17}$$

and

$$C = \begin{bmatrix} h_1 & 0 & 0 \end{bmatrix} \tag{5.18}$$

5.1.1 Estimator

The estimation law is taken directly from [Basin et al., 2006] and is

$$\dot{\hat{\mathbf{x}}} = E(f(\mathbf{x},t)) + PC^\top (BB^\top)^{-1}(y - C\mathbf{x}) \tag{5.19}$$

$$\dot{P} = E([\mathbf{x}-\hat{\mathbf{x}}]f^\top(\mathbf{x},t)) + E(f(\mathbf{x},t)[\mathbf{x}-\hat{\mathbf{x}}]^\top) + bb^\top - PC^\top (BB^\top)^{-1} CP \tag{5.20}$$

Where $P(\mathbf{x},t) \triangleq E[(\mathbf{x}(t) - \hat{\mathbf{x}}(t))(\mathbf{x}(t) - \hat{\mathbf{x}}(t))^\top]$ is the covariance matrix. The three terms with $E(\cdot)$ will now be derived to write the estimation law in closed form. First the term in (5.19) is derived, then the terms in (5.20).

Term in $\dot{\hat{\mathbf{x}}}$ Starting with $E(f(\mathbf{x},t))$ (Note subscripts on f in the following) gives

$$E(f_1(\mathbf{x},t)) = \frac{\beta_d}{h_1 v_1}(q_p(t) - h_2 \hat{x}_2) \tag{5.21}$$

$$E(f_3(\mathbf{x},t)) = 0 \tag{5.22}$$

The 2nd element is a bit more complicated

$$E(f_2(\mathbf{x},t)) = \frac{a_2}{h_2} E(h_1 x_1 - p_c(t) - h_3 h_2^2 x_3 x_2^2) \tag{5.23}$$

$$= \frac{a_2}{h_2}(h_1 \hat{x}_1 - p_c(t) - h_3 h_2^2 E(x_3 x_2^2)) \tag{5.24}$$

The last term is derived in Appendix C (Equation (C.11)) and is

$$E(x_3 x_2^2) = 2\hat{x}_2 P_{32} + \hat{x}_3 P_{22} + \hat{x}_3 \hat{x}_2^2 \tag{5.25}$$

where P_{ij} is the ij^{th} element of P. Inserting (5.25) into (5.24) gives

$$E(f_2(\mathbf{x},t)) = \frac{a_2}{h_2}(h_1 \hat{x}_1 - p_c(t) - 2h_2 \hat{x}_2 P_{32} - h_2^2 h_3 (\hat{x}_3 P_{22} - \hat{x}_3 \hat{x}_2^2)) \tag{5.26}$$

Equations (5.21), (5.22) and (5.26) are collected and give

$$E(f(\mathbf{x},t)) = F(\hat{\mathbf{x}}, P, t) \tag{5.27}$$

with

$$F(\hat{\mathbf{x}}, P, t) = \begin{bmatrix} \frac{\beta_d}{h_1 v_1}(q_p(t) - h_2 \hat{x}_2) \\ \frac{h_1 a_2}{h_2}\hat{x}_1 - \frac{a_2}{h_2} p_c(t) - h_2 h_3 a_2 (2\hat{x}_2 P_{32} + \hat{x}_3 P_{22} + \hat{x}_2^2 \hat{x}_3) \\ 0 \end{bmatrix} \tag{5.28}$$

And at last the estimates for the states are

$$\dot{\hat{\mathbf{x}}} = F(\hat{\mathbf{x}}, P, t) + PC^\top (BB^\top)^{-1}(y - C\hat{\mathbf{x}}) \tag{5.29}$$

Terms in $\dot{P}$ Starting with $E([\mathbf{x}-\hat{\mathbf{x}}]f^\top(\mathbf{x},t))$ from Equation (5.20) and take one element at the time gives

$$E([\mathbf{x}-\hat{\mathbf{x}}]f_1(\mathbf{x},t)) = E\left([\mathbf{x}-\hat{\mathbf{x}}]\frac{\beta_d}{h_1 v_1}(q_p(t)-h_2x_2)\right) \tag{5.30}$$

$$= E\left([\mathbf{x}-\hat{\mathbf{x}}]\frac{\beta_d}{h_1 v_1}q_p(t)\right) - \frac{h_2\beta_d}{h_1 v_1}E([\mathbf{x}-\hat{\mathbf{x}}]x_2) \tag{5.31}$$

$$= 0 - \frac{h_2\beta_d}{h_1 v_1}E\left([\mathbf{x}-\hat{\mathbf{x}}](x_2-\hat{x}_2)+\hat{x}_2[\mathbf{x}-\hat{\mathbf{x}}]\right) \tag{5.32}$$

$$= -\frac{h_2\beta_d}{h_1 v_1}E\left([\mathbf{x}-\hat{\mathbf{x}}](x_2-\hat{x}_2)\right) \tag{5.33}$$

$$= -\frac{h_2\beta_d}{h_1 v_1}P_{*2} \tag{5.34}$$

where P_{*2} is the second column of P. The third element is simply

$$E([\mathbf{x}-\hat{\mathbf{x}}]f_3(\mathbf{x},t)) = 0 \tag{5.35}$$

The second element is nonlinear and requires some calculations

$$E([\mathbf{x}-\hat{\mathbf{x}}]f_2(\mathbf{x},t)) = \frac{a_2}{h_2}P_{*1} - h_2h_3a_2E([\mathbf{x}-\hat{\mathbf{x}}]x_3x_2^2) \tag{5.36}$$

A closer look at the last term in Equation (5.36) reveals

$$E([\mathbf{x}-\hat{\mathbf{x}}]x_3x_2^2) = E\left([\mathbf{x}-\hat{\mathbf{x}}]((x_3-\hat{x}_3)x_2^2+\hat{x}_3x_2^2)\right) \tag{5.37}$$

$$= E\left([\mathbf{x}-\hat{\mathbf{x}}](x_3-\hat{x}_3)x_2^2\right) + \hat{x}_3E([\mathbf{x}-\hat{\mathbf{x}}]x_2^2) \tag{5.38}$$

Equations (C.25) and (C.30) state that

$$E([\mathbf{x}-\hat{\mathbf{x}}](x_3-\hat{x}_3)x_2^2) = \hat{x}_2^2P_{*3} \tag{5.39}$$

and

$$E([\mathbf{x}-\hat{\mathbf{x}}]\hat{x}_3x_2^2) = 2\hat{x}_2\hat{x}_3P_{*2} \tag{5.40}$$

The nonlinear term in (5.36) is then given by (5.39) and (5.40) and is

$$E([\mathbf{x}-\hat{\mathbf{x}}]x_3x_2^2) = \hat{x}_2^2P_{*3} + 2\hat{x}_2\hat{x}_3P_{*2} \tag{5.41}$$

And at last, Equation (5.41) into (5.36) gives the expression

$$E([\mathbf{x}-\hat{\mathbf{x}}]f_2(\mathbf{x},t)) = h_2h_3a_2(P_{*1}-\hat{x}_2^2P_{*3}-2\hat{x}_2\hat{x}_3P_{*2}) \tag{5.42}$$

The terms in $\dot{P}$ can now be written (with the use of Equations (5.34), (5.42) and (5.35)) as

$$E([\mathbf{x}-\hat{\mathbf{x}}]f^\top(\mathbf{x},t)) = PG(\hat{\mathbf{x}},t) \tag{5.43}$$

with

$$G(\hat{\mathbf{x}},t) = \begin{bmatrix} 0 & h_2h_3a_2 & 0 \\ -\frac{\beta_d h_2}{v_1 h_1} & -2h_2h_3a_2\hat{x}_2\hat{x}_3 & 0 \\ 0 & -h_2h_3a_2\hat{x}_2^2 & 0 \end{bmatrix} \tag{5.44}$$

And the estimation laws are

$$\dot{\hat{\mathbf{x}}} = F(\hat{\mathbf{x}},t) + PC^\top(BB^\top)^{-1}(y - C\hat{\mathbf{x}}) \tag{5.45}$$

$$\dot{P} = PG(\hat{\mathbf{x}},t) + G^\top(\hat{\mathbf{x}},t)P + bb^\top - PC^\top(BB^\top)^{-1}CP \tag{5.46}$$

5.2 Comparison with Kalman-filter

Kalman filter [Kalman, 1960] is a well known and robust filter technique, which is applied in many industrial applications. The most common use is a discrete filter, but to compare with the Optimal Polynomial Filter the continuous Kalman filter [Kalman and Bucy, 1961] is used. Since the system is non-linear, the Extended Kalman-Bucy filter [Gelb, 1974] must be applied.

A general non-linear system, with linear measurements, can be written

$$\dot{\mathbf{x}} = f(\mathbf{x},t) + w(t) \tag{5.47}$$

$$y = C\mathbf{x} + v(t) \tag{5.48}$$

where $w(t)$ and $v(t)$ are independent white noise functions.

The Kalman filter for the system in Equations (5.47) and (5.48) is [Gelb, 1974]

$$\dot{\hat{\mathbf{x}}} = f_k(\hat{\mathbf{x}},t) + K(y - C\hat{\mathbf{x}}) \tag{5.49}$$

where $f_k(\hat{\mathbf{x}},t) = f_k(\mathbf{x},t)|_{\mathbf{x}(t)=\hat{\mathbf{x}}(t)}$, $K = PC^\top R^{-1}$ is the Kalman gain, $R = E[vv^\top]$ and C is the measurement matrix.

The derivate of the covariance matrix is

$$\dot{P} = F_kP + PF_k^\top - PC^\top R^{-1}CP \tag{5.50}$$

Since the system is non-linear, F_k is given as the Jacobi determinant of Equation (5.17)

$$F_k = \left.\frac{\partial f_k}{\partial \mathbf{x}}\right|_{\mathbf{x}(t)=\hat{\mathbf{x}}(t)} \tag{5.51}$$

For the simplified drilling system $f(\hat{\mathbf{x}},t)$ is found from Equation (5.17) as

$$f_k(\hat{\mathbf{x}},t) = \begin{bmatrix} \frac{\beta_d}{v_1}(q_p(t) - \hat{x}_2) \\ a_2(\hat{x}_1 - p_c(t) - \hat{x}_2^2\hat{x}_3) \\ 0 \end{bmatrix} \tag{5.52}$$

and F_k is

$$F_k(\hat{\mathbf{x}},t) = \begin{bmatrix} 0 & -\frac{\beta_d}{v_1} & 0 \\ a_2 & -2a_2\hat{x}_2\hat{x}_3 & -a_2\hat{x}_2^2 \\ 0 & 0 & 0 \end{bmatrix} \tag{5.53}$$

Table 5.1: Summary of parameters used for Optimal Polynomial and Kalman filter.

Parameter	Value
H	diag(2, 0.1, 1)
B	1
b	H/diag(1 0.001 500)
R	1
Γ	diag(2000, 10^{-9})
$\hat{x}(0)$	$[0.5p_p(0) \quad 0.5q_{bit}(0) \quad F_d + 2F_a]$
$P(0)$	diag(10^{-3},10^{-3},10^{-3})

5.2.1 Comparison

To see the differences between the Optimal Polynomial Filter and the Kalman filter a comparison of the functions will be done, before simulations are presented. The results gave very similar results. It is argued in e.g. [Basin and Skliar, 2005] that the Optimal filter should perform better than the conventional Kalman filter, but for the system considered here, the differences are insignificant.

Differences in $\dot{\hat{\mathbf{x}}}$ Assume $h_i = 1$ in the following. It can then be seen from Equations (5.28) and (5.52) that

$$\dot{\hat{\mathbf{x}}}_{Kalman} - \dot{\hat{\mathbf{x}}}_{Poly} \tag{5.54}$$

$$= f_k(\hat{\mathbf{x}}, t) - F_K(\hat{\mathbf{x}}, t) \tag{5.55}$$

$$= \begin{bmatrix} 0 \\ 2\hat{x}_2 P_{32} + \hat{x}_3 P_{22} \\ 0 \end{bmatrix} \tag{5.56}$$

The only difference is that the polynomial filter has two terms from the covariance matrix. It is difficult to say something if this is an advantage or not for the estimation of $x_2 = q_{bit}$, but from simulations it does not seem to give any difference.

Differences in $\dot{P}$ The time derivative for the to estimators are given in equations (5.46) and (5.50). Taking a closer look at $F_k(\hat{\mathbf{x}}, t)$ in the Kalman filter and $G(\hat{\mathbf{x}}, t)$ in the polynomial filter (Equations (5.53) and (5.44)) reveals that $G^\top(\hat{\mathbf{x}}, t) = F_k(\hat{\mathbf{x}}, t)$. Inserting $G^\top(\hat{\mathbf{x}}) = F_k(\hat{\mathbf{x}}, t)$ into (5.50), together with $R = BB^\top$ shows that the two expressions are equal.

5.2.1.1 Simulation results

The same step-test as described for the Stamnes observer in Section 3.4 was also done for the Optimal Polynomial Filter and the Kalman filter. The design

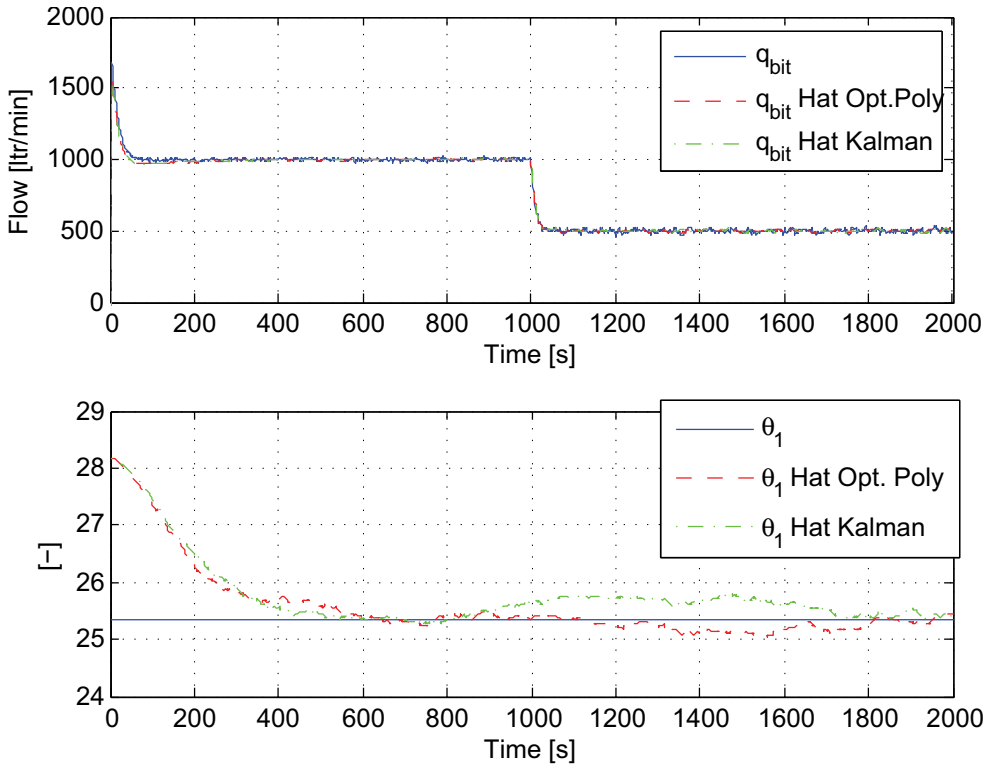

Figure 5.1: Step test for Optimal Polynomial Filter and Kalman filter.

parameters are summarized in Table 5.1. Since these observers are driven by noise, normal distributed noise was added to the measurements. The results are shown in Figure 5.1[1] and show that the polynomial filter and the Kalman filter are equally good. Remember this simulation is done with the simplified system, so it is difficult to compare with the other observers, but the results are promising.

In [Rognmo, 2008] an evaluation of Kalman filter for estimation of bottom hole pressure was done. The report concluded with promising results, but the Kalman filter has problems with observability when estimating the parameters. This should also be expected for the Optimal Polynomial Filter when applied to the total drilling system.

5.3 Proof of convergence.

It is desirable to prove convergence of the Optimal Polynomial Filter, but [Reif et al., 2000] points out that the stability and convergence properties of the continuous extended Kalman filter are hard to analyze. From Section 5.2

[1] In the last row F is divided by M to get θ_1 as for the other observers.

it is concluded that the optimal filter is very similar to the Kalman filter, so a proof may be difficult also for the polynomial filter.

However, a proof based on Lyapunov analysis is tried in the following with the following Lyapunov candidate

$$V = \tilde{\mathbf{x}}^\top P^{-1}\tilde{\mathbf{x}} \geq 0 \tag{5.57}$$

Remember that P is the covariance matrix and is positive semi-definite.

$$\dot{V} = \dot{\tilde{\mathbf{x}}}^\top P^{-1}\tilde{\mathbf{x}} + \tilde{\mathbf{x}}^\top \dot{P}^{-1}\tilde{\mathbf{x}} + \tilde{\mathbf{x}}^\top P^{-1}\dot{\tilde{\mathbf{x}}} \tag{5.58}$$

$$= 2\tilde{\mathbf{x}}^\top P^{-1}\dot{\tilde{\mathbf{x}}} - \tilde{\mathbf{x}}^\top P^{-1}\dot{P}P^{-1}\tilde{\mathbf{x}} \tag{5.59}$$

As a typical Lyapunov approach, the error dynamics should be something including $\dot{\tilde{\mathbf{x}}} = -\tilde{\mathbf{x}}$. To achieve this for our problem, Equations (5.14) and (5.29) are written with a linear and a non-linear part

$$\dot{\mathbf{x}} = F^*(\mathbf{x}, t)\mathbf{x} + f^*(\mathbf{x}, t) \tag{5.60}$$

and

$$\dot{\hat{\mathbf{x}}} = F^*(\hat{\mathbf{x}}, t)\hat{\mathbf{x}} + f^*(\hat{\mathbf{x}}, P, t) \tag{5.61}$$

The error dynamics are then

$$\dot{\tilde{\mathbf{x}}} = \dot{\mathbf{x}} - \dot{\hat{\mathbf{x}}} \tag{5.62}$$

$$= F^*(\mathbf{x}, t)\mathbf{x} + f^*(t) - F^*(\hat{\mathbf{x}}, t)\hat{\mathbf{x}} - f^*(\hat{\mathbf{x}}, t) - PC^\top(BB^\top)^{-1}C\tilde{\mathbf{x}} \tag{5.63}$$

$$= F^*(\hat{\mathbf{x}}, t)(\mathbf{x} - \hat{\mathbf{x}}) + (F^*(\mathbf{x}, t) - F^*(\hat{\mathbf{x}}, t))\mathbf{x} + f^*(t) - f^*(\hat{\mathbf{x}}, t) - PC^\top(BB^\top)^{-1}C\tilde{\mathbf{x}} \tag{5.64}$$

$$= \hat{F}^*\tilde{\mathbf{x}} - PC^\top(BB^\top)^{-1}C\tilde{\mathbf{x}} + \tilde{F}^*\mathbf{x} + \tilde{f}^* \tag{5.65}$$

where $\hat{F}^* \triangleq F^*(\hat{\mathbf{x}}, t)$, $\tilde{F}^* \triangleq (F^*(\mathbf{x}, t) - F^*(\hat{\mathbf{x}}, t))$ and $\tilde{f}^* \triangleq (f^*(t) - f^*(\hat{\mathbf{x}}, P, t))$.

Inserting Equations (5.46) and (5.65) into Equation (5.59) gives

$$\dot{V} = 2\tilde{\mathbf{x}}^\top P^{-1}(\hat{F}^*\tilde{\mathbf{x}} - PC^\top(BB^\top)^{-1}C\tilde{\mathbf{x}} + \tilde{F}^*\mathbf{x} + \tilde{f}^*) - \tilde{\mathbf{x}}^\top P^{-1}(PG(\hat{\mathbf{x}}, t) + G^\top(\hat{\mathbf{x}}, t)P - PC^\top(BB^\top)^{-1}CP)P^{-1}\tilde{\mathbf{x}} \tag{5.66}$$

$$= \tilde{\mathbf{x}}^\top P^{-1}(2\hat{F}^* - 2PC^\top(BB^\top)^{-1}C + PC^\top(BB^\top)^{-1}C)\tilde{\mathbf{x}} + 2\tilde{\mathbf{x}}^\top P^{-1}(\tilde{F}^*\mathbf{x} + \tilde{f}^*) - \tilde{\mathbf{x}}^\top(\hat{G}P^{-1} + P^{-1}\hat{G}^\top)\tilde{\mathbf{x}} \tag{5.67}$$

$$= \tilde{\mathbf{x}}^\top(2P^{-1}\hat{G}^\top - \hat{G}P^{-1} - P^{-1}\hat{G}^\top)\tilde{\mathbf{x}} - \tilde{\mathbf{x}}^\top C^\top(BB^\top)^{-1}C\tilde{\mathbf{x}} + 2\tilde{\mathbf{x}}^\top P^{-1}(\tilde{F}^*\mathbf{x} + \tilde{f}^*) \tag{5.68}$$

$$= 2\tilde{\mathbf{x}}^\top(P^{-1}\hat{G}^\top)\tilde{\mathbf{x}} - \underbrace{\tilde{\mathbf{x}}^\top(P^{-1}\hat{G})\tilde{\mathbf{x}}}_{=\tilde{\mathbf{x}}^\top(\hat{G}^\top P^{-1}\tilde{\mathbf{x}}} - \tilde{\mathbf{x}}^\top(P^{-1}\hat{G}^\top)\tilde{\mathbf{x}} - \tilde{\mathbf{x}}^\top(C^\top(BB^\top)^{-1}C)\tilde{\mathbf{x}} + 2\tilde{\mathbf{x}}^\top P^{-1}(\tilde{F}^*\mathbf{x} + \tilde{f}^*) \tag{5.69}$$

$$= -\tilde{\mathbf{x}}^\top C^\top(BB^\top)^{-1}C\tilde{\mathbf{x}} + 2\tilde{\mathbf{x}}^\top P^{-1}(\tilde{F}^*\mathbf{x} + \tilde{f}^*) \tag{5.70}$$

The first term is a good term, but the last therm is difficult to say anything about. A try was made to insert $\tilde{F}^*$ and $\tilde{f}^*$ to see if it could be written as something like $-\bar{F}\tilde{\mathbf{x}}$, but it did not lead to a this desired result.

The derivation is left at this stage and serves as stepping stones for further research.

Chapter 6

The Grip observer

A new observer is derived for a general system by H. Grip in [Grip et al., 2009], where an example of application to bottom hole pressure estimation is also shown. [Kaasa, 2009] gives some more introductions to applications of the estimator. These ideas are further investigated in this chapter. The observer is presented, before convergence is proved. Simulations are performed to compare with the other observers.

The Grip-observer design is a two stage procedure. First update laws for the parameters $\boldsymbol{\theta}$ are designed with the full perturbation, ψ, assumed to be known. This update law is exponentially stable. As stage two, an estimate of ψ is used to implement the law for $\hat{\boldsymbol{\theta}}$.

6.1 Observer

The design model from Chapter 2 is

$$\dot{p}_p = a_1(q_p - q_{bit} - \dot{V}_d) \tag{6.1}$$

$$\frac{V_a}{\beta_a}\dot{p}_c = q_{bit} + q_{back} + q_{res} - q_{choke} - \dot{V}_a \tag{6.2}$$

$$\dot{q}_{bit} = a_2(p_p - p_c) - a_2(F_d + F_a)|q_{bit}|q_{bit} + a_2(\rho_d - \rho_a)gv_3 \tag{6.3}$$

The design procedure is first to rewrite Equation (6.3) as

$$\dot{q}_{bit} = f_0(t) + \psi \tag{6.4}$$

where $f_0(t) = a_2(p_p - p_c)$ is the known signals and $\psi = \boldsymbol{\phi}^\top \boldsymbol{\theta}$ is the terms including unknown constants. The constants and the signals are defined as

$$\boldsymbol{\theta} \triangleq \begin{bmatrix} a_2(F_d + F_a) \\ a_2(\rho_d - \rho_a)g \end{bmatrix} \tag{6.5}$$

$$\boldsymbol{\phi} \triangleq \begin{bmatrix} -|q_{bit}|q_{bit} \\ v_3 \end{bmatrix} \tag{6.6}$$

Remember that F_a and ρ_a are the unknown parameters.

As proposed in [Grip et al., 2009] ψ is first assumed to be known. The following estimator for $\boldsymbol{\theta}$ is then used

$$\dot{\hat{\boldsymbol{\theta}}} = \boldsymbol{\Gamma}\boldsymbol{\phi}(t, q_{bit})(\psi - \boldsymbol{\phi}^\top \hat{\boldsymbol{\theta}}) \tag{6.7}$$

where $\boldsymbol{\Gamma} > 0$ is an adaptation gain. This adaptation law is exponentially stable.

Since ψ is unknown, an estimator for it is needed. This is proposed as

$$\hat{\psi} = \gamma_0(q_{bit} - \hat{q}_{bit}) + \boldsymbol{\phi}^\top \hat{\boldsymbol{\theta}} \tag{6.8}$$

where $\gamma_0 > 0$ is the adaptation gain. The error expression for ψ is

$$\tilde{\psi} = -\gamma_0 \tilde{q}_{bit} + \boldsymbol{\phi}^\top \tilde{\boldsymbol{\theta}} \tag{6.9}$$

The observer for q_{bit} is taken as

$$\dot{\hat{q}}_{bit} = f_0(t) + \hat{\psi} + \gamma_0^{-1} \boldsymbol{\phi}^\top \dot{\hat{\boldsymbol{\theta}}} \tag{6.10}$$

Inserting the expression for $\hat{\psi}$ into Equations (6.7) and (6.10) give the Grip-observer

$$\dot{\hat{\boldsymbol{\theta}}} = \boldsymbol{\Gamma}\boldsymbol{\phi}(t, q_{bit})(\hat{\psi} - \boldsymbol{\phi}^\top \hat{\boldsymbol{\theta}}) \tag{6.11}$$

$$\dot{\hat{q}}_{bit} = a_2(p_p - p_c) + \gamma_0(q_{bit} - \hat{q}_{bit}) + \boldsymbol{\phi}^\top \hat{\boldsymbol{\theta}} + \gamma_o^{-1} \boldsymbol{\phi}^\top \dot{\hat{\boldsymbol{\theta}}} \tag{6.12}$$

6.2 Proof of convergence

In this section a Lyapunov proof for convergence is derived. First the error dynamics are stated, before the proof is derived in the next sub section.

6.2.1 Error dynamics

To find the error dynamics are quite straight forward for both $\boldsymbol{\theta}$ and ψ. First for $\boldsymbol{\theta}$ the dynamics are

$$\dot{\tilde{\boldsymbol{\theta}}} \triangleq \dot{\boldsymbol{\theta}} - \dot{\hat{\boldsymbol{\theta}}} \tag{6.13}$$

Remembering $\dot{\boldsymbol{\theta}} = 0$, inserting Equation (6.11) and replacing $\hat{\psi} = \psi - \tilde{\psi}$ gives

$$\dot{\tilde{\boldsymbol{\theta}}} = -\boldsymbol{\Gamma}\boldsymbol{\phi}\boldsymbol{\phi}^\top \tilde{\boldsymbol{\theta}} - \boldsymbol{\Gamma}\boldsymbol{\phi}\tilde{\psi} \tag{6.14}$$

Also the error dynamics for ψ is straight forward

$$\dot{\tilde{\psi}} \triangleq \dot{\psi} - \dot{\hat{\psi}} \tag{6.15}$$

where $\dot{\psi} = \dot{\boldsymbol{\phi}}^\top \boldsymbol{\theta}$ and $\dot{\hat{\psi}}$ is found by taking the time derivate of Equation (6.8), and then insert Equation (6.4)

$$\dot{\tilde{\psi}} = \gamma_0(f_0 + \psi) - \gamma_0(f_0 + \hat{\psi} + \gamma_o^{-1}\boldsymbol{\phi}^\top\dot{\hat{\boldsymbol{\theta}}}) + \dot{\boldsymbol{\phi}}^\top\hat{\boldsymbol{\theta}} + \boldsymbol{\phi}^\top\dot{\hat{\boldsymbol{\theta}}} \tag{6.16}$$

$$= \gamma_0(\psi - \hat{\psi}) + \dot{\boldsymbol{\phi}}\hat{\boldsymbol{\theta}} \tag{6.17}$$

The error dynamics for $\tilde{\psi}$ are then

$$\dot{\tilde{\psi}} = \dot{\psi} - \dot{\hat{\psi}} \tag{6.18}$$

$$= -\gamma_0\tilde{\psi} + \dot{\boldsymbol{\phi}}^\top\tilde{\boldsymbol{\theta}} \tag{6.19}$$

6.2.2 Proof

To prove the convergence of the complete system from Section 2.4 we follow [Grip et al., 2009] and divide the proof into to stages. First convergence with $\tilde{\psi} = 0$ will be derived, before the full estimator is taken into consideration.

6.2.2.1 ψ known

With ψ known, the following Lyapunov candidate is used

$$V_1 = \frac{1}{2}\tilde{\boldsymbol{\theta}}^\top(\boldsymbol{\Gamma}^{-1} - \mu\int_t^\infty e^{t-\tau}S(\tau, x(\tau))d\tau)\tilde{\boldsymbol{\theta}} \tag{6.20}$$

where $\mu > 0$ is a constant yet to be specified. Define

$$S(t, x(t)) \triangleq \boldsymbol{\phi}(\tau, x(\tau))^\top\boldsymbol{\phi}(\tau, x(\tau)) \tag{6.21}$$

and assume

$$\int_t^{t+T} S(\tau, x(\tau))d\tau \geq \epsilon\mathbf{I} \tag{6.22}$$

where $T > 0$ and $\epsilon > 0$.

To confirm that $\dot{V}_1$ is positive-definite it can be seen that
$\frac{1}{2}(\lambda_{min}(\boldsymbol{\Gamma}^{-1} - \mu\lambda_S)||\tilde{\boldsymbol{\theta}}||^2 \leq V_1 \leq \frac{1}{2}\lambda_{max}(\boldsymbol{\Gamma}^{-1})||\tilde{\boldsymbol{\theta}}||^2$,
where $\lambda_S = \sup\lambda_{max}(S(t, x(t)))$.

The time derivative of V_1 is

$$\dot{V}_1 = \tilde{\boldsymbol{\theta}}^\top(\boldsymbol{\Gamma}^{-1} - \mu\int_t^\infty e^{t-\tau}S(\tau, x(\tau))d\tau)\dot{\tilde{\boldsymbol{\theta}}}$$
$$+ \frac{1}{2}\tilde{\boldsymbol{\theta}}^\top(-\mu\frac{d}{dt}\int_t^\infty e^{t-\tau}S(\tau, x(\tau))d\tau))\tilde{\boldsymbol{\theta}} \tag{6.23}$$

The error dynamics are inserted from Equation (6.14) and the *Leibniz integral-rule* has been applied.

$$\begin{aligned}
\dot{V}_1 &= -\tilde{\boldsymbol{\theta}}^\top(\boldsymbol{\Gamma}^{-1} - \mu\int_t^\infty e^{t-\tau}S(\tau,x(\tau))d\tau\boldsymbol{\Gamma}\overbrace{\boldsymbol{\phi}\boldsymbol{\phi}^\top}^{S})\tilde{\boldsymbol{\theta}} \\
&\quad - \frac{1}{2}\tilde{\boldsymbol{\theta}}^\top\mu(\int_t^\infty e^{t-\tau}S(\tau,x(\tau))d\tau - S(t,x(t)))\tilde{\boldsymbol{\theta}} \qquad (6.24)\\
&= -\tilde{\boldsymbol{\theta}}^\top S(t,x(t))\tilde{\boldsymbol{\theta}} + \frac{1}{2}\tilde{\boldsymbol{\theta}}^\top\mu S(t,x(t))\tilde{\boldsymbol{\theta}} \\
&\quad + \tilde{\boldsymbol{\theta}}^\top\mu\int_t^\infty e^{t-\tau}S(\tau,x(\tau))d\tau\boldsymbol{\Gamma}S(t,x(t))\tilde{\boldsymbol{\theta}} \\
&\quad - \frac{1}{2}\tilde{\boldsymbol{\theta}}^\top\mu\int_t^\infty e^{t-\tau}S(\tau,x(\tau))d\tau\tilde{\boldsymbol{\theta}} \qquad (6.25)\\
&= -(1-\frac{1}{2}\mu)\tilde{\boldsymbol{\theta}}^\top S(t,x(t))\tilde{\boldsymbol{\theta}} \\
&\quad + \tilde{\boldsymbol{\theta}}^\top\mu\int_t^\infty e^{t-\tau}S(\tau,x(\tau))d\tau(\boldsymbol{\Gamma}S(t,x(t)) - \frac{1}{2})\tilde{\boldsymbol{\theta}} \qquad (6.26)
\end{aligned}$$

Since

$$\begin{aligned}
\int_t^\infty e^{t-\tau}S(\tau,x(\tau))d\tau &\geq \int_t^T e^{t-\tau}S(\tau,x(\tau))d\tau \\
&\geq e^{-T}\int_t^T S(\tau,x(\tau))d\tau \geq e^{-T}\epsilon \qquad (6.27)
\end{aligned}$$

the derivative becomes

$$\begin{aligned}
\dot{V}_1 &\leq -(1-\frac{1}{2}\mu)\tilde{\boldsymbol{\theta}}^\top S(t,x(t))\tilde{\boldsymbol{\theta}} - \frac{1}{2}\mu\tilde{\boldsymbol{\theta}}^\top e^{-T}\epsilon\tilde{\boldsymbol{\theta}} \\
&\quad + \tilde{\boldsymbol{\theta}}^\top\mu\int_t^\infty e^{t-\tau}S(\tau,x(\tau))d\tau\boldsymbol{\Gamma}S(t,x(t))\tilde{\boldsymbol{\theta}} \qquad (6.28)
\end{aligned}$$

Assume $||S(t,x(t))|| \leq M_S$ and $||\boldsymbol{\Gamma}|| < \gamma$, then

$$\begin{aligned}
\dot{V}_1 &\leq -(1-\frac{1}{2}\mu)\tilde{\boldsymbol{\theta}}^\top S(t,x(t))\tilde{\boldsymbol{\theta}} - \frac{1}{2}\mu\tilde{\boldsymbol{\theta}}^\top e^{-T}\epsilon\tilde{\boldsymbol{\theta}} \\
&\quad + \tilde{\boldsymbol{\theta}}^\top\mu\int_t^\infty e^{t-\tau}M_S d\tau\boldsymbol{\Gamma}S(t,x(t))\tilde{\boldsymbol{\theta}} \qquad (6.29)\\
&= -(1-\frac{1}{2}\mu)\tilde{\boldsymbol{\theta}}^\top S(t,x(t))\tilde{\boldsymbol{\theta}} - \frac{1}{2}\mu\tilde{\boldsymbol{\theta}}^\top e^{-T}\epsilon\tilde{\boldsymbol{\theta}} + \tilde{\boldsymbol{\theta}}^\top\mu M_S\boldsymbol{\Gamma}S(t,x(t))\tilde{\boldsymbol{\theta}} \qquad (6.30)\\
&= -(1-\frac{1}{2}\mu - \mu M_S\gamma)\tilde{\boldsymbol{\theta}}^\top S(t,x(t))\tilde{\boldsymbol{\theta}} - \frac{1}{2}\mu\tilde{\boldsymbol{\theta}}^\top e^{-T}\epsilon\tilde{\boldsymbol{\theta}} \qquad (6.31)
\end{aligned}$$

which requires

$$\mu < \frac{2}{1+2M_S\gamma} \qquad (6.32)$$

to guarantee $\dot{V}_1 \leq 0$.

The conclusion is then that $\tilde{\boldsymbol{\theta}} \to 0$ as $t \to \infty$ if ψ is known.

6.2.2.2 ψ unknown

To complete the derivation, the assumption of $\tilde{\psi} = 0$ is removed and the following Lyapunov candidate is used

$$V = V_1 + \frac{1}{2}\tilde{\psi}^2 \tag{6.33}$$

Taking the time derivative and inserting the error dynamics from (6.14) and (6.19) give

$$\dot{V} = \dot{V}_1 - \tilde{\boldsymbol{\theta}}\boldsymbol{\phi}\tilde{\psi} + \tilde{\boldsymbol{\theta}}^\top \mu \int_t^\infty e^{t-\tau} S(\tau, x(\tau)) d\tau \boldsymbol{\Gamma}\boldsymbol{\phi}\tilde{\psi} - \gamma_0\tilde{\psi}\tilde{\psi} + \tilde{\psi}\dot{\boldsymbol{\phi}}^\top\tilde{\boldsymbol{\theta}} \tag{6.34}$$

Using the same derivation as for $\dot{V}_1$ Equation (6.34) can be written

$$\dot{V} \leq \dot{V}_1 - \tilde{\boldsymbol{\theta}}^\top(1 - \mu M_S\gamma)\boldsymbol{\phi}\tilde{\psi} - \gamma_0\tilde{\psi}\tilde{\psi} + \tilde{\boldsymbol{\theta}}^\top\dot{\boldsymbol{\phi}}\tilde{\psi} \tag{6.35}$$

Define $\gamma_2 \triangleq 1 - \mu M_S\gamma > 0$ (This is fulfilled with Equation (6.32)) and remembering that γ and M_S are bounds on $||\boldsymbol{\Gamma}||$ and $||S(t, x(t))||$ gives

$$\begin{aligned}
\dot{V} &\leq -(1 - \frac{1}{2}\mu - \mu M_S\gamma)\tilde{\boldsymbol{\theta}}^\top S(t, x(t))\tilde{\boldsymbol{\theta}} - \frac{1}{2}\mu e^{-T}\epsilon\tilde{\boldsymbol{\theta}}^\top\tilde{\boldsymbol{\theta}} \\
&\quad - \gamma_0\tilde{\psi}\tilde{\psi} - \gamma_2\tilde{\boldsymbol{\theta}}^\top\boldsymbol{\phi}\tilde{\psi} + \tilde{\boldsymbol{\theta}}^\top\dot{\boldsymbol{\phi}}^\top\tilde{\psi} && (6.36) \\
&= -(1 - \frac{1}{2}\mu - \mu M_S\gamma)\tilde{\boldsymbol{\theta}}^\top S(t, x(t))\tilde{\boldsymbol{\theta}} - \frac{1}{2}\mu e^{-T}\epsilon\tilde{\boldsymbol{\theta}}^\top\tilde{\boldsymbol{\theta}} \\
&\quad - \tilde{\boldsymbol{\theta}}^\top(\gamma_2\boldsymbol{\phi} - \dot{\boldsymbol{\phi}}^\top)\tilde{\psi} - \gamma_0\tilde{\psi}\tilde{\psi} && (6.37) \\
&= -(1 - \frac{1}{2}\mu - \mu M_S\gamma)\tilde{\boldsymbol{\theta}}^\top S(t, x(t))\tilde{\boldsymbol{\theta}} - \zeta^\top Q\zeta && (6.38)
\end{aligned}$$

with $\zeta \triangleq [\tilde{\boldsymbol{\theta}}, \quad \tilde{\psi}]^\top$ and

$$Q = \begin{bmatrix} \frac{1}{2}\mu e^{-T}\epsilon & \gamma_2\boldsymbol{\phi} \\ -\dot{\boldsymbol{\phi}}^\top & \gamma_0 \end{bmatrix} \tag{6.39}$$

To check for positive-definiteness of Q, note that the first-order leading principal minor is $\frac{1}{2}\mu e^{-T}\epsilon > 0$. The second-order leading principal minor is $\frac{1}{2}\mu e^{-T}\epsilon\gamma_0 + \gamma_2\boldsymbol{\phi}\dot{\boldsymbol{\phi}}^\top$, which is positive if

$$\gamma_0 > \frac{2B_3(1 - \mu M_S\gamma)}{\mu e^{-T}\epsilon} \tag{6.40}$$

where $|\boldsymbol{\phi}\dot{\boldsymbol{\phi}}| < B_3$ for some $B_3 > 0$. This requirement does not conflict (6.32) as long as $\gamma_0 > \frac{B_3}{e^{-T}\epsilon}$.

The conclusion is then that $\tilde{\boldsymbol{\theta}}$, $\tilde{\psi} \to 0$ as $t \to \infty$. From Equation (6.9) it can be seen that also $\tilde{q}_{bit} \to 0$ when $\tilde{\psi} \to 0$ and $\tilde{\boldsymbol{\theta}} \to 0$.

Table 6.1: Summary of the Grip observer

Observer	$\dot{\hat{q}}_{bit} = a_2(p_p(t) - p_c(t)) + \gamma_0(q_{bit} - \hat{q}_{bit}) + \boldsymbol{\phi}^\top \hat{\boldsymbol{\theta}} + \gamma_o^{-1} \boldsymbol{\phi}^\top \dot{\hat{\boldsymbol{\theta}}}$ $\hat{p}_{bit} = p_c + M_a(a_2(p_p - p_c) - \hat{\theta}_1 \lvert\hat{q}_{bit}\rvert \hat{q}_{bit} + \hat{\theta}_2 v_3$ $+(M\hat{\theta}_1 - F_d)\lvert\hat{q}_{bit}\rvert\hat{q}_{bit} + (\rho_d g - M\hat{\theta}_2)v_3$
Adaptation	$\dot{\hat{\boldsymbol{\theta}}} = \boldsymbol{\Gamma}\boldsymbol{\phi}(t, q_{bit})(\hat{\psi} - \boldsymbol{\phi}^\top \hat{\boldsymbol{\theta}})$ $\hat{\psi} = \gamma_0(q_{bit} - \hat{q}_{bit}) + \boldsymbol{\phi}^\top \hat{\boldsymbol{\theta}}$
Properties	$\lim_{t\to\infty} \tilde{\theta} = 0$ $\lim_{t\to\infty} \tilde{\psi} = 0$ $\lim_{t\to\infty} \tilde{q}_{bit} = 0$ $\lim_{t\to\infty} \tilde{p}_{bit} = 0$

6.3 Summary of the Grip observer

The Grip observer is summarized in Table 6.1, where the observer, adaptation law and the main properties are repeated.

6.4 Simulation result

The step-test for the Grip observer is shown in Figure 6.1. The simulation does not seem to agree with the theoretical results of convergence for $\hat{\boldsymbol{\theta}}$. There may be two reasons for this. One is that more excitation is needed; the other is that it takes much longer time before the error is zero. Note however that $\hat{\theta}_2$ is very, very close to the correct value. This was not the case with the Stamnes observer. It is not possible that just one of $\hat{\theta}_1$ and $\hat{\theta}_2$ converges, so the estimate is not exactly correct. This is the same result as for for the passive identifier with and without the low pass filter.

It should also be noted that the estimate of p_{bit} in Figure 6.1(b) is much slower than for the Stamnes observer, even though exactly the same initial conditions were used. The estimation of q_{bit} on the other hand is fast and correct.

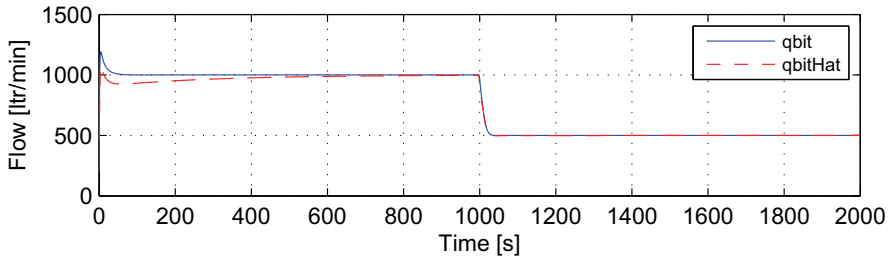

(a) q_{bit} and $\hat{q}_{bit}$.

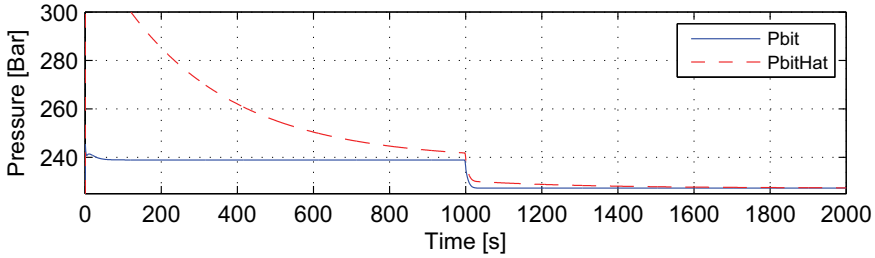

(b) p_{bit} and $\hat{p}_{bit}$.

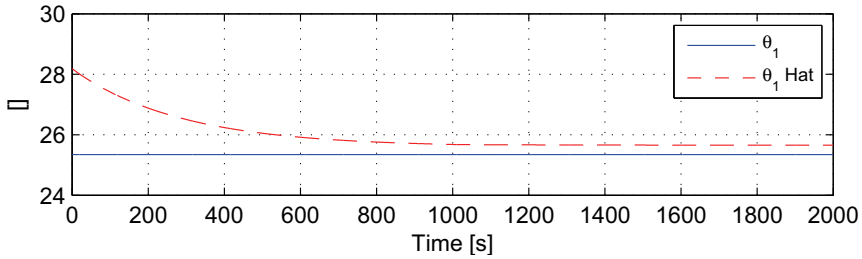

(c) θ_1 and $\hat{\theta}_1$

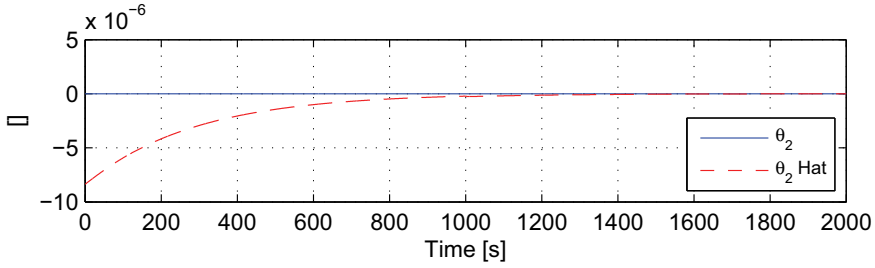

(d) θ_2 and $\hat{\theta}_2$

Figure 6.1: States and parameters for step test with Grip observer.

Chapter 7

Case simulations

This chapter presents simulations of a pipe connection case done for the observers from Chapters 3-6. The friction parameter F_a and the density ρ_a are assumed unknown.

Pipe connection is a realistic drilling procedure where new pipes are added to the drill string. Each drill pipe is about 27 m, and with a drilling speed of 15 m per hour a pipe connection must be done about every second hour. When a pipe connection is done, the main mud pump is ramped down and stopped to reduce the pressure in the drill string. The pump pressure should be equal to 1 bar and to simulate this, the pump rate is set negative for some time. (This is known as a bleed off).

The back pressure pump is increased from 200 liter/min to 400 liter/min when the main mud pump is below to 400 ltr/min. The mud pump and back pressure pump are showed in Figure B.3. A simple PI-controller was used to keep constant choke pressure.

As pointed out in [Stamnes, 2007] a pipe connection may lead to large modeling errors due to zero flow from the mud pump. A pragmatic approach to modifications is given in the reference, but the original observer is used in this chapter. The modified observer will be tested in Chapter 11 when the pipe connection case is revisited.

The simulations show that that there are just minor differences between the observers. All simulations show converges of the bit flow and bottom hole estimations, but all observers have problems with zero flow (as expected). None of the observers managed to estimate the parameters correctly.

For all simulations the plant parameters are given in Table 7.1. See the Nomenclature in the beginning of the thesis for parameter descriptions.

Table 7.1: Summary of plant parameters used in simulations.

Parameter	Value	Parameter	Value
V_a	96.1327 [m^3]	F_a	$0.02080 \cdot 10^6$ [-]
V_d	28.2743 [m^3]	ρ_d	1250 [kg/m^3]
β_d	1400 [bar]	ρ_a	1250 [kg/m^3]
β_d	1400 [bar]	p_0	1 [bar]
M_a	1600.9 [kg/m^4]	g	9.81 [m/s^2]
M_d	5729.6 [kg/m^4]	K_c	0.0046 [-]
F_d	$0.16500 \cdot 10^6$ [-]		

7.1 The Stamnes observer

Table 7.2 lists the design parameters used for the Stamnes observer and Figures 7.1 and 7.2 show how the Stamnes observer handles the pipe connection. The changes in the choke opening can be seen in Figure 7.1(a). The choke is closed when the pump rate is reduced to maintain the reference choke pressure. Also note that the back pressure pump is running when the mud pump is below 400 ltr/min.

Table 7.2: Design parameters used in pipe connection for Stamnes observer.

Parameter	Value
Γ	$\text{diag}([5 \cdot 10^4, 5 \cdot 10^{-9}]$
l_1	10^{-7}
K_p	1
K_i	1
$\hat{q}_{bit}(0)$	700 [ltr/min]
$\hat{\theta}_1(0)$	28.1836 [-]
$\hat{\theta}_2(0)$	$-8.3640 \cdot 10^{-6}$ [-]

The bottom hole pressure estimate can be seen in Figure 7.1(b). The estimate is good except the period where $q_{bit} = 0$. In this interval the estimate error is about 5 bar. This agrees with the theoretical results from Chapter 3. The same can be seen for the bit flow estimation in Figure 7.1(c). The estimate is very good, but with no bit flow the estimate diverges.

The parameter estimates are shown in Figure 7.2. As expected from the theoretical results the parameters do not converge to their true values, but they become constants in steady state.

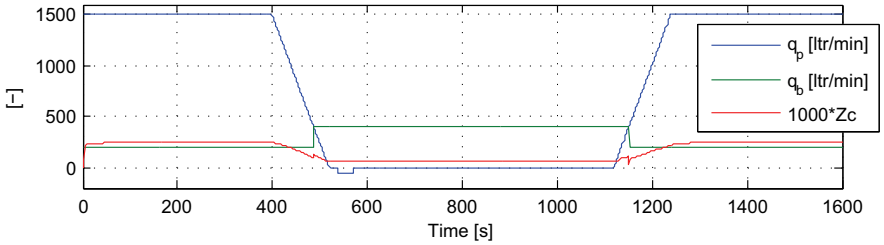

(a) Flows q_p and q_b and choke opening z_c.

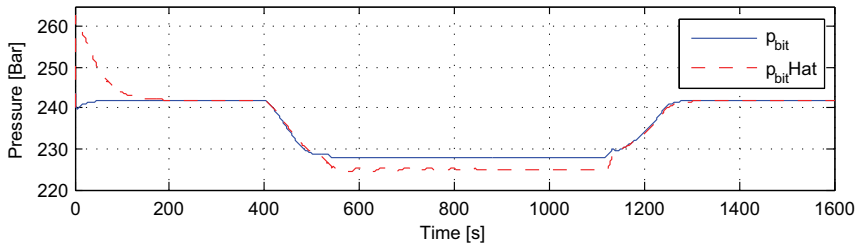

(b) Pressures p_{bit} and $\hat{p}_{bit}$.

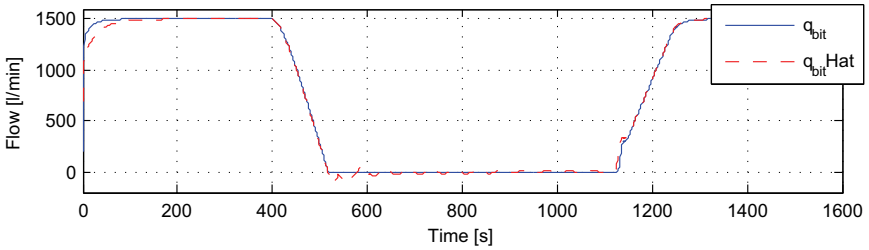

(c) Flows q_{bit} and $\hat{q}_{bit}$.

Figure 7.1: Simulation results for pipe connection with Stamnes observer.

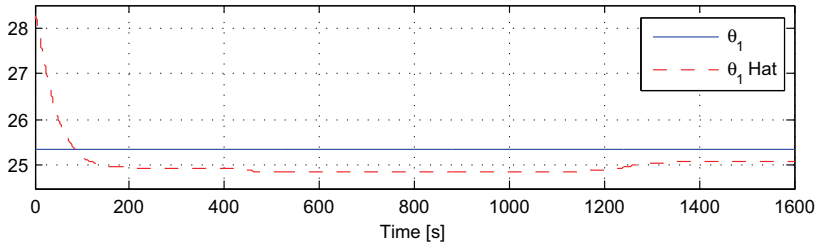

(a) θ_1 and $\hat{\theta}_1$.

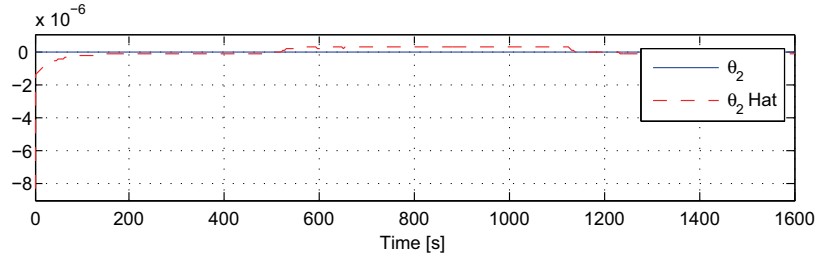

(b) θ_2 and $\hat{\theta}_2$.

Figure 7.2: Parameter estimation with Stamnes observer. Pipe connection.

7.2 Passive identifier

The estimation laws from Chapter 4 are simulated in Figures 7.3-7.6. The first is driven by $\tilde{q}_{bit}$, while the latter is driven by the low pass filtered $\tilde{q}_{bit}$. The results are similiar, but the low pass filter introduces oscillations.

The pressure estimate for the passive identifier without a low pass filter (Figure 7.3(b)) shows good results in steady state. But when the pump is ramped down, the estimate shows a inverse response. This might be because q_{bit} is derived from $\dot{p}_p$, which may introduce some transients. The convergence is also slower for $\hat{q}_{bit}$ as can be seen in Figure 7.3(c). The estimate is also a bit wrong while the pump is ramped down and up.

Table 7.3: Design parameters used in pipe connection for passive identifier.

Parameter	Value
Γ	$\text{diag}([5 \cdot 10^4, 5 \cdot 10^{-9}]$
l_1	$1 \cdot 10^{-7}$
K_p	1
K_i	1
τ_f	$\{1, 20, 50\}$
$\hat{q}_{bit}(0)$	700 [ltr/min]
$\hat{\theta}_1(0)$	28.1836 [-]
$\hat{\theta}_2(0)$	$-8.3640 \cdot 10^{-6}$ [-]

The parameters are shown in Figure 7.3. The parameter estimations are more wrong than for the Stamnes observer, but the flow estimate is still correct.

The low pass filter is introduced in Figure 7.5. It can be concluded from Figures 7.5(b) and 7.5(c) that the low pass filter introduces oscillations. The oscillations increase with increased time constant, τ_f. When the time constant is small ($\rightarrow 0$) the behavior tends to the results in Figures 7.3 and 7.4. From the simulations done in this thesis the low pass filter does not improve the estimates.

The time constant in the low pass filter has some influence on the parameter estimation. The parameters does not reach the same value, but as for the other observers, none of the estimates are correct.

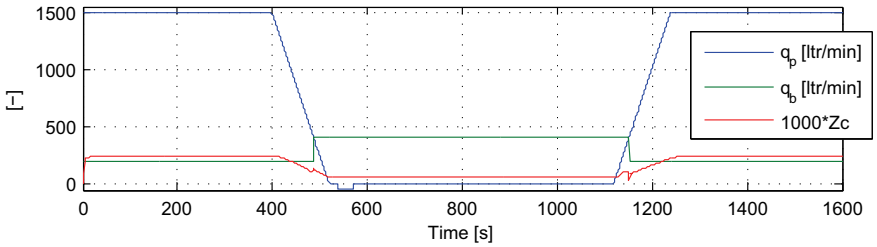

(a) Flows q_p and q_b and choke opening z_c.

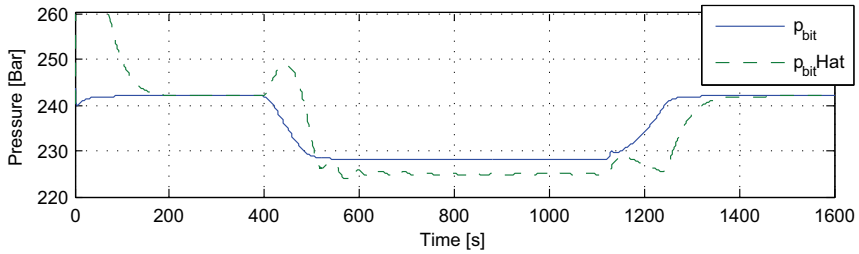

(b) Pressures p_{bit} and $\hat{p}_{bit}$.

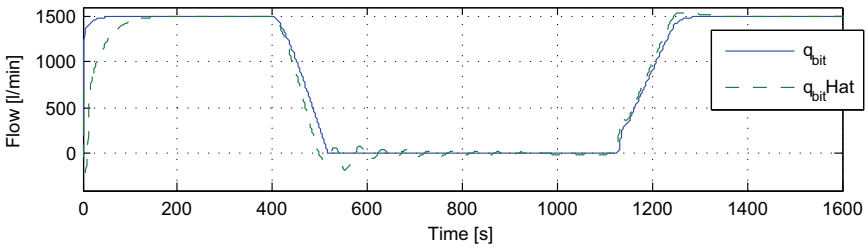

(c) Flows q_{bit} and $\hat{q}_{bit}$.

Figure 7.3: Simulation results for pipe connection with passive identifier.

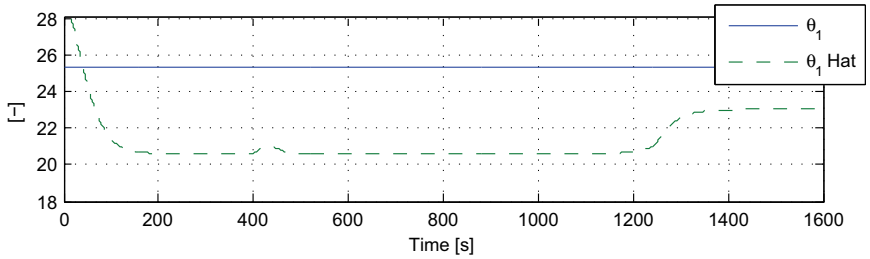

(a) θ_1 and $\hat{\theta}_1$.

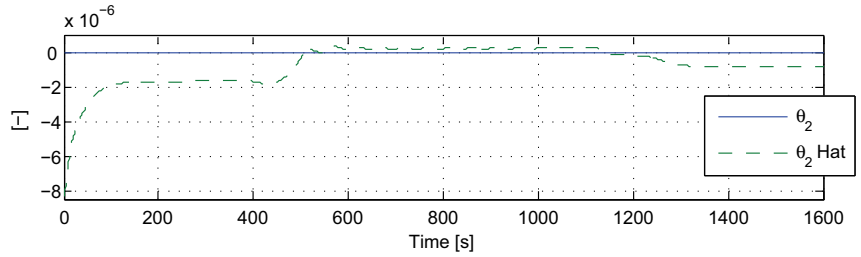

(b) θ_2 and $\hat{\theta}_2$.

Figure 7.4: Parameter estimation with passive identifier. Pipe connection.

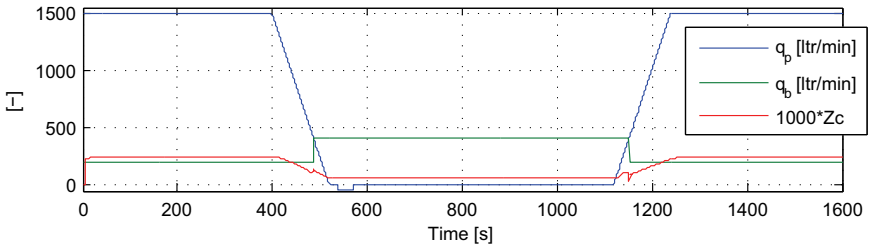

(a) Flows q_p and q_b and choke opening z_c.

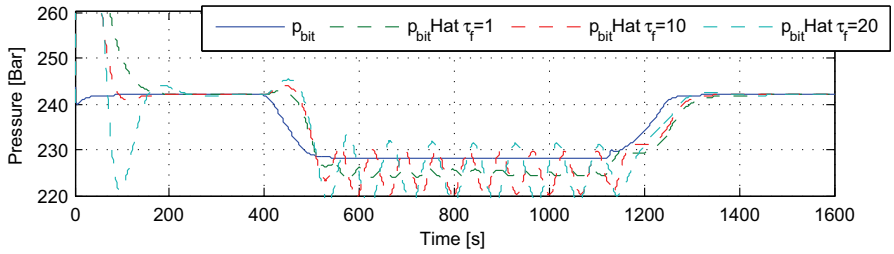

(b) Pressures p_{bit} and $\hat{p}_{bit}$.

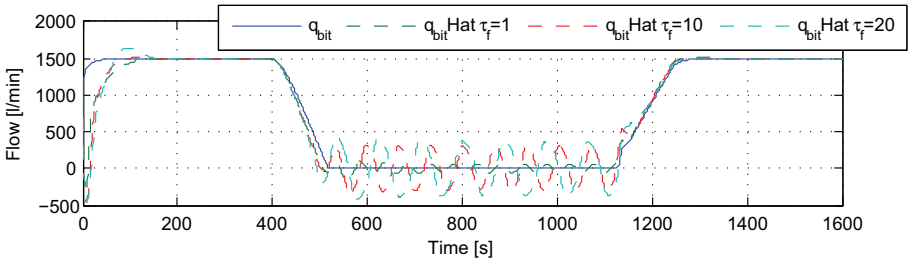

(c) Flows q_{bit} and $\hat{q}_{bit}$.

Figure 7.5: Simulation results for passive identifier driven by filtered $\tilde{q}_{bit}$, pipe connection. $\tau_f = \{1, 10, 20\}$

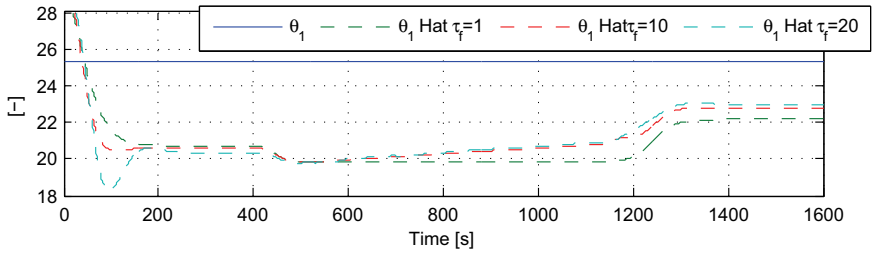

(a) θ_1 and $\hat{\theta}_1$.

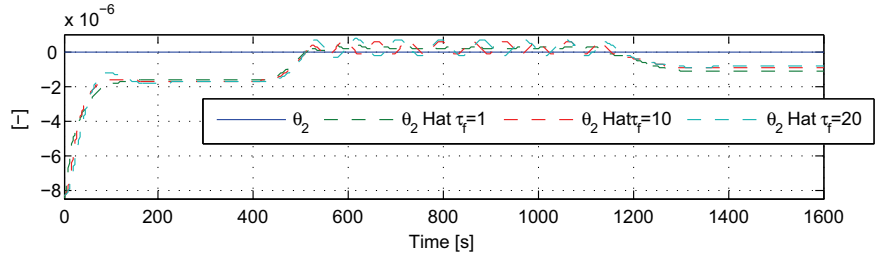

(b) θ_2 and $\hat{\theta}_2$.

Figure 7.6: Parameter estimation with passive identifier. Pipe connection. $\tau_f = \{1, 10, 20\}$

7.3 Optimal Polynomial Filter

Simulations with the optimal estimator for polynomial systems were also performed. Remember that this estimator uses a simplified system, with the friction parameter as the only unknown. This make the estimation task simpler.

The results are shown in Figure 7.7. $\hat{q}_{bit}$ converges very fast, but is a bit off for zero flow. The parameter estimation also shows promising behavior in Figure 7.7(b)[1]. Since there is only one unknown, this estimate should converge, which is does. Remember that the filter is driven by noise, so it is not expected that the parameter converges exactly to the correct value, but oscillates around the value.

More simulations with the complete drilling system from Chapter 2 should be done better evaluate the filter. The filter did not get the main focus in this thesis, since the proof did not lead to a result.

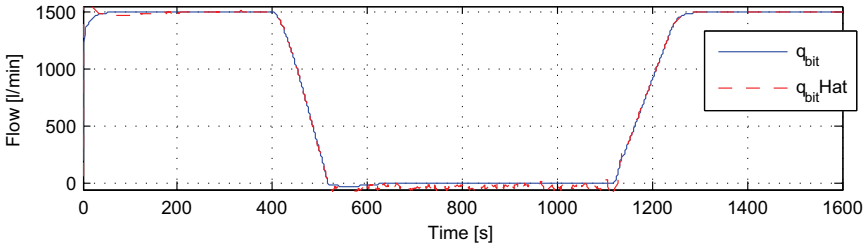

(a) Flows q_{bit} and $\hat{q}_{bit}$.

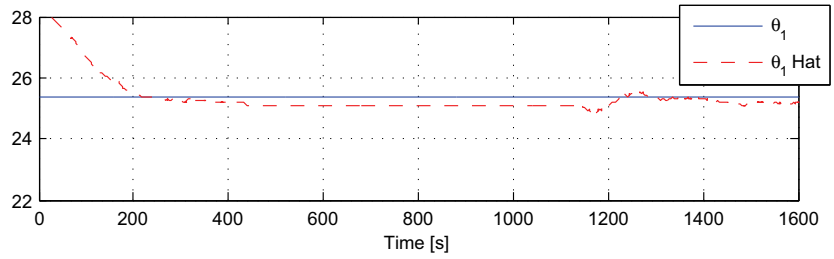

(b)

Figure 7.7: Simulation results for pipe connection with Optimal Polynomial Estimator.

[1]In the derivation the friction factor F was estimated, but this is divided by M in the figure to get θ_1

7.4 The Grip observer

The simulations from the pipe connection case with the Grip observer are shown in Figures 7.8 and 7.9. The pressure estimate in Figure 7.8(b) shows good steady state behavior, but has some problems during changes in the mud pump. The estimate is somewhat too low (5 bar) when the bit flow is zero. This is about the same error as for the Stamnes observer.

The bit flow estimate in Figure 7.8(c) on the other hand is very good. It has the fastest convergence, and the estimate is correct also for zero flow, except the time with bleed off. The estimate is this good since $\dot{p}_p = 0$, which leads to a correct calculation of q_{bit} from the top side measurement as described in Chapter 6.

Table 7.4: Design parameters used in pipe connection for Grip observer.

Parameter	Value
Γ	$\text{diag}([5 \cdot 10^4, 5 \cdot 10^{-9}]$
γ_0	10^{-7}
K_p	1
K_i	1
$\hat{q}_{bit}(0)$	700 [ltr/min]
$\hat{\theta}_1(0)$	28.1836 [-]
$\hat{\theta}_2(0)$	$-8.3640 \cdot 10^{-6}$ [-]

The parameter estimations in Figure 7.9 coincide with the results from the other observers.

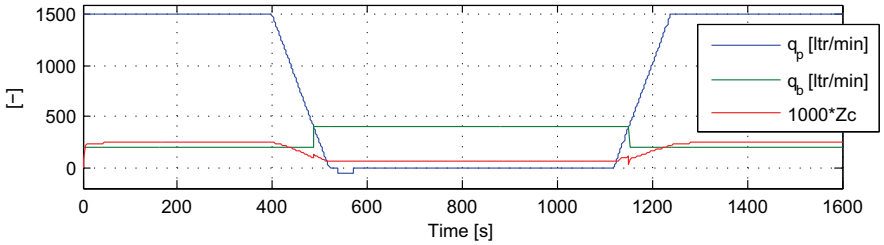

(a) Flows q_p and q_b and choke opening z_c.

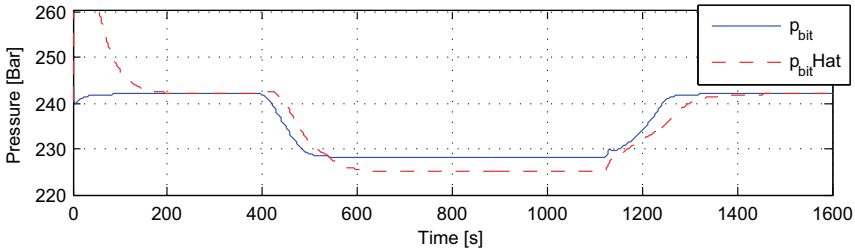

(b) Pressures p_{bit} and $\hat{p}_{bit}$.

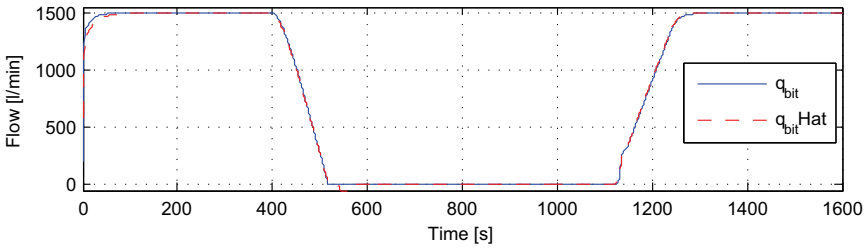

(c) Flows q_{bit} and $\hat{q}_{bit}$.

Figure 7.8: Simulation results for pipe connection with the Grip observer.

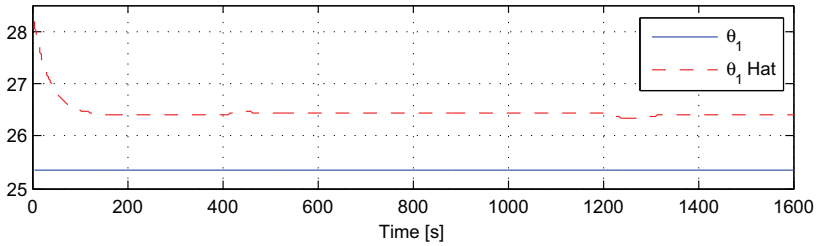

(a) θ_1 and $\hat{\theta}_1$.

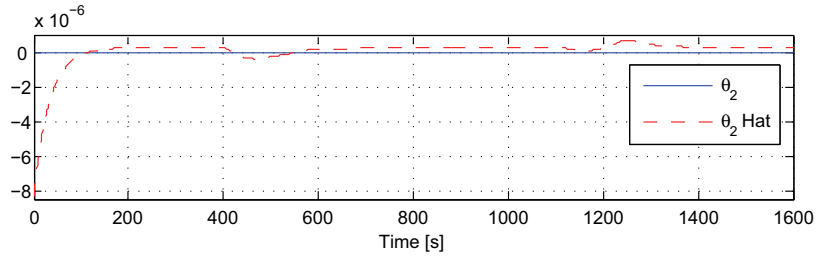

(b) θ_2 and $\hat{\theta}_2$.

Figure 7.9: Parameter estimation with Grip observer. Pipe connection.

Chapter 8

Summary of the Observers

This short chapter summarizes the observers and gives advantages and disadvantages for each observer from Chapters 3-6.

The main conclusion from the simulations is that the performances were equally good for the cases considered. All the observers estimated the bit flow and the bottom hole pressure very good, but none of them managed to estimate the unknown parameters correctly.

All observers are driven by $\tilde{q}_{bit}$ in some way, and it seems to be a inherent property of the drilling system that the bit flow estimates converges too fast for the parameters to reach the correct value. Instead, "wrong and wrong becomes correct" and the bit flow estimate converges when both $\hat{\theta}_1$ and $\hat{\theta}_2$ are wrong. One solution that might work is to use a small negative adaption gain for the bit flow estimation. This could possibly slow down the estimation so the parameters converge. This idea is not tested out in simulations in this thesis, but could be further research.

The Stamnes observer stands out from the others with a smart implementation of the adaptation law. A change of coordinates walks around the need for q_{bit} to be known, which is an advantage. However, q_{bit} is available as a low sample measurement and this should be used to some extend.

The Grip observer is also proved to converge in this thesis. An advantage with this proof is that it includes a PE-condition[1], which can be used in implementation to stop the adaptation if the signal does not fulfill the condition. This will result in a more robust estimator. The simulations did not confirm convergence as expected from the proof. As pointed out earlier, it might be that the parameters will converge after a very long time or that more excitement is needed in the signals. There is also a possibility that an assumption from the proof is not fulfilled.

If the passive identifier and the Grip observer is compared, the two expressions for $\dot{\hat{\theta}}$ can both be written $\dot{\hat{\theta}} = \Gamma \boldsymbol{\phi}(\hat{q}_{bit}, v_3)\tilde{q}_{bit}$ and there are only minor differences in the expressions for $\dot{\hat{q}}_{bit}$. This should explain why these results

[1] A condition for the signal to be persistent excitation

are almost the same.

The advantages and disadvantages for each observer are summarized in Table 8.1.

Table 8.1: Summary of the observers.

Observer	**Advantages**	**Disadvantages**
Stamnes observer	Does not use q_{bit} Comprehensive proofs Smart implementation	Should use q_{bit} measurement when available. PE-conditions not known.
Grip observer	Proof of convergence. PE-conditions in proof.	Uses q_{bit}
Passive Identifier	Simple implementation Uses top side values	Uses q_{bit}
Filtered Passive Identifier	Simple implementation Can filter out noise.	Uses q_{bit}. Introduces oscillations. Lack of theoretical proofs.
Optimal Poly. Est.	Handles noise	Lack of theoretical proofs.

Part III

Friction modeling

Chapter 9

Friction modeling

In Section 2.2 the pressure drop due to friction in the annulus and the drill string were assumed to be given by $P_{fric} = (F_a + F_d)|q_{bit}|q_{bit}$ (assuming $q_{res} = 0$), with F_a as an unknown parameter. From drilling experience this model is known not to fit the real friction loss very well, which motivates for a better friction model. A more realistic model will improve the bottom hole pressure estimate and is derived in this chapter.

The new friction model is based on steady state conditions in measurement data from the North Sea. Steady state conditions make it easy to find the hydrostatic pressure and the friction curves for the annulus and drill string, but is still a simplification of the real friction which might have more difficult behavior.

Since the drilling tests were done mid April, it was not possible to use the new friction model in most of this thesis, but some simulations are done in the next chapters.

9.1 Getting the friction curves

The friction curves are made from drilling data collected for StatoilHydro in April 2009. The tests are done at the Gullfaks C field in the North Sea. Several tests were done for research use and the case used here is a step the mud pump down from 2000 ltr/min to 0 ltr/min, back up to 2000 ltr/min. Each step was about 100 ltr/min. This period of the drilling test is used to find the friction model.

Equations (2.4) and (2.5) are used to find steady state friction curves for drill string and annulus by plotting

1. $f^a_{fric} = p_{bit} - P_c - \rho g h_{bit}$ for the annulus.

2. $f^d_{fric} = p_p - p_{bit} + \rho g h_{bit}$ for drill string.

for $q_p (= q_{bit}$ in steady state) from 0 to 2000 ltr/min (all steady state measurements). p_p, p_{bit} and p_c are known from measurements, but $\rho g h_{bit}$ has to be calculated.

9.1.1 Finding the hydrostatic pressure

First the hydrostatic pressure ($p_{hydro} = \rho g h_{bit}$) has to be found. By assuming $p_{fric} = 0$ for zero flow and rearranging Equations (2.4) and (2.5), p_{hydro} is given as

$$p_{hydro_1} = \rho g h_{bit} = -p_p + p_{bit} \tag{9.1}$$

$$p_{hydro_2} = \rho g h_{bit} = p_{bit} - p_c \tag{9.2}$$

These two values should in theory be equal, but in the data set they differ with about 1 bar. To cope with this, measurement errors and to take noise into account to some extent, the average of p_{hydro_1} and p_{hydro_2} for the time period with $q_p = 0$ was used as p_{hydro}. The period is shown in Figure B.2.

The average value was found to be

$$\boxed{p_{hydro} = 263.6[\text{bar}]} \tag{9.3}$$

and will be used in the rest of this thesis as the correct hydrostatic friction.

9.1.2 Finding friction curves

As mentioned, the pump was stepped down in the drilling test with about 100 ltr/min each step. To get the values needed for the friction plots, the index for each step was collected from Figure B.2. It is assumed that the system reaches steady state before each new step. There is no flow from the back pressure pump during the test.

The drill string friction, p^d_{fric} is shown in Figure 9.1(a) where $p^d_{fric}(q_p) = p_p - p_{bit} + p_{hydro}$ is plotted for each of the steady state q_p values. The friction curve for the annulus is found by plotting $p^a_{fric}(q_p) = p_{bit} - p_c - p_{hydro}$, as shown in Figure 9.1(b).

9.1.3 Comparison with quadratic friction

Figure 9.2 shows the friction model from measurements compared with the quadratic friction model assumed in Section 2.2. The friction factors are taken as $F_d = 4.5833 \cdot 10^{-5}$[1] and $F_a = 5.7778 \cdot 10^{-6}$, which are taken from [Stamnes, 2007].

As Figure 9.2(a) shows, the assumption of quadratic friction is quite good for the drill string. There is a bias of about 3.5 bar for flows below 600

[1] The values for F_d and F_a are scaled to match q_{bit} with ltr/min as unit. The values are given in Table 7.1 for SI-units.

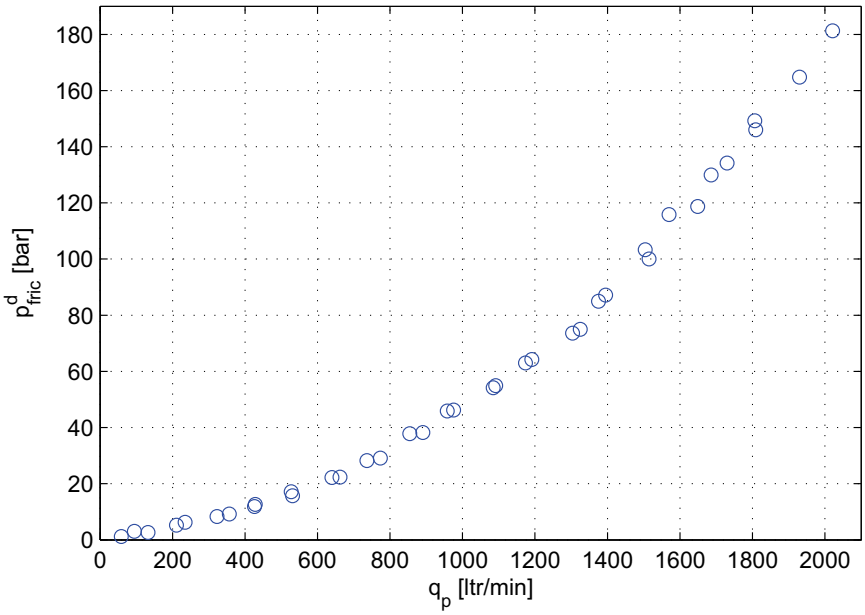

(a) Drill string

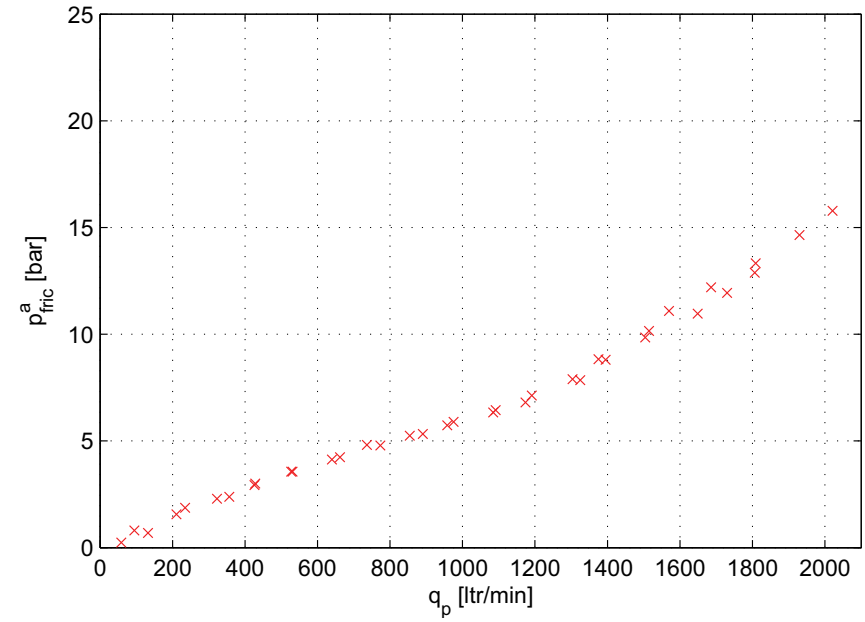

(b) Annulus

Figure 9.1: Friction curves from measurement data.

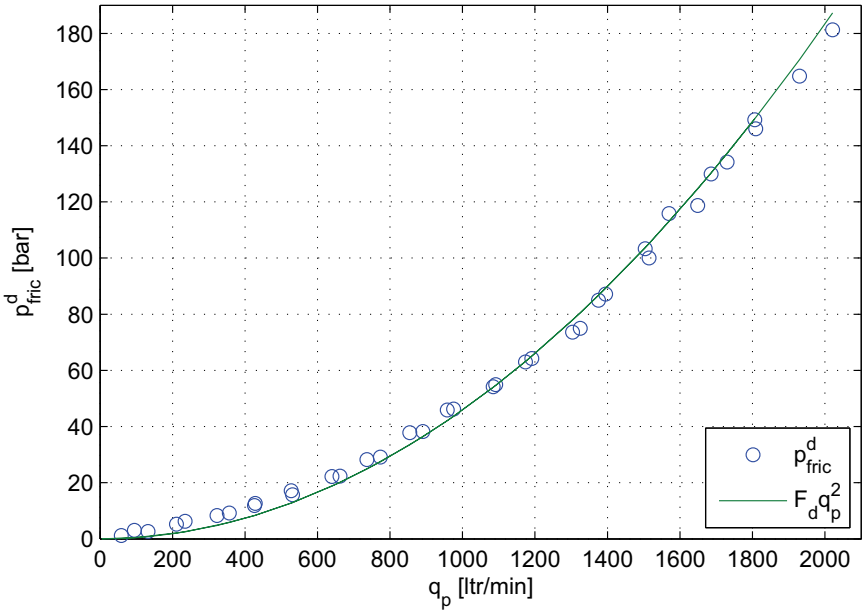

(a) Drill string. $F_d = 4.5833 \cdot 10^{-5}$

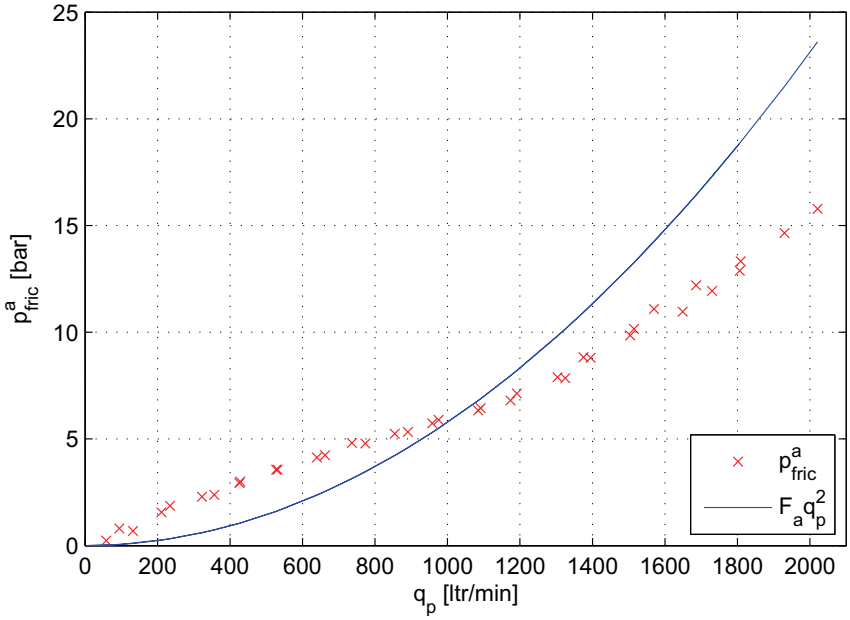

(b) Annulus. $F_a = 5.7778 \cdot 10^{-6}$

Figure 9.2: Comparison of quadratic friction and friction from measurements.

ltr/min. For the rest of the flow rates, the quadratic model is good. The quadratic friction model $p^d_{fric} = F_d|q_{bit}|q_{bit}$ is assumed to be good enough and will be used throughout this thesis. A better model can easily be made, but since estimation is the main focus of the thesis, the unknown annulus friction is most important and used for testing in the following.

The friction pressure in annulus, Figure 9.2(b), on the other hand does not show the same good results. (Note that the y-axes are different for the two figures.) The curve shape is different and the bias is increasing for increased flow. The quadratic model gives too little friction pressure for flows below 1000 ltr/min and too much loss for flows over 1000 ltr/min. A new friction model for the annulus friction loss will be derived in the next chapter.

Chapter 10

Estimation of friction curve

As shown in Section 9.1.3, the quadratic friction assumption for the friction pressure in the annulus is not satisfactory. To estimate the annulus friction curve, an approximation of the curve is built up from basis functions and the weighted sum of these functions is estimated. This method gives many possibilities and great flexibility for both approximation and estimation.

First an example of function approximation is presented, before three different approximations to the annulus friction are tested. Two of these approximations are simulated with a ramp in the mud pump to see if the parameters converge.

Since the drilling data were available late in the progress with this thesis, only one adaptation law is considered in this chapter.

10.1 Function approximation

A function $f(x)$ can be approximated as $\bar{f}(x) = \sum_{i=1}^{N} \phi_i(x)\theta_i = \boldsymbol{\phi}^\top \boldsymbol{\theta}$, where $\boldsymbol{\phi} = [\phi_1(x) \quad \phi_2(x) \quad ... \quad \phi_N(x)]^\top$ are basis functions and $\boldsymbol{\theta} = [\theta_1 \quad \theta_2 \quad ... \quad \theta_N]^\top$ are weights or scaling of each basis function. θ_i can generally be time depended, but is taken as constant here.

The contribution from $\phi_i(x)$ to $f(x)$ is known as *support*. If $\phi_i(x)$ is nonzero only for some values of x, it is said that $\phi_i(x)$ has *local support*. *Center of support* is defined as the mid point for $\phi_i(x)$ and *radius of support* is the subset of x where $\phi_i(x) \neq 0$.

A simple example of a function build up from two basis functions is shown in Figure 10.1. The basis functions are shown in the last row, while the normalized[1] weighted sum ($\bar{f}(x) = \boldsymbol{\phi}^\top \boldsymbol{\theta}$) is shown in the first row. The weighting used is $\boldsymbol{\theta} = [0.8 \quad 1.2]^\top$, while $c_i = \{0.25, 0.75\}$ (centers of support) and $\mu_{1,2} = 0.5$ (radius for each basis function).

[1] For this case the basis functions were normalized, as shown in the middle row. Normalization will be described in more details later in the thesis.

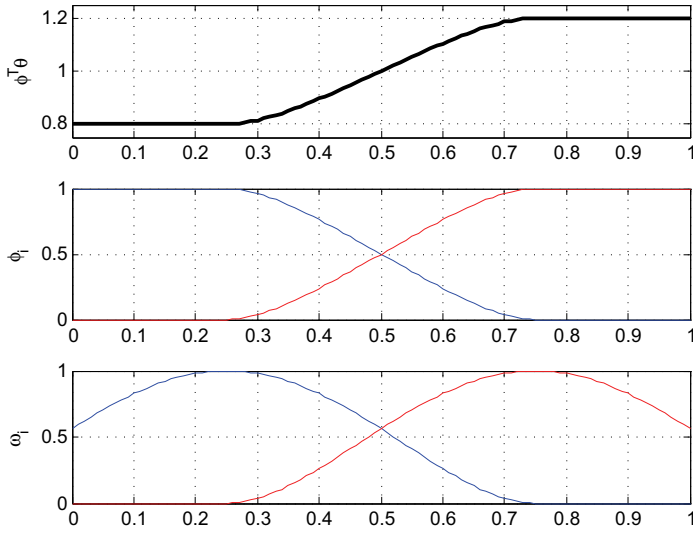

Figure 10.1: Simple example of how the sum of basis functions (bottom) builds a new function (top). N = 2, $c_i = \{0.25, 0.75\}, \mu_i = 0.5, \boldsymbol{\theta} = [0.8 \quad 1.2]^\top$.

10.2 Friction curve approximation

Two different basis functions are examined for friction approximation in this thesis. Both functions give local support, where the first is a continuous function and the second is 1^{st}-order b-splines. The latter is used to build up the friction curve with a set of four basis functions and a set of 10 functions. With 10 basis functions the approximation should be better, but with only four functions the number of parameters is reduced, which should give easier estimation.

To see how the parameters converge, the simulations in this chapter use $p^a_{fric}(q_{bit}, \theta)$ as the true friction and $\hat{p}^a_{fric}(\hat{q}_{bit}, \hat{\theta})$ as the estimated friction. This means that the pressure estimate is compared to the approximation with the current basis functions, not the true friction from Figure 9.1(b).

A more realistic simulation case, with friction from Chapter 9 and both the passive identifier and the Stamnes observer can be seen in Chapter 11 when the pipe connection is revisited.

10.3 System and adaptation laws

Since a new friction model was derived in Section 9.1, some modifications of the system and the adaptation law are done. It is assumed that the weights, θ_i, are the only unknowns. As before, the drill string friction is taken as $p^d_{fric} = F_d|q_{bit}|q_{bit}$ where F_d is known. The density in annulus, ρ_a, is also assumed known.

The system is taken as

$$\frac{V_d}{\beta_d}\dot{p}_p = q_p - q_{bit} \tag{10.1}$$

$$\frac{V_a}{\beta_a}\dot{p}_c = q_{bit} - q_c - \dot{V}_a \tag{10.2}$$

$$M\dot{q}_{bit} = p_p - p_c - F_d|q_{bit}|q_{bit} - p^a_{fric}(q_{bit})\text{sgn}(q_{bit}) + (\rho_d - \rho_a)gh_{bit} \tag{10.3}$$

where p^a_{fric} is the unknown friction loss in annulus.

The adaptation law is taken from the passive identifier in Section 4.1 and is

$$\begin{aligned}\dot{\hat{\theta}} &= \mathbf{\Gamma}\boldsymbol{\phi}(\hat{q}_{bit})\tilde{q}_{bit} \\ &= \mathbf{\Gamma}\boldsymbol{\phi}(\hat{q}_{bit})(q_p - \frac{V_d}{\beta_d}\dot{p}_p - \dot{V}_d - \hat{q}_{bit})\end{aligned} \tag{10.4}$$

where $\boldsymbol{\phi}(\hat{q}_{bit})$ are the basis functions.

One important point for estimation with basis functions with local support is that only functions that have support for a given flow are changed. As an example, in Figure 10.2 only two weights are changed for any q_{bit}. (Since the other does not have support). This limits the number of parameters that are estimated for a given flow, which gives better and faster estimation.

10.4 Continous basis functions

In theory, any function can be used as basis functions, but [Imsland, 2009] introduces a continuous basis function which is also used in this section. The continuous local functions is taken as

$$\omega_i(q_{bit}) = \begin{cases}(1 - (\frac{|q_{bit}-c_i|}{\mu_i})^2)^2, & \text{if } |q_{bit} - c_i| < \mu_i \\ 0, & \text{otherwise}\end{cases} \tag{10.5}$$

where c_i is the center of support and μ_i is the radius of support.

The normalized basis functions are given by

$$\phi_i(q_{bit}) = \frac{\omega_i(q_{bit})}{\sum_{i=1}^{N}\omega_i(q_{bit})} \tag{10.6}$$

Normalized basis functions have several advantages, e.g. the interpretation of θ_i is simpler than for the non-normalized functions. The normalized approach is used for the continuous basis functions in this thesis.

To approximate the friction curve for the annulus, a total of 5 normalized basis functions are used. The center points and the support radius is found off-line with trail and error. The centers of support are taken as

$c_i = \{0, 500, 1000, 1500, 2000\}$, while the radii are taken as $\mu_i = 500$. The weights are found to be

$$\boldsymbol{\theta} = [0.1, 3.5, 6.0, 9.6, 15.1]^\top \tag{10.7}$$

Figure 10.2 shows the basis functions and the approximated friction curve. The approximation to the true friction curve is quite good, catching the main behavior. There are some steps in the transitions between basis functions that gives some deviation from the true friction. However, the error is less than one bar and assumed to be good enough.

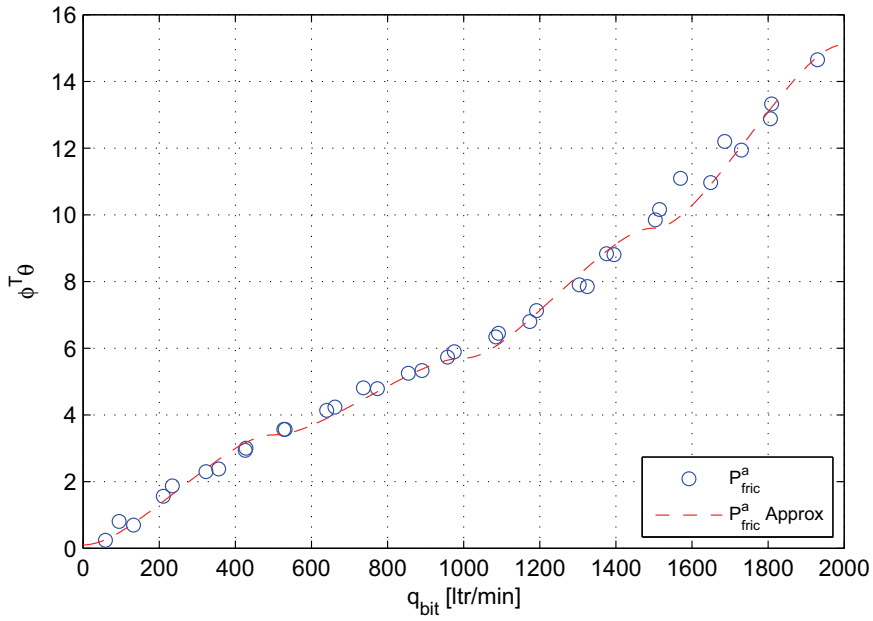

(a) Friction approximation.

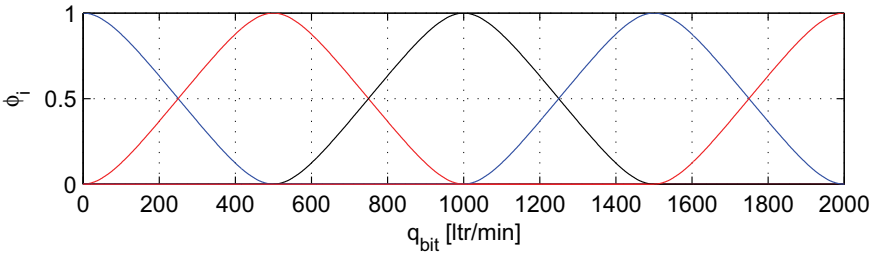

(b) Basis functions.

Figure 10.2: Continuous basis function and friction approximation.

10.4.1 Simulations with continuous basis functions

To see how $\hat{\boldsymbol{\theta}}$ converges, the mud pump was ramped as shown in Figure B.4(a). The flow was increased from 200 ltr/min to 2000 ltr/min within 90 seconds. 2000 ltr/min were kept for 30 seconds, before the pump was ramped back down to 200 ltr/min. This procedure was repeated for the time span showed in the following figures. To ramp the pump is a realistic case for estimating the friction. It is also important to note that q_p spans all the basis functions, which is necessary for all parameters to converge. Mud pump flow, choke pressure, pump pressure and bottom hole pressure are shown in Figure B.4. These results are as expected when the pump is ramped up and down. In

Table 10.1: Design parameters for simulation with continuous basis functions.

Parameter	Value
Γ	diag([80, 50, 50, 50,100])
c	$\{0, 500, 1000, 1500, 2000\}$
μ	$\{600, 600, 600, 600, 600\}$
$\boldsymbol{\theta}$	$[0.1, 3.4, 5.7, 9.6, 15.1]^\top$
$\boldsymbol{\theta}(0)$	$\mathbf{0}_{5\times 1}$

Figure 10.3 the actual pressure loss and the estimated loss, together with the error, are showed. The initial conditions are $\hat{\theta} = 0$ and the figure clearly shows how the error tends to zero, while $\hat{\theta}$ converges to the true value.

The development for each $\hat{\theta}_i$ is showed in Figure 10.4. The figure shows that all weights converge to their true value, within reasonable time.

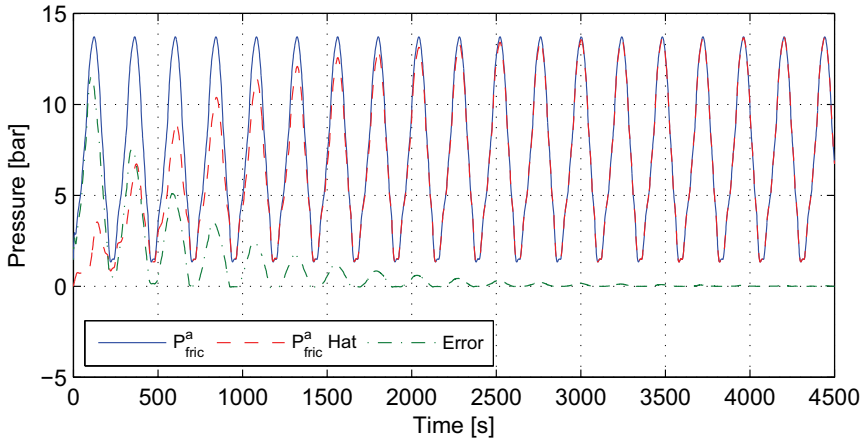

Figure 10.3: Annulus friction pressure and estimation for simulation with continuous basis functions.

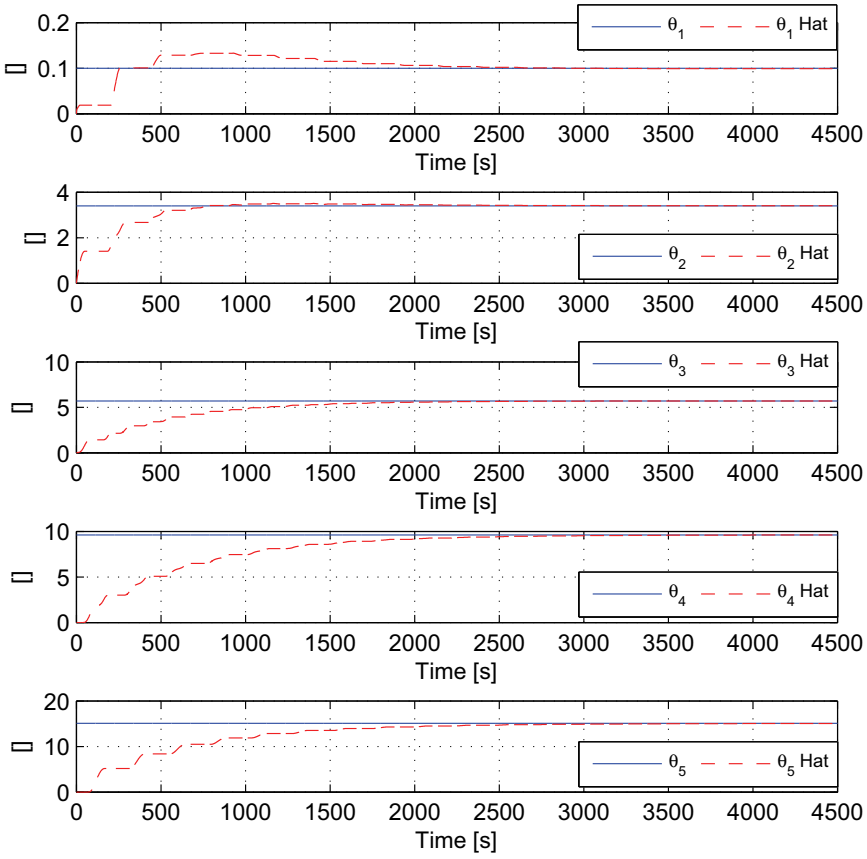

Figure 10.4: Parameter convergence for simulation with continuous basis functions.

Another interesting figure is Figure 10.5. Here is the development for $\hat{p}^a_{fric}$ showed. It is easy to see how the friction estimate has zero as initial condition, and builds up as the time elapse and each weight converges.

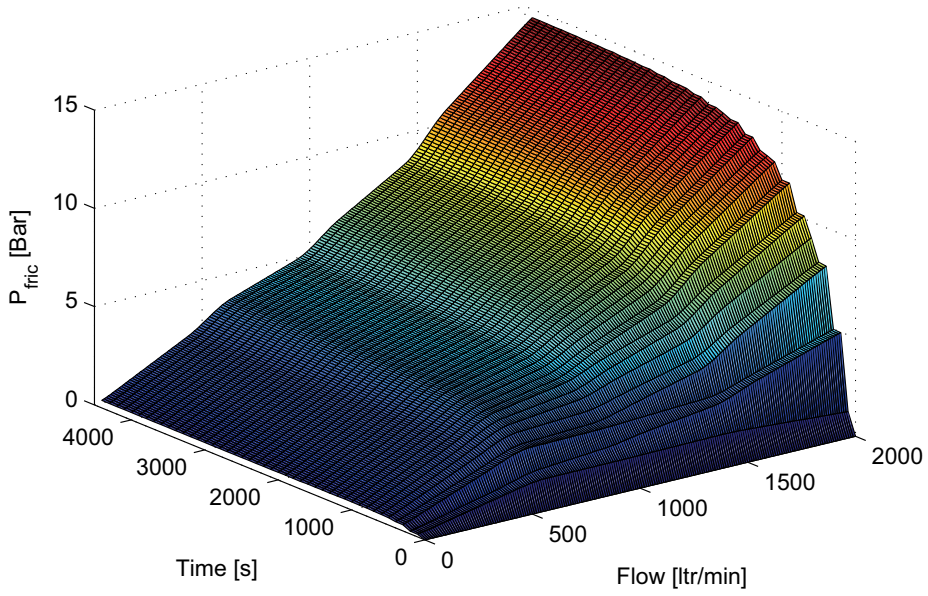

Figure 10.5: Development of friction estimation with continuous basis functions.

10.5 B-spline basis functions

As another approach to approximate the friction curve, b-spline functions are used. The b-spline of k^{th}-degree is recursively defined as [Farrell and Polycarpou, 2006]

$$\phi_i^k(q_{bit}) = \left(\frac{q_{bit} - c_i}{c_{i+k} - c_i}\right)\phi_i^{k-1}(q_{bit}) + \left(\frac{c_{i+k+1} - q_{bit}}{c_{i+k+1} - c_{i+1}}\right)\phi_{i+1}^{k-1}(q_{bit}) \tag{10.8}$$

where $i = [1, 2, ..., N]$ is the basis function number and the 0^{th}-degree b-spline is defined as

$$\phi_i^0(q_{bit}) \triangleq \begin{cases} 1 & \text{if } q_{bit} \in [c_i, c_{i+1}) \\ 0, & \text{otherwise} \end{cases} \tag{10.9}$$

The recursive formula in Equation (10.8) can be slow to compute for high order b-splines, but is not a problem for the work done here.

The b-splines does not have a parameter to explicit set the radius of support, such as μ for the continuous basis functions in Section 10.4. Instead, both center of support and radius are set by c_i for each ϕ_i. Each basis function ϕ_i has support on the interval $[c_i, \quad c_{i+k+1})$.

In this thesis the degree is set to $k = 1$ and first the approximation is done with four basis functions. The resulting approximation is showed in Figure 10.6(a), where $c_i = \{0, 500, 1000, 1500, 2000, 2500\}$ and
$\boldsymbol{\theta} = [3.1 \quad 6.0 \quad 9.7 \quad 15.0]^\top$. Since the true friction is quite linear (piecewise), the linear basis functions give a good approximation, even though the number of basis functions are reduced from five to four compared with Section 10.4. To get a even better approximation, a total of 10 basis functions where also tested. The resulting approximation is found in Figure 10.7(a), with
$c = \{0, 200, 400, 600, 800, 1000, 1200, 1400, 1600, 1800, 2000, 2500\}$ and
$\boldsymbol{\theta} = [1.4, 2.6, 4.0, 5.0, 6.0, 6.8, 8.5, 11.0, 13.0, 15.1]^\top$

The approximation is a bit closer to the true friction, but not radically better. It does not seems to be worth to increase the number of basis functions from four to 10, so only simulations for 4 b-splines approximation are showed.

10.5.1 Simulations with b-spline approximation

The same pump ramp as for continuous basis functions was used for the b-splines simulation.

Figure 10.8 shows the same behavior as seen in the last section. The friction estimate is zero in the beginning, but after some ramps, the estimate tends to the correct value. The parameters converge after some time, which implies convergence for the friction loss estimate. This is confirmed by Figure 10.9, where it is shown that the parameters converge to their true values. Note that this case needs more time before convergence than the continuous basis

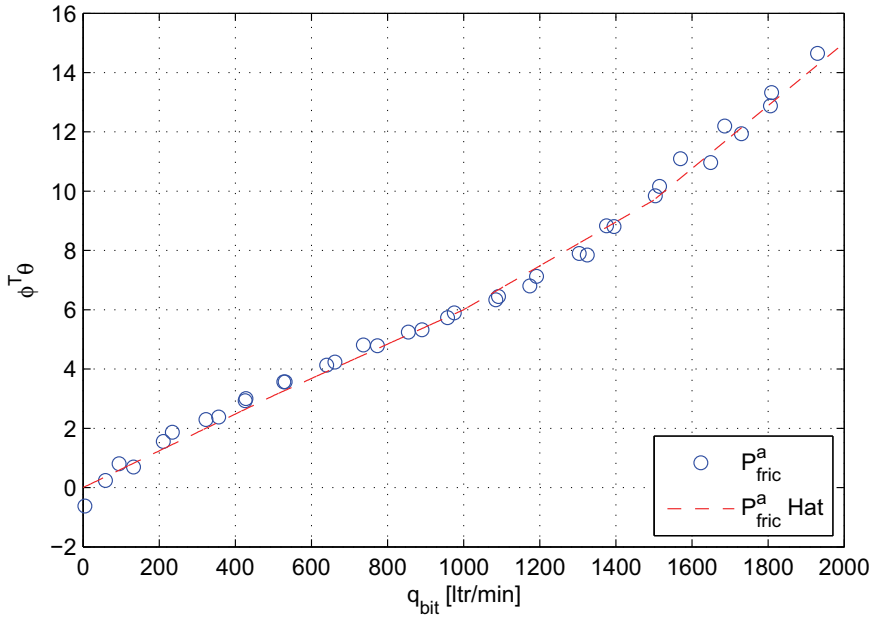

(a) Friction approximation.

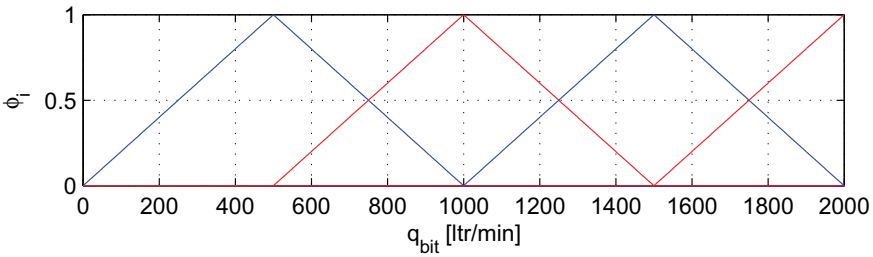

(b) Basis functions.

Figure 10.6: Friction approximation with four 1st order b-spline functions.

functions in the last section. This might be because each θ is larger when the number of basis functions is reduced, so zero as initial value is more far from the true value. It should also be noted that the friction loss estimate is smoother for the continuous basis functions, than for the b-splines. This might be because the 1^{st} order b-splines have discontinuities at the centers of support.

Figure 10.10 shows the entire development of the friction estimation when using 4 b-splines. There are just minor differences from the case with continuous basis functions.

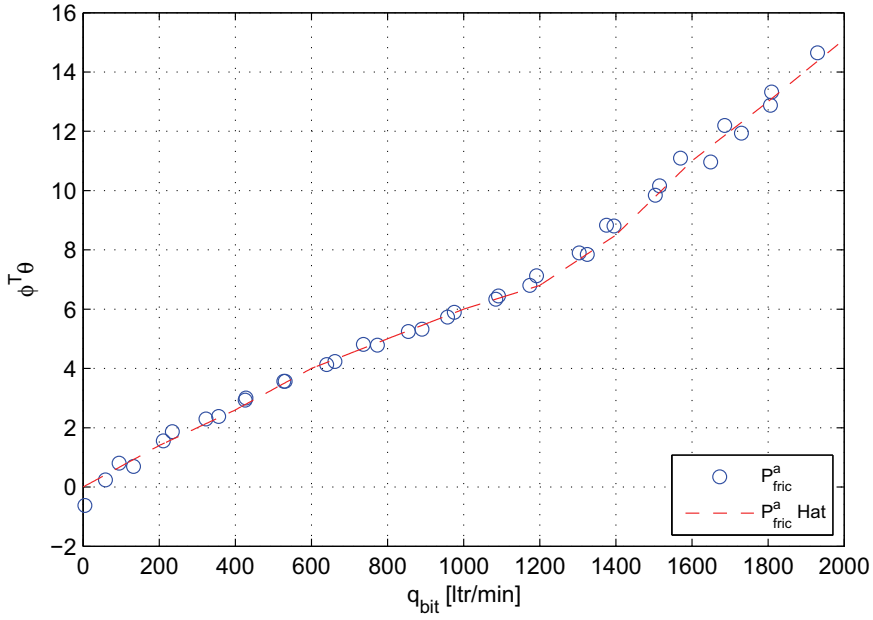

(a) Friction approximation.

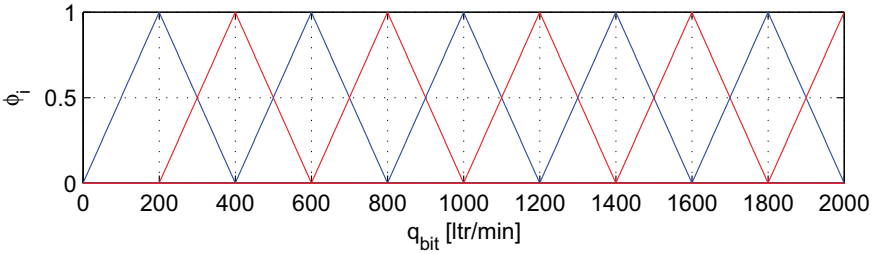

(b) Basis functions.

Figure 10.7: Friction approximation with 10 1st order b-spline functions.

Table 10.2: Design parameters for simulation with 4 b-spline basis functions.

Parameter	Value
Γ	diag([8, 9, 10, 40])
c	$\{0, 500, 1000, 1500, 2000, 3000\}$
$\boldsymbol{\theta}$	$[3.1, 6.0, 9.7, 15.0]^\top$
$\boldsymbol{\theta}(0)$	$\mathbf{0}_{4\times1}$

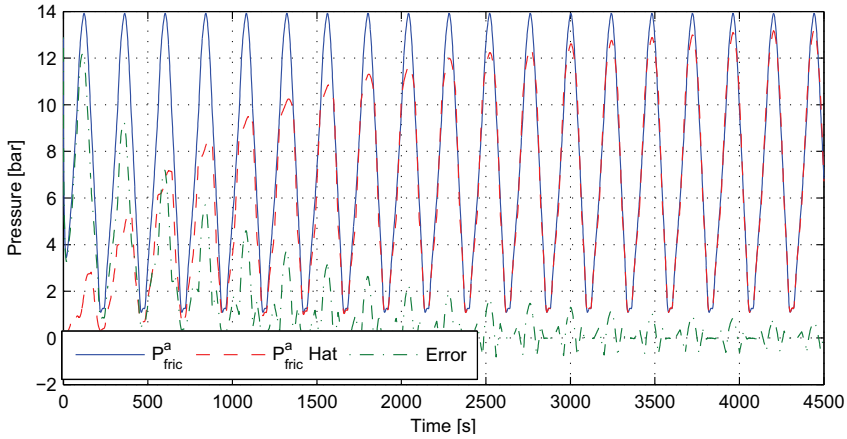

Figure 10.8: Annulus friction pressure and estimation for simulation with 4 b-spline basis functions.

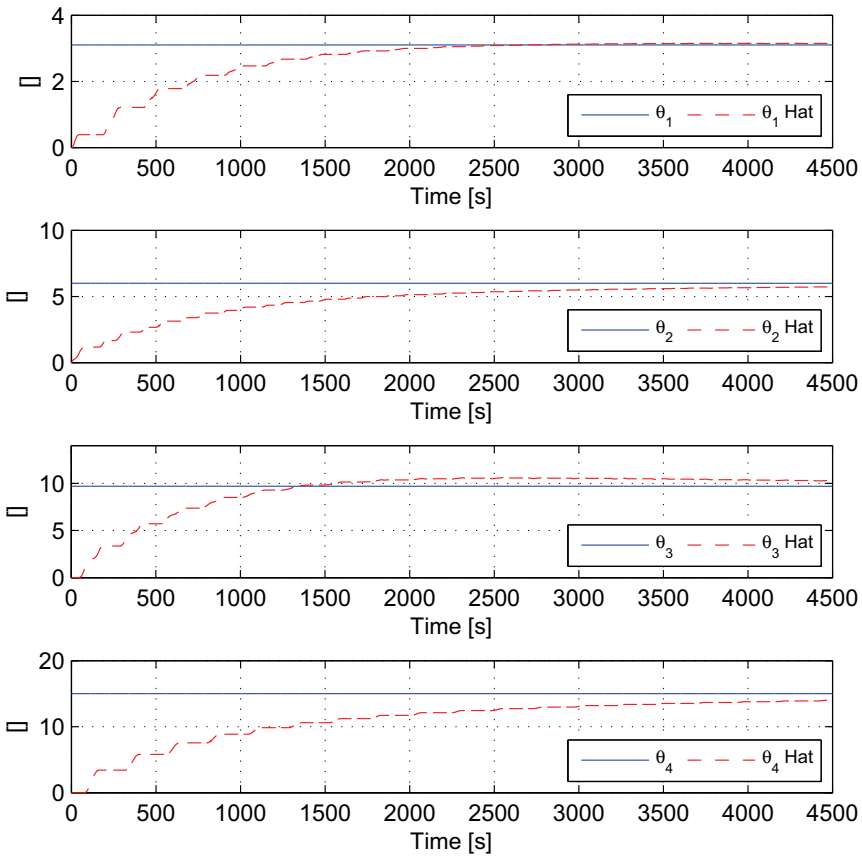

Figure 10.9: Parameter convergence for simulation with 4 b-spline basis functions.

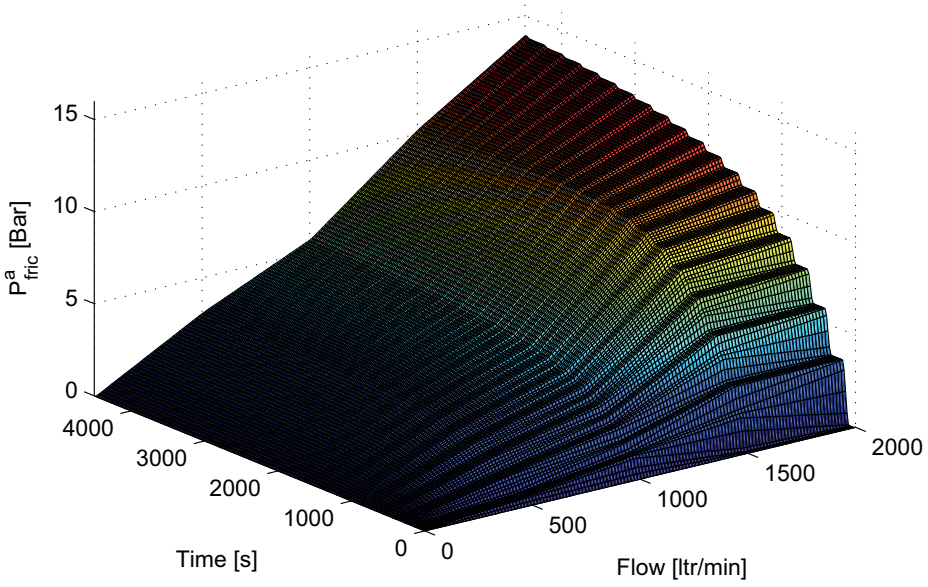

Figure 10.10: Development of friction estimation with 4 b-spline basis functions.

10.6 Summary of friction approximation

Three different methods for friction approximation have been derived in this chapter. The first case used five continuous basis functions; while the last two used four and 10 b-spline functions respectively.

All three methods gave good approximation to the real friction curve derived in Chapter 9, but since 4 b-splines was almost as good as 10 b-splines only the first one was presented[2]. Both continuous and 4 b-spline functions gave convergence for the parameters.

With number of parameters and simplicity in mind, the use of four b-splines to approximate the friction are recommended as the best solution. Simulations with this approximation, compared to the best curve fit friction will be presented in the next chapter for both the passive identifier and the Stamnes observer.

[2]A simulation with 10 b-splines was also tried and gave the same results

Chapter 11

Simulations with improved friction model

In the last two chapters a new friction model for the annulus friction was derived, approximated and estimated. The simulations showed that different approximations were possible and that the parameters converged when compared to friction given by the correct parameters.

In this chapter the approximation with four b-spline basis functions is again simulated, but this time the friction is compared directly with the friction model developed in Section 9.1.2. A curve fit analysis is done to get a continuous friction curve and the passive identifier and the Stamnes observer will be simulated.

The case considered is the same as in Chapter 7; *a pipe connection*.

11.1 Getting a continuous friction model

To be able to compare the estimated approximation with the real friction, a continuous model is needed. The model is based on the friction curve in Section 9.1.2 and is showed in Figure 11.1. The continuous friction curve was found with Matlab and `Tools->Basic fitting`. The resulting model is

$$\boxed{p^a_{fric}(q_{bit}) = 2.1 \cdot 10^{-9} q^3_{bit} - 4.7 \cdot 10^{-6} q^2_{bit} + 8.9 \cdot 10^{-3} q_{bit} - 0.21} \qquad (11.1)$$

and will be used as the correct friction in the rest of this chapter. Since the approximations in the last chapter are quite good, the use of Equation (11.1) should not introduce any problems.

11.2 Simulation results

Different estimation laws will be tested with the pipe connection case in this section. As in Chapter 7 the mud pump will be ramped down, but this time

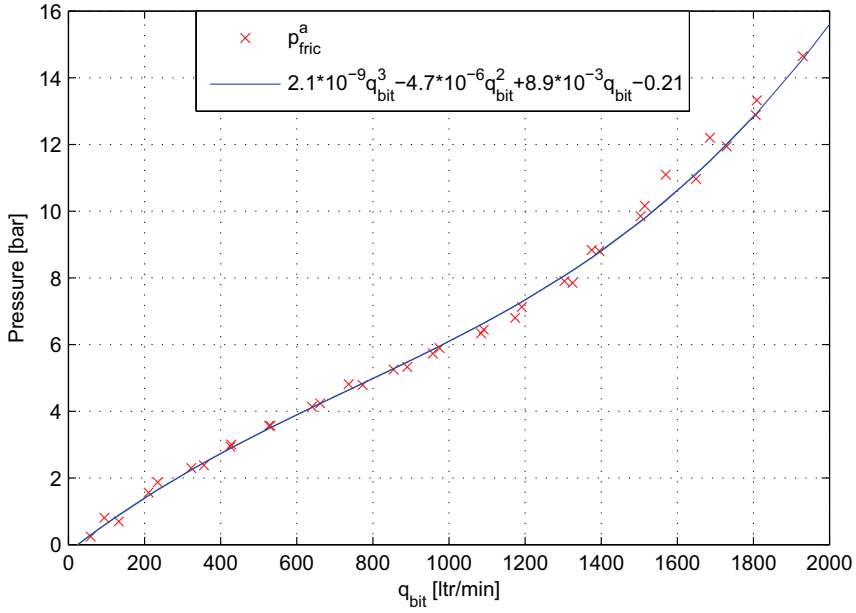

Figure 11.1: Annulus friction and continuous friction model made from curve fit analysis.

from 1800 ltr/min to zero flow. The back pressure pump is used for mud pump flow below 400 ltr/min as shown in Figure B.3. The choke will be closed to maintain the down hole pressure, controlled by a PI controller.

The weights for the basis functions are assumed to be the only unknowns.

The modified version of the observer for q_{bit} is used as proposed in [Stamnes, 2007, Sec. 4.4.1]. As explained in the reference, $q_p = 0$ and $\Delta\rho = 0$ (as is the case for this simulation) will introduce a large modeling error that affects $\hat{q}_{bit}$ and $\hat{p}_{bit}$. The solution proposed is to modify $\dot{\hat{\xi}}_1$ and $\hat{p}_{bit}$ if $\hat{q}_{bit} \leq 0$ as follows

$$\dot{\hat{\xi}}_1 = l_1 a_1 q_p \tag{11.2}$$

$$\hat{p}_{bit} = p_c + \rho_d g v_3 \tag{11.3}$$

where (11.2) and (11.3) is used if $\hat{q}_{bit} \leq 0$ and $p_p < p_c$. This solution will act as projections on $\hat{q}_{bit}$ to prevent it to be negative. With two unknown parameters in Chapter 7 the error in parameter estimation prevented $\hat{q}_{bit}$ to be negative, but for the friction case the estimation becomes wrong if the original observer is used.

11.2.1 Identifier driven by $\tilde{q}_{bit}$

The first simulation considers the simple identifier from Section 4.1. This was also the adaptation law used in the last chapter where the friction approxi-

mations were simulated.

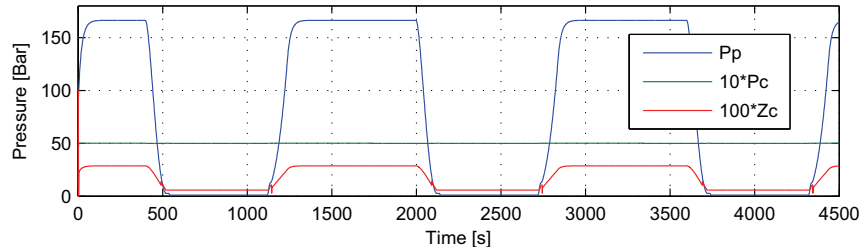

(a) Pump pressure, back pressure pump and choke opening.

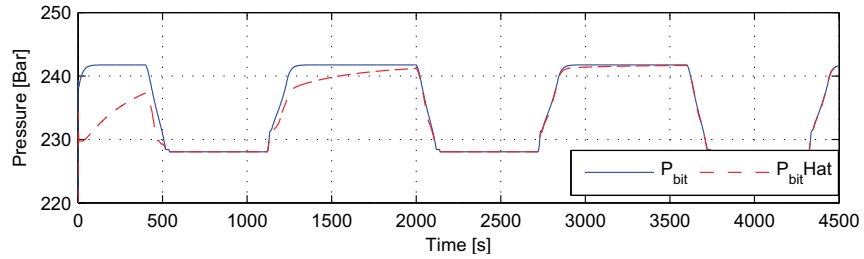

(b) Pressures p_{bit} and $\hat{p}_{bit}$.

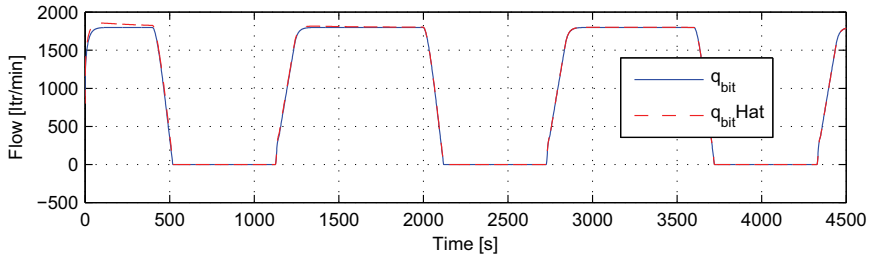

(c) Flows q_{bit} and $\hat{q}_{bit}$.

Figure 11.2: Pipe connection simulation results for passive identifier, with improved friction model.

Figure 11.2 shows the main results from the simulation. Since the initial values for $\hat{\theta} = 0$ the estimations are far from the correct value in the beginning. When the mud pump ramps up and down, the parameters converge (Figure 11.4(b)), which results in convergence also for the estimated states.

Figure 11.4(a) shows that the friction estimation is almost correct after few ramps in the mud pump. Remember that p^a_{fric} is the friction from Equation (11.1), while $\hat{p}^a_{fric}$ is build up from basis functions. This results in small deviations even if $\hat{\theta} = \theta$. As seen in Figure 11.4(b) the parameters converge to their true value as expected. As for the test in the previous chapter there are some small deviations, but a long time simulation showed that the parameters converged. However, it might be a disadvantage with the non-continuous basis functions that the convergence is not smooth. It may also be a good idea to

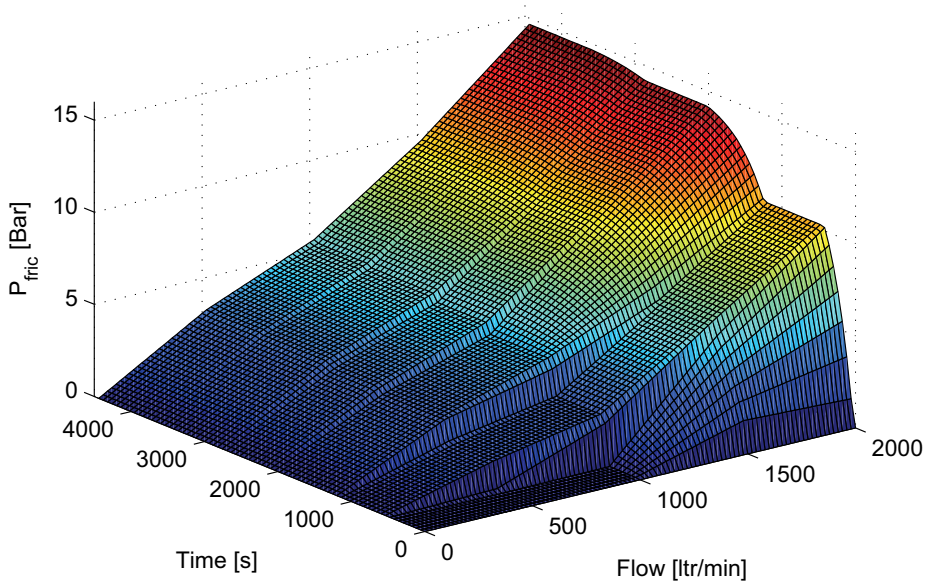

Figure 11.3: Friction estimation passive identifier.

use smaller gains and let the parameters use longer time to converge. This will give a smoother behavior.

How the friction estimates changes with time and flow is showed in Figure 11.3. This supports the other results for the simulation.

This case confirms that there are no problems with comparing to the real friction. This is as expected since the friction approximation is quite good. It should also be noted that zero flow does not influence on the estimation. This is also as expected since none of the basis functions have support for zero flow.

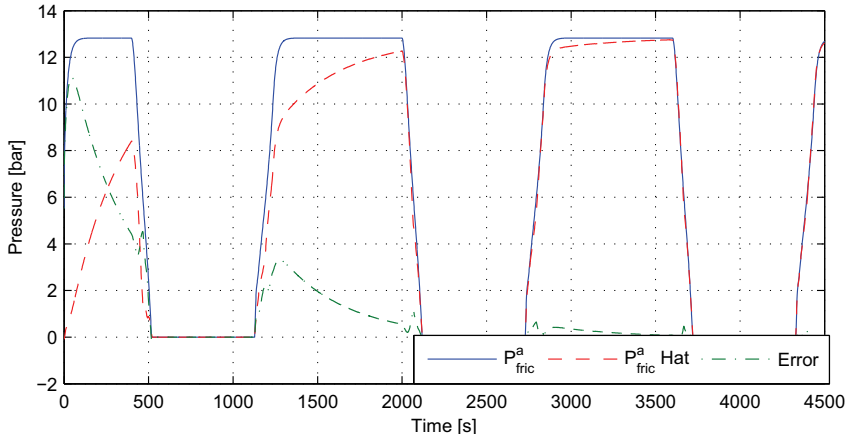

(a) Friction estimation

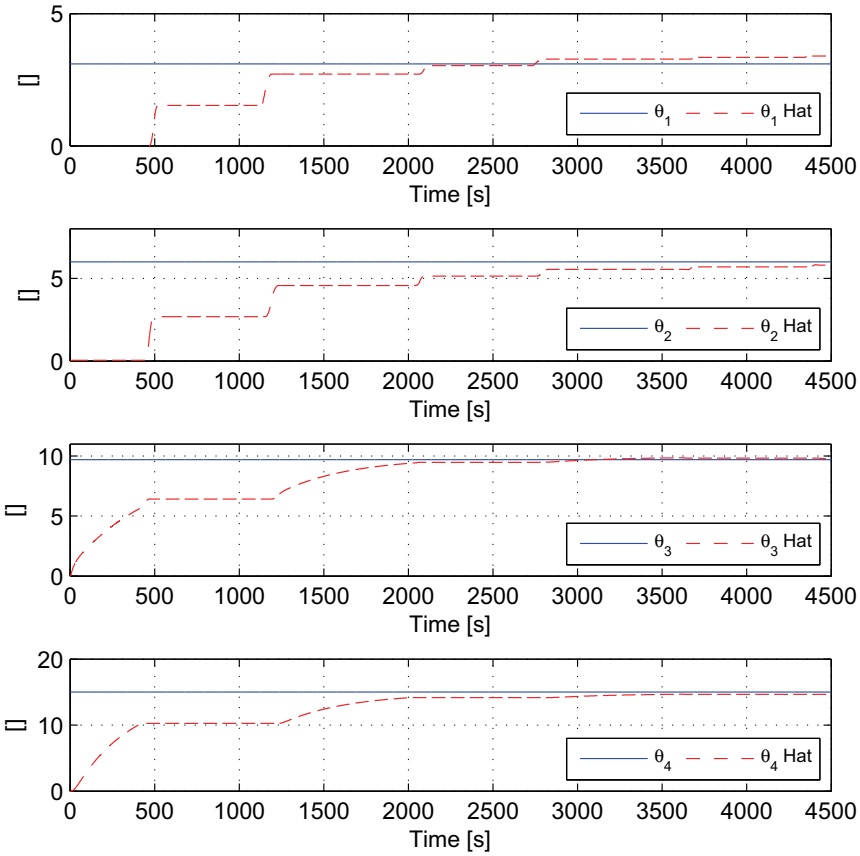

(b) Parameter convergence.

Figure 11.4: Parameter convergence for pipe connection with passive identifier.

11.2.2 Stamnes observer

The Stamnes observer from Chapter 3 was not simulated in the last section, but the pipe connection case is now simulated. First, the observer is modified to fit to the basis function estimation, before the pipe connected case is simulated and commented.

11.2.2.1 Modification to observer

One step in the derivation of the adaptation law for the Stamnes observer is to integrate the regressor $\boldsymbol{\phi}(\hat{q}_{bit})$ w.r.t. $\hat{q}_{bit}$ (See Section 3.2 and [Stamnes, 2007]). Since the regressor is changed, the integration must be done again.

When using basis function approximation, the regressor is

$$\boldsymbol{\phi}(\hat{q}_{bit}) = \begin{bmatrix} \phi_1(\hat{q}_{bit}) \\ \phi_2(\hat{q}_{bit}) \\ \phi_3(\hat{q}_{bit}) \\ \phi_4(\hat{q}_{bit}) \end{bmatrix} \tag{11.4}$$

where ϕ_i are basis functions defined in Equation (10.8).

Since ϕ_i has support in the interval $[c_i, c_{i+2})$ only, this is used as the limits for the integral. Since $\hat{q}_{bit}$ may be outside these limits, the min-function is used. (If $\hat{q}_{bit}$ is outside the interval, the integral will have the same lower and upper limits, which gives zero as solution and stops the adaptation as it should.)

Using $q = \hat{q}_{bit}$ to simplify notation, the integral of $\phi_i^1(\hat{q}_{bit})$ is

$$\nu_i(\hat{q}_{bit}) \triangleq \int_{\min(q,c_i)}^{\min(q,c_{i+2})} \phi_i^1(z)dz \tag{11.5}$$

$$= \int_{\min(q,c_i)}^{\min(q,c_{i+1})} \frac{z - c_i}{c_{i+1} - c_i}dz + \int_{\min(q,c_i+1)}^{\min(q,c_{i+2})} \frac{c_{i+2} - z}{c_{i+2} - c_{i+1}}dz \tag{11.6}$$

$$= \frac{\frac{1}{2}z^2 - c_i z}{c_{i+1} - c_i}\Bigg|_{\min(q,c_i)}^{\min(q,c_{i+1})} + \frac{c_{i+2}z - \frac{1}{2}z^2}{c_{i+2} - c_{i+1}}\Bigg|_{\min(q,c_{i+1})}^{\min(q,c_{i+2})} \tag{11.7}$$

$$\begin{aligned} = &\frac{\frac{1}{2}(\min(q, c_{i+1}))^2 - c_i \min(q, c_{i+1})}{c_{i+1} - c_i} \\ &- \frac{\frac{1}{2}(\min(q, c_i))^2 - c_i \min(q, c_i)}{c_{i+1} - c_i} \\ &+ \frac{c_{i+2}\min(q, c_{i+2}) - \frac{1}{2}(\min(q, c_{i+2}))^2}{c_{i+2} - c_{i+1}} \\ &- \frac{c_{i+2}\min(q, c_{i+1}) - \frac{1}{2}(\min(q, c_{i+1}))^2}{c_{i+2} - c_{i+1}} \end{aligned} \tag{11.8}$$

Using Equation (3.21) the expression for $\eta_i(\hat{q}_{bit})$ becomes

$$\eta_i(\hat{q}_{bit}) = \Gamma_{ii}\frac{-\nu_i}{l_1 a_1} \tag{11.9}$$

where ν_i is given in Equation (11.8). The partial derivatives are also needed in the adaptation law. These are given as

$$\frac{\partial \eta_i}{\partial \hat{q}_{bit}} = \Gamma_{ii} \frac{\phi_i^1(\hat{q}_{bit})}{l_1 a_1} \tag{11.10}$$

To summarize, the Stamnes observer is given in Chapter 3, but the expression for $\boldsymbol{\eta}$ is modified and given in Equation 11.9

11.2.2.2 Simulation results

The simulation results for the pipe connection case with the adaptation from Section 11.2.2.1 are shown in Figures 11.5 - 11.7. The design variables are given in Table 11.1.

Table 11.1: Summary of parameters used for pipe connection case with the observer from Stamnes.

Parameter	Value
l_1	10^{-6}
Γ	diag(75, 125, 50, 50)
$\hat{\boldsymbol{\theta}}(0)$	$\mathbf{0}_{4\times 1}$

As for the passive identifier Figure 11.5(a) shows that the estimation of the bit pressure converges after some pipe connections. The modifications to the observer when the mud pump is turned off ensure that the estimate is correct also for zero flow. There are some small errors when the pump rampes up and down, which is because of some problems with the paramter convergence, explained below.

The bit estimation is very good, as shown in Figure 11.5(b). The convergence is faster than for $\hat{p}_{bit}$.

The friction estimate and the parameter convergence are shown in Figure 11.6. From this it is concluded that the adaptation law from the Stamnes observer can be used to estimate the basis function weights. There are however some problem. The convergence for $\hat{\theta}_1$ and $\hat{\theta}_2$ in particular have some bad responses each time they give support. The reason for this might be the modifications done to the observer, and problems with zero flow. It might also be better if the gains were smaller. The non-continuous basis functions may also contribute with bad responses or it may be disturbances from the back pressure pump, which is stepped up and down then the main pump is turned off/on. This should be further analyzed and tested with drilling data as future work.

Figure 11.7 shows nicely how the friction estimate builds up.

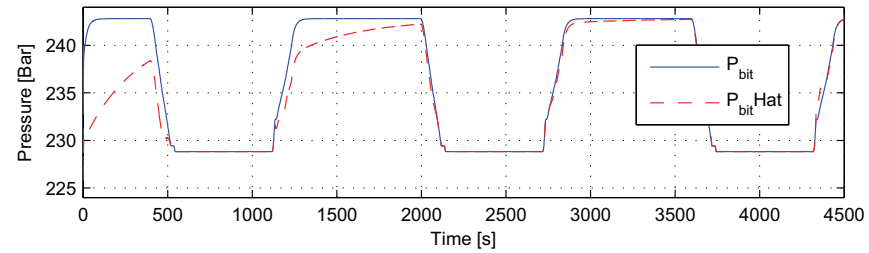

(a) Pressures p_{bit} and $\hat{p}_{bit}$.

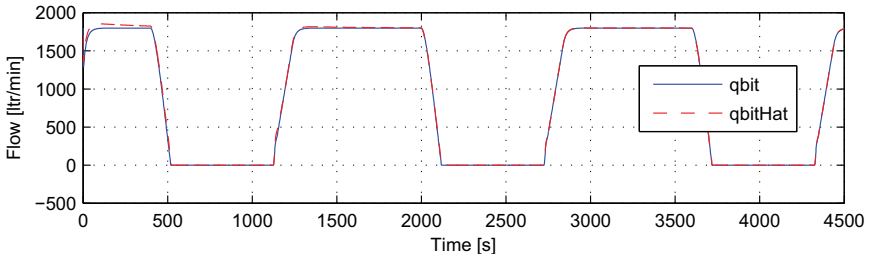

(b) Flows q_{bit} and $\hat{q}_{bit}$.

Figure 11.5: Pipe connection simulation results for Stamnes observer, with improved friction model.

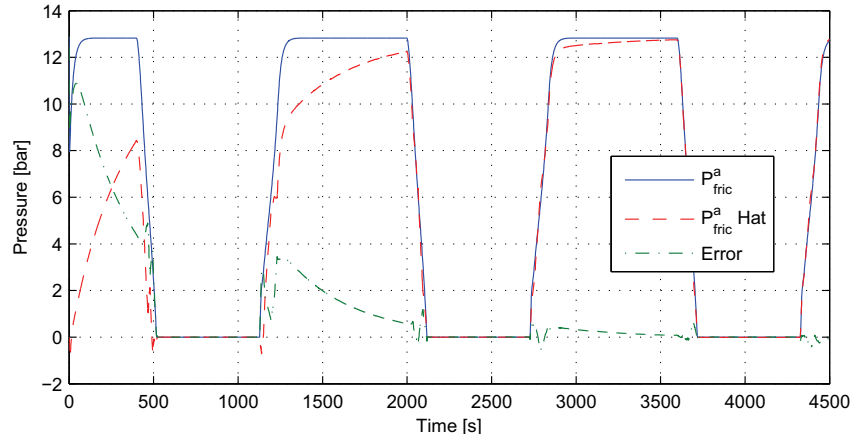

(a) Friction estimation

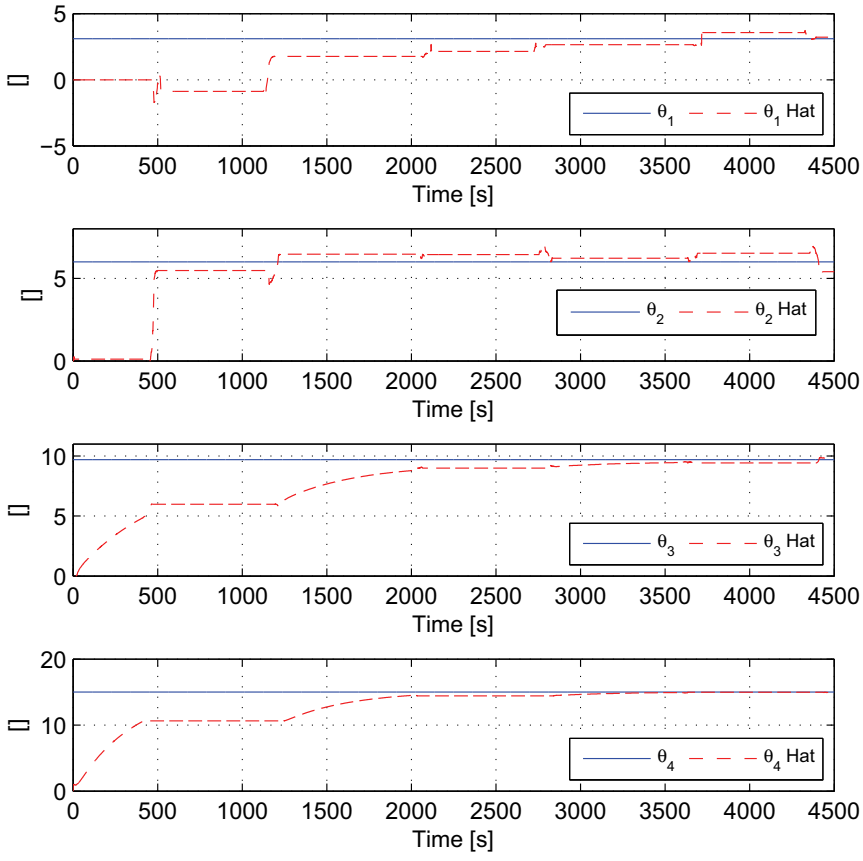

(b) Parameter convergence.

Figure 11.6: Parameter convergence for pipe connection with Stamnes observer.

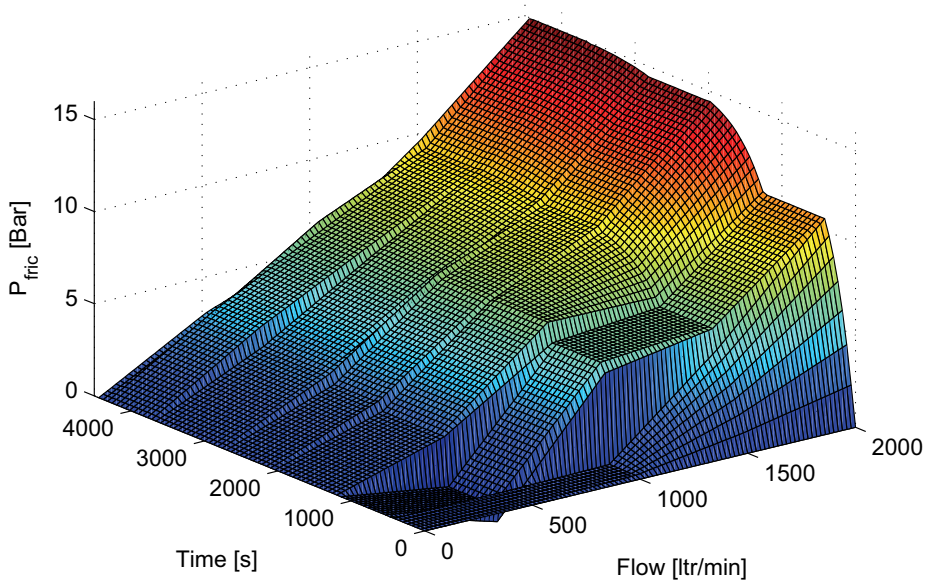

Figure 11.7: Friction estimation Stamnes observer.

Part IV

Conclusion

Chapter 12

Conclusion and Further Work

12.1 Conclusion

Part 2 of the thesis presented different observers for the bottom hole pressure and unknown parameters. Simulations showed that there were just minor differences between the performances. None of the estimation laws managed to estimate the parameters correct when more than one parameter were unknown. All observers are driven by the bit flow estimation error and it seems to be an inherent property of the drilling system that $\hat{q}_{bit}$ converges too fast for the parameters to converge.

A valid proof of convergence was not derived for the Optimal Polynomial Estimator. Instead, some ideas and stepping stones were presented. For the Grip observer a proof based on Lyapunov analysis was derived.

The Stamnes observer is the only observer that not use q_{bit} in the estimation. This, together with rigid proofs and simulations, suggest this to be the best observer.

Part 3 of the thesis considered friction modeling in the drill string and annulus. The quadratic friction loss assumption was found to be reasonable for the drill string, but not good enough for the annulus. A new friction model for the annulus was presented. The friction curve was approximated with a weighted sum of basis functions.

The use of basis functions gave the desired behavior and simulations were done to verify that the parameters converged. The use of four 1^{st}-order b-spline functions gave good approximation and convergence of the estimates. Increasing complexity or number of basis functions did not give better results.

It was also showed that the Stamnes observer could be used to estimate the weights for basis functions, but some more analysis are needed.

12.2 Further Work

Suggested further work are

- Take the Optimal Filter approach into closer analysis, both theoretical and with simulations.
- Test the observers against real drilling log data and later do a test run offshore with the best observer.
- Do more simulations with the improved friction model, preferably with drilling log data.
- Derive and test the Stamnes observer for basis function estimation and other unknowns, such as annulus density and/or bulk modulus in annulus.

References

M. Basin and M. Skliar. Optimal filtering for partially measured polynomial system states. In *American Control Conference, 2005. Proceedings of the 2005*, pages 4022–4027, 2005.

M. Basin, J. Perez, and M. Skliar. Optimal filtering for polynomial system states with polynomial multiplicative noise. *International Journal of Robust and Nonlinear Control*, 16(6):303, 2006.

M. Basin, D. Calderon-Alvarez, and M. Skliar. Optimal filtering for incompletely measured polynomial states over linear observations. 2007.

O. Egeland and J.T. Gravdahl. *Modeling and simulation for automatic control*. Marine Cybernetics, 2002.

J. A. Farrell and M. M. Polycarpou. *Adaptive Approximation Based Control*. New Jersey: John Wiley and Sons, 2006.

A. Gelb. *Applied optimal estimation*. MIT press, 1974.

H. F. Grip, T. A. Johansen, L. Imsland, and G.-O. Kaasa. Parameter Estimation and Compensation in Systems with Nonlinearly Parameterized Perturbations. [Preprint submittet to Automatica January 2009], 2009.

D. Hannegan, J. Richard, M. David, et al. MPD-Uniquely Applicable to Methane Hydrate Drilling. *SPE/IADC*, 91560, 2004.

L. Imsland. Adaptive friction approximation. [Internal note; Cybernetica, Trondheim, 2009.

G.-O. Kaasa. A simple dynamic model of drilling for control. StatoilHydro Research Centre, Porsgrunn, 2007.

G.-O. Kaasa. Note on passive adaptive observers for managed pressure drilling. Internal note; StatoilHydro Research Centre, Porsgrunn, 2009.

R.E. Kalman. A new approach to linear filtering and prediction problems. *Journal of basic Engineering*, 82(1):35–45, 1960.

R.E. Kalman and R.S. Bucy. New results in linear filtering and prediction. *Journal of Basic Engineering (ASME), 83D*, 95108, 1961.

H. E. Merritt. *Hydraulic Control Systems*. Wiley, 1967.

K. Reif, S. Gunther, E. Yaz, and R. Unbehauen. Stochastic stability of the continuous-time extended Kalman filter. *IEE Proceedings-Control Theory and Applications*, 147(1):45–52, 2000.

T. Rognmo. Evaluation of Kalman filters for estimation of the annular bottomhole pressure during drilling. Master's thesis, NTNU, 2008.

P. Skalle. Pressure control during drilling. Tapir akademisk forlag, 2005.

Ø. N. Stamnes. Adaptive observer for bottomhole pressure during drilling. Master's thesis, NTNU, 2007.

Ø. N. Stamnes. Application of optimal estimator for polynominal systems. NTNU, 2008.

Ø. N. Stamnes, J. Zhou, G.O. Kaasa, and O.M. Aamo. Adaptive observer design for the bottomhole pressure of a managed pressure drilling system. In *Decision and Control, 2008. 47th IEEE Conference on*, 2008.

Y. Tan, I. Kanellakopoulos, and Z.P. Jiang. Nonlinear observer/controller design for a class of nonlinearsystems. In *Decision and Control, 1998. Proceedings of the 37th IEEE Conference on*, volume 3, 1998.

Part V

Appendices

Appendix A

Model Derivation

Some derivations for the design model is done in this appendix. More can be found in [Kaasa, 2007; Stamnes, 2007].

A.1 Pressure dynamics

The system is divided into two control volumes (Figure 2.1, the drill string and the annulus. Conservation of mass [Merritt, 1967] gives

$$\sum m_{in} - \sum m_{out} = \dot{m} \tag{A.1}$$

$$= \frac{d\rho V}{dt} \tag{A.2}$$

$$= V\frac{d\rho}{dt} + \rho\frac{dV}{dt} \tag{A.3}$$

From [Egeland and Gravdahl, 2002] we have

$$\frac{d\rho}{\rho} = \frac{dp}{\beta} \tag{A.4}$$

Where β is the bulk modulus and is given as [Merritt, 1967]

$$\beta = -V_0\frac{\partial p}{\partial V}|_{T_o} \tag{A.5}$$

The mass balance can now be written as

$$\sum m_{in} - \sum m_{out} = V\frac{\rho}{\beta}\frac{d\rho}{dt} + \rho\frac{dV}{dt} \tag{A.6}$$

If we assume that $\sum m = \sum q\rho$ we can write (A.6) as

$$\frac{V}{\beta}\dot{p} = \sum q_{in} - \sum q_{out} - \dot{V} \tag{A.7}$$

Appendix B

Additional Simulations

This chapter contains additional simulation results.

B.1 Step test simulations for the observers.

These figures show the behavior for the states for the step test done for each observer. The states behavior are qualities of the system, so it is equal for all observers. The figure shows that the pump pressure and choke pressure decreases when the pump flow is ramped down at 1000 sec. After some time, also the bit flow reach a new steady state value.

The back pressure pump was not used in this simulation.

B.2 Getting the friction curves

Figure B.2 shows how the mud pump was ramped down and up in the drilling test done at the Gullfaks C field. Steady state values was taken at the measurements marked with crosses. The measurements around number 3000 were used to calculate the hydrostatic friction in Section 9.1.1.

B.3 Pipe connection simulation

The mud pump and back pressure pump flows for the pipe connection case are shown in Figure B.3. For the pipe connection with basis functions the mud pump is ramped from/to 1800 ltr/min to ensure that all basis functions have support in the course of the simulation.

B.4 Friction simulations

To estimate the weight parameters in Chapter 10 the mud pump was ramped up and down as shown in Figure B.4(a). The ramp was repeated for the

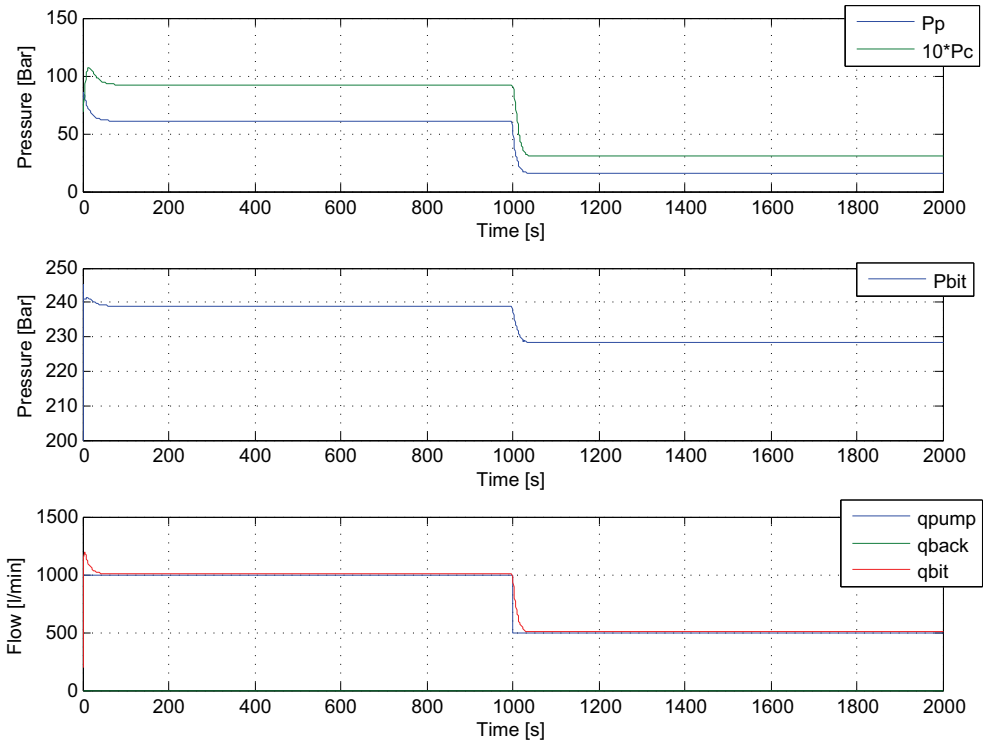

Figure B.1: States response results for step in mud pump.

entire timespan in each simulation. Note that the pump rates span all the basis functions, so all parameters can converge.

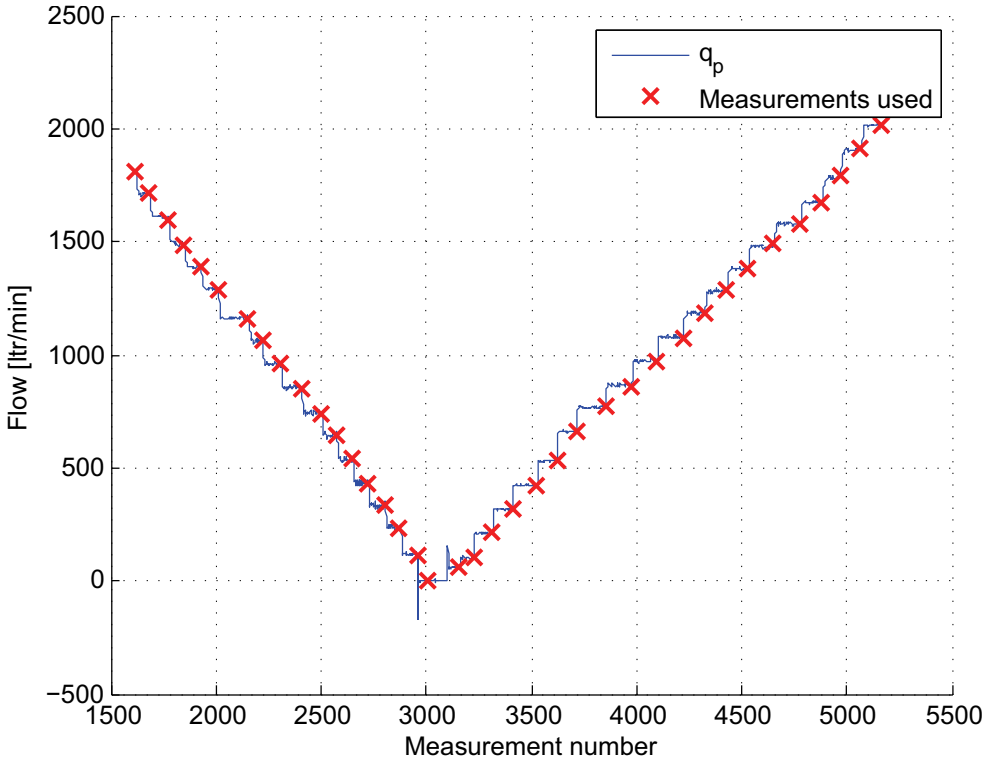

Figure B.2: Pump flow during the ramp test. The measurement numbers used to find friction curves are marked with ×.

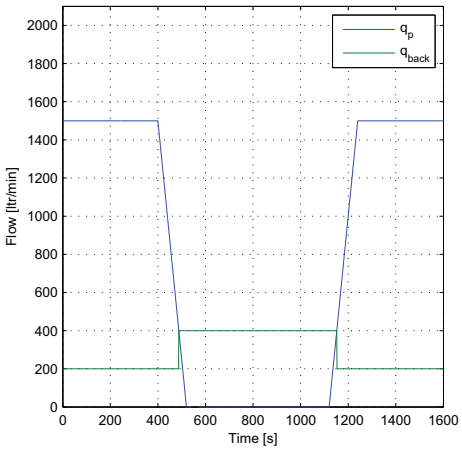

Figure B.3: Pump flows for the case simulations.

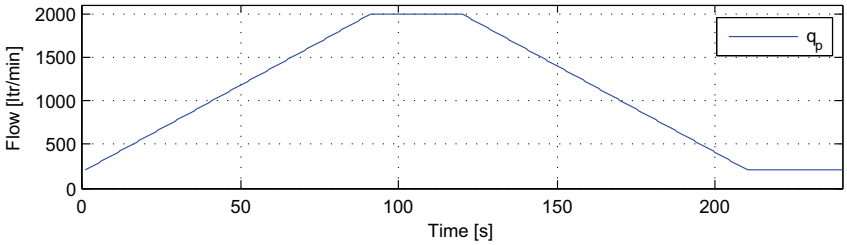

(a) Mud pump flow

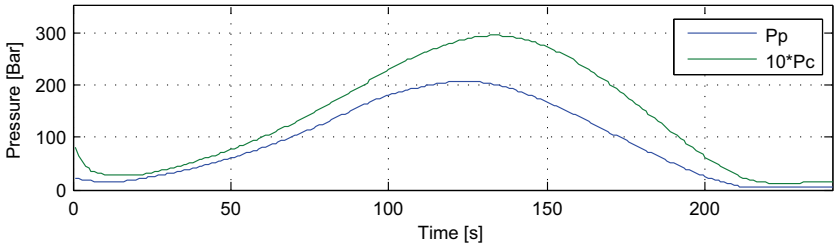

(b) Pump and choke pressure.

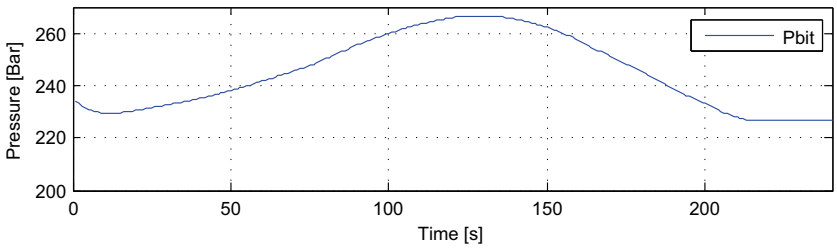

(c) Bit pressure

Figure B.4: States for simple friction simulations.

Appendix C

Derivation of Optimal Estimator for Polynomial Systems

Here the terms in the plynomial estimator are derived.

C.1 Derivation

Term in $\dot{\hat{x}}$ There is one difficult terms in $\dot{\hat{x}}$

$$
\begin{aligned}
E(x_3x_2^2) &= E((x_3-\hat{x}_3)x_2^2) + E(\hat{x}_3x_2^2) && \text{(C.1)}\\
&= E((x_3-\hat{x}_3)[(x_2-\hat{x}_2)^2 + 2x_2\hat{x}_2 - \hat{x}_2^2]) + E(\hat{x}_3x_2^2) && \text{(C.2)}\\
&= \underbrace{E((x_3-\hat{x}_3)(x_2-\hat{x}_2)^2)}_{\text{3rd moment}\Rightarrow 0} + 2E(x_3-\hat{x}_3)x_2\hat{x}_2)... && \text{(C.3)}\\
&\quad - E((x_3-\hat{x}_3)\hat{x}_2^2) + E(\hat{x}_3x_2^2) && \text{(C.4)}\\
&= 2\underbrace{E((x_3-\hat{x}_3)(x_2-\hat{x}_2)}_{P_{32}}\hat{x}_2) + \underbrace{2E((x_3-\hat{x}_3)\hat{x}_2^2)}_{\text{3rd moment}\Rightarrow 0}... && \text{(C.5)}\\
&\quad - \underbrace{E((x_3-\hat{x}_3)\hat{x}_2^2)}_{\text{3rd moment}\Rightarrow 0} + E(\hat{x}_3x_2^2) && \text{(C.6)}\\
&= 2\hat{x}_2P_{32} + \hat{x}_3E(x_2^2) && \text{(C.7)}\\
&= 2\hat{x}_2P_{32} + \hat{x}_3[E((x_2-\hat{x}_2)^2 + 2x_2\hat{x}_2 - \hat{x}_2^2)] && \text{(C.8)}\\
&= 2\hat{x}_2P_{32} + \hat{x}_3[P_{22} + 2E(x_2)\hat{x}_2\hat{x}_2 - \hat{x}_2] && \text{(C.9)}\\
&= 2\hat{x}_2P_{32} + \hat{x}_3[P_{22} + 2\hat{x}_2^2 - \hat{x}_2] && \text{(C.10)}\\
&= 2\hat{x}_2P_{32} + \hat{x}_3P_{22} + \hat{x}_3\hat{x}_2^2 && \text{(C.11)}
\end{aligned}
$$

Terms in $\dot{P}$ There are two terms in $\dot{P}$ which is not trivial. We start with $E([x-\hat{x}]f_2^\top(x,t))$

$$E([x-\hat{x}]f_2(x,t)) = E\left([x-\hat{x}](\frac{1}{M}x_1 - \frac{1}{M}p_c(t) - \frac{1}{M}x_3x_2^2)\right) \tag{C.12}$$

$$= \frac{1}{M}E([x-\hat{x}]x_1) - \frac{1}{M}E([x-\hat{x}]p_c(t))... \tag{C.13}$$

$$- \frac{1}{M}E([x-\hat{x}]x_3x_2^2) \tag{C.14}$$

$$= \frac{1}{M}P_{*1} - 0 - \frac{1}{M}E([x-\hat{x}]x_3x_2^2) \tag{C.15}$$

We now take a closer look at the last term in (C.15)

$$E([x-\hat{x}]x_3x_2^2) = E\left([x-\hat{x}]((x_3-\hat{x}_3)x_2^2 + \hat{x}_3x_2^2)\right) \tag{C.16}$$

$$= E\left([x-\hat{x}](x_3-\hat{x}_3)x_2^2\right) + \hat{x}_3E([x-\hat{x}]x_2^2) \tag{C.17}$$

Once again we take one term at the time from (C.17)

$$E([x-\hat{x}](x_3-\hat{x}_3)x_2^2)... \tag{C.18}$$

$$= E([x-\hat{x}]((x_3-\hat{x}_3)(x_2-\hat{x}_2)^2 + 2x_2\hat{x}_2(x_3-\hat{x}_3) - \hat{x}_2^2(x_3-\hat{x}_3))) \tag{C.19}$$

$$= E([x-\hat{x}]((x_3-\hat{x}_3)(x_2-\hat{x}_2)^2 + 2(x_2-\hat{x}_2)\hat{x}_2(x_3-\hat{x}_3)... \tag{C.20}$$

$$+ 2\hat{x}_2^2(x_3-\hat{x}_3) - \hat{x}_2^2(x_3-\hat{x}_3))) \tag{C.21}$$

$$= E\left([x-\hat{x}](x_3-\hat{x}_3)(x_2-\hat{x}_2)^2\right) + E\left([x-\hat{x}]2(x_2-\hat{x}_2)\hat{x}_2(x_3-\hat{x})\right)... \tag{C.22}$$

$$+ E\left([x-\hat{x}]2\hat{x}_2^2(x_3-\hat{x}_3)\right) - E\left([x-\hat{x}]\hat{x}_2^2(x_3-\hat{x}_3)\right) \tag{C.23}$$

$$= 0 + 0 + 2\hat{x}_2^2E([x-\hat{x}](x_3-\hat{x}_3)) - \hat{x}_2^2E([x-\hat{x}](x_3-\hat{x}_3)) \tag{C.24}$$

$$= \hat{x}_2^2P_{*3} \tag{C.25}$$

We then take the last term in (C.17)

$$E([x-\hat{x}]\hat{x}_3x_2^2) = E\left([x-\hat{x}]((x_2-\hat{x}_2)^2\hat{x}_3 + 2x_2\hat{x}_2\hat{x}_3 - \hat{x}_2^2\hat{x}_3)\right) \tag{C.26}$$

$$= E([x-\hat{x}](x_2-\hat{x}_2)^2\hat{x}_3 + 2\hat{x}_2(x_2-\hat{x}_2)\hat{x}_3 \tag{C.27}$$

$$+ 2\hat{x}_2^2\hat{x}_3 - \hat{x}_2^2\hat{x}_3) \tag{C.28}$$

$$= 2\hat{x}_2\hat{x}_3E([x-\hat{x}](x_2-\hat{x}_2)) \tag{C.29}$$

$$= 2\hat{x}_2\hat{x}_3P_{*2} \tag{C.30}$$

We collect (C.25) and (C.30) and put them into (C.17)

$$E([x-\hat{x}]x_3x_2^2) = \hat{x}_2^2P_{*3} + 2\hat{x}_2\hat{x}_3P_{*2} \tag{C.31}$$

And at last (C.31) into (C.15) give the expression

$$E([x-\hat{x}]f_2(x,t)) = \frac{1}{M}(P_{*1} - \hat{x}_2^2P_{*3} - 2\hat{x}_2\hat{x}_3P_{*2}) \tag{C.32}$$

vir prudens non contra ventum mingit